



Fluid flow and CO₂–fluid–mineral interactions during CO₂–storage in sedimentary basins[☆]



Niko Kampman^{a,b,c}, Mike Bickle^a, Max Wigley^a, Benoit Dubacq^{a,d,e}

^a Department of Earth Sciences, University of Cambridge, Downing Street, Cambridge CB2 3EQ, UK

^b Lancaster Environment Centre, Lancaster University, Bailrigg, Lancaster, LA1 4YW, UK

^c British Geological Survey, NERC Isotope Geosciences Laboratory, Keyworth, Nottingham, NG12 5GG, UK

^d UPMC, Université Pierre et Marie Curie, ISTEP, Institut des Sciences de la Terre de Paris, F-75005, Paris, France

^e CNRS, Centre National de la Recherche Scientifique, UMR 7193, F-75005, Paris, France

ARTICLE INFO

Article history:

Received 26 March 2013

Received in revised form 12 November 2013

Accepted 12 November 2013

Available online 27 November 2013

Editor: J. Fein

Keywords:

Carbon sequestration

Geochemistry

Fluid–mineral reactions

Injection experiments

Natural CO₂ analogues

ABSTRACT

Modelling the progress of geochemical processes in CO₂ storage sites is frustrated by uncertainties in the rates of CO₂ flow and dissolution, and in the rates and controlling mechanisms of fluid–mineral reactions that stabilise the CO₂ in geological reservoirs. Dissolution of CO₂ must be controlled by the complexities of 2-phase flow of CO₂ and formation brines and the smaller-scale heterogeneities in the permeability in the reservoirs which increase the fluid contact areas. The subsequent fluid mineral reactions may increase storage security by precipitating CO₂ in carbonate minerals but the consequences of fluid–mineral reactions on caprock rocks or potential leakage pathways up fault zones are less certain as the CO₂-charged brines may either corrode minerals or decrease permeabilities by precipitating carbonates.

Observations from CO₂-injection experiments and natural analogues provide important constraints on the rates of CO₂ and brine flow and on the progress of CO₂ dissolution and mineral–fluid reactions. In these experiments brines in contact with the propagating plume appear to rapidly saturate with CO₂. Dissolution of the CO₂ drives the dissolution of oxide and carbonate minerals, on times scales of days to weeks. These reactions buffer fluid pH and produce alkalinity such that carbonate dissolution moves to carbonate precipitation over time-scales of weeks to months. The dissolution of Fe-oxide grain coatings and the release of Fe to solution is important in stabilising insoluble Fe–Mg–Ca carbonate minerals but the rate limiting step for carbonate mineral precipitation is the transport of CO₂-charged brines and silicate mineral dissolution rates. Observations from CO₂-EOR experiments and natural analogues suggest that the silicate mineral dissolution reactions are initially fast in the low pH fluids surrounding the CO₂ plume but that reaction progress over months to years drives minerals towards thermodynamic equilibrium and dissolution rates slow over 2–5 orders of magnitude as equilibrium is approached. The sluggish dissolution of silicate minerals is likely to preside over the long-term fate of the CO₂ in geological reservoirs. Observations from injection experiments and natural analogues suggest that the potentially harmful trace elements mobilised by the drop in pH are immobilised as adsorbed and precipitated phases as fluid pH is buffered across mineral reaction fronts.

There are very few observations of caprock exposed to CO₂-rich brines. Preliminary examination of core recently recovered from scientific drilling of a natural CO₂ accumulation in Utah suggests that the diffusion of CO₂ into reservoir caprocks drives dissolution of Fe-oxides but subsequent precipitation of carbonate minerals likely retards the diffusion distance of the CO₂. At this site thin siltstone layers are shown to be effective seals to the CO₂-charged fluids, which has significant implications for the long term security of CO₂ in geological reservoirs.

© 2013 The Authors. Published by Elsevier B.V. All rights reserved.

Contents

1.	Introduction	23
2.	Modelling of flow and reaction	24
2.1.	Flow and dissolution of CO ₂ in brine	24
2.2.	Controls on fluid–fluid and fluid–rock reactions	26
2.2.1.	CO ₂ –brine phase relationships	26
2.2.2.	CO ₂ –wellbore interactions	26

[☆] This is an open-access article distributed under the terms of the Creative Commons Attribution-NonCommercial-No Derivative Works License, which permits non-commercial use, distribution, and reproduction in any medium, provided the original author and source are credited

2.2.3.	Supercritical CO ₂ –rock reactions	27
2.2.4.	CO ₂ –fluid–rock reactions	27
3.	CO ₂ –fluid–rock interactions in CO ₂ injection experiments	30
3.1.	CO ₂ injection experiments and CO ₂ -EOR projects	30
3.2.	Sampling CO ₂ injection experiments	30
3.3.	Monitoring of CO ₂ dissolution and CO ₂ saturation	31
3.3.1.	Direct measurements of dissolved CO ₂ and CO ₂ saturation	31
3.3.2.	Indirect estimation of dissolved CO ₂ concentrations and CO ₂ -gas saturation	31
3.3.3.	Fluid–rock interactions inferred from CO ₂ injection experiments	33
3.3.4.	Trace metal mobilisation	35
3.4.	Organic contaminants	37
4.	Long term fluid–rock interactions in injection experiments and CO ₂ -EOR studies	37
4.1.	Ionic trapping	37
4.2.	Carbonate mineral precipitation	37
4.2.1.	Pembina-Cardium EOR project	37
4.2.2.	Salt Creek EOR project	37
5.	Long term fluid–rock reactions – observations from natural analogues	38
5.1.	Noble gas constraints on the long term fate of natural CO ₂	38
5.2.	Fluid–mineral reactions in natural reservoirs	40
5.2.1.	Implications for carbonate mineral deposition	41
5.3.	Green River, Utah	41
5.3.1.	Green River active system	42
5.3.2.	Scientific drilling	42
5.3.3.	Fluid–rock reaction	43
5.3.4.	Green River exhumed reservoir	43
6.	Conclusions and future work	44
	Acknowledgements	46
	References	46

1. Introduction

Carbon capture and storage equipped power generation from fossil fuels needs to form a significant fraction of new power generation capabilities by 2035 to satisfy global energy needs while limiting the rise in atmospheric CO₂ and mitigating potential climate instabilities (Metz et al., 2005). Such geological storage in saline aquifers and depleted oil and gas reservoirs represents a practical and safe method of CO₂ disposal as demonstrated by the several current large-scale injection programs (e.g. Hosa et al., 2011) and the retention of CO₂ in natural geological reservoirs for millions of years (e.g. Zhou et al., 2012). Secure long-term storage in geological reservoirs must be demonstrated to satisfy operational and regulatory criteria, public acceptance, and auditing of carbon credits for the stored CO₂. Regulation requires, for example, 'that the stored CO₂ will be completely and permanently contained' (EU DIRECTIVE 2009/31/EC). Uncertainty over the security of storage is seen as a major risk factor which has significant impact on the overall costs (e.g. DECC (UK Department of Energy and Climate Change), 2012).

Geological carbon storage involves separating CO₂ at power stations or other industrial plants, compressing it and injecting it into permeable strata at depths where it remains in a dense supercritical state (Fig. 1). Previously exploited oil and gas fields and saline aquifers offer the most storage potential (Hendriks et al., 2004). Injection into, and reaction with, basaltic or peridotitic rocks is also being explored as alternative sites in appropriate settings, where the CO₂ is often pre-dissolved in water prior to injection (e.g. Newark, Assayag et al., 2009b; CarbFix, Keleman and Matter, 2008; Gislason et al., 2010). At the pressure and temperatures in most potential storage sites, the CO₂ is less dense than formation brines and will rise. Secure storage therefore requires that the CO₂ is trapped under an impermeable caprock. Major concerns include; 1) that the CO₂ may exploit permeable pathways such as faults to escape upwards; 2) the acid fluids formed when the CO₂ dissolves in formation brines may corrode caprocks or fault seals, allowing CO₂ to migrate upwards; 3) changes in stress related to injection may fracture caprocks; 4) carbonate mineralisation in faults and fractures

may generate stresses by the force of crystallisation, inducing leakage; 5) migrating CO₂-charged brines might mobilise trace metals and organic compounds and contaminate overlying potable aquifers; 6) displacement of brines distant from the injection site may contaminate overlying aquifers and; 7) CO₂ storage reservoirs will be hard to monitor to verify that the stored CO₂ remains in place.

Several processes may act to further stabilise the CO₂ trapped by geological structures (Fig. 2; Metz et al., 2005). In residual trapping, between 10 and 35% of the pore space is occupied by CO₂ after a CO₂ plume has passed, held immobile by capillary forces (Bachu and Bennion, 2009). The fraction of CO₂ so trapped depends both on the magnitude of the residual CO₂ saturation and on the volume of the reservoir swept by the CO₂ plume (Hesse et al., 2008). Dissolution trapping occurs as CO₂ dissolves into formation brines and is facilitated by large brine–CO₂ contact surface areas, the negative buoyancy of CO₂-saturated brine and density driven convective mixing. Ionic trapping of dissolved CO₂ as bicarbonate ions and its subsequent trapping as precipitated carbonate minerals result from reaction between CO₂-bearing brines and the reservoir rock and are therefore dependent on the rates of dissolution trapping, on the flow paths of the CO₂-saturated brines and on the kinetics of subsequent fluid–mineral reactions.

There are a number of potentially significant consequences of fluid–mineral reactions. 1) The rapid mineral dissolution, especially of carbonates, may corrode caprocks, wellbores and fault seals, potentially leading to migration of CO₂ into overlying formations, 2) carbonate precipitation in caprocks may reduce their permeability, stabilising storage, 3) mineral dissolution or precipitation in reservoirs may alter the permeability and the flow of CO₂ and CO₂-saturated brines and 4) sequestration of CO₂ into carbonate minerals may contribute to the long-term storage security. The general impacts of CO₂-injection on fluid–rock reactions are reviewed in Gaus (2010).

The nature and especially the rates of the geochemical processes in CO₂ storage reservoirs are very poorly constrained. This arises from a combination of factors: 1) there are a limited number of anthropogenic CO₂ injection experiments and their short duration, combined with

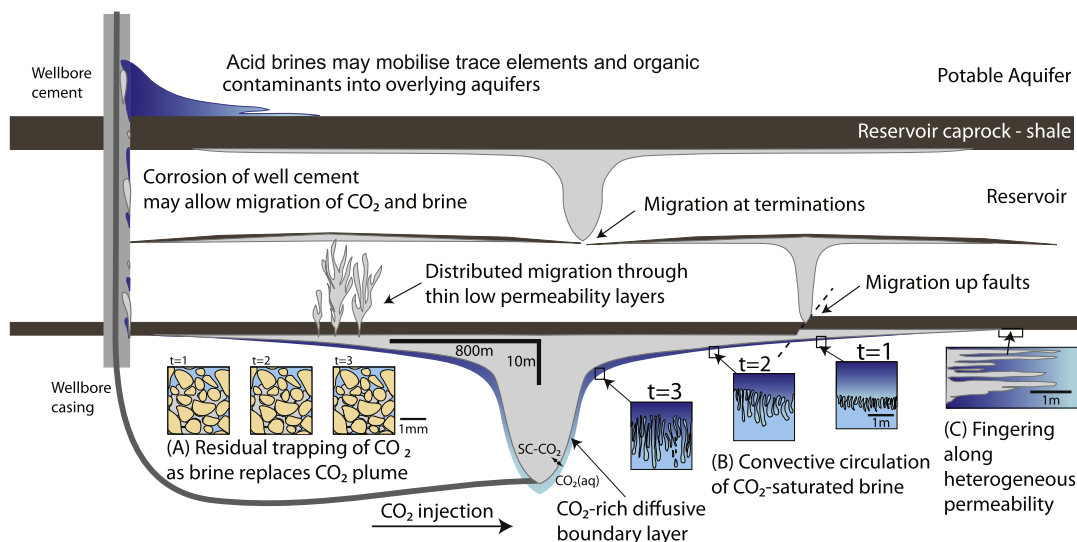


Fig. 1. Diagrammatic illustration of geological carbon storage. CO₂ from concentrated sources is separated from other gases, compressed and injected into porous geological strata at depths >800 m where it is in a dense or supercritical phase. The CO₂ is lighter than formation brines, rises and is trapped by impermeable strata. The risks are that the light CO₂ will exploit faults or other permeable pathways to escape upwards and acid CO₂-charged brines might corrode the caprocks or fault zones. A variety of processes will tend to stabilise the CO₂ including 1) capillary trapping in bubbles of CO₂ after the CO₂ plume has passed (inset A), 2) dissolution in formation brines which forms a denser fluid which will sink (inset B), where fingering along bedding-related heterogeneities will enhance dissolution (inset C), and 3) precipitation of CO₂ in solid form as carbonate minerals as a result of reactions between CO₂-charged brines and silicate minerals.

the difficulty of observing dissolution and mineral reactions and the sluggish nature of these reactions, results in a very limited observational data base. 2) A key process, the rate of dissolution of CO₂ in the brine, will be strongly moderated by reservoir heterogeneities on scales less than ~10 m which is below that resolvable by remote observation. 3) The kinetics of fluid–mineral reactions are often not well known and there are order-of-magnitude discrepancies between reaction rates determined in the laboratory and those recovered from natural field settings (e.g. White and Brantley, 2003). 4) Monitoring the progress of CO₂ dissolution by direct sampling of CO₂-rich fluids is complicated by the limited sampling opportunities and CO₂ degassing as samples are collected.

In this paper we review the state of knowledge of these fluid flow and geochemical processes and how understanding of these processes might be improved. Theoretical modelling of the flow of CO₂ and brine

in potential CO₂ storage sites combined with prediction of the nature and rates of fluid–fluid and mineral–fluid reactions from laboratory experiments and imaging of two-phase flow in rock core provide a framework in which to evaluate the observations from field sites. These predictions are compared with the results of completed or on-going CO₂ injection experiments and studies of natural analogues. In particular we focus on the results from small scale CO₂-injection experiments at Frio, Texas and on-going CO₂-EOR projects in Canada and the USA and present initial results from our work on a CO₂-EOR project (Salt Creek, Wyoming). We present preliminary results from scientific drilling of a natural CO₂ accumulation at Green River, Utah. An important conclusion of the work is that monitoring the geochemical evolution of brines provides a unique set of constraints on the complex interactions of CO₂ flow, fluid–fluid and fluid–mineral reactions in the reservoirs. We conclude that, if these processes, including the critical impact of small scale heterogeneities on flow and reaction in the reservoirs, are to be quantified it will be essential to carry out additional experiments to sample, analyse and model the geochemical evolution of the brines.

2. Modelling of flow and reaction

2.1. Flow and dissolution of CO₂ in brine

The progress of fluid–fluid and fluid–rock reactions in geological storage sites will critically depend on the flow of CO₂ in the reservoir and the dissolution of CO₂ into formation brine and flow of the CO₂-rich brines. CO₂ has limited solubility and is therefore immiscible in formation brines, and is typically the non-wetting phase. Its flow is therefore dependent on the complex multiphase flow properties of the reservoir rocks. Important consequences of such multiphase flow are (Jacob, 1972): 1) that the injected CO₂ will only occupy a fraction of the pore space depending on the pore structure, capillary pressure and flow dynamics, 2) the effective permeability of the formation to CO₂ reduces rapidly with decreasing saturation of the CO₂ ('relative permeability'), 3) caprocks with very small pores and permeabilities will have high capillary entry pressures, increasing their effectiveness as seals (Bildstein et al., 2010), 4) where brines replace a migrating CO₂ plume a significant fraction of the CO₂ remains trapped in the

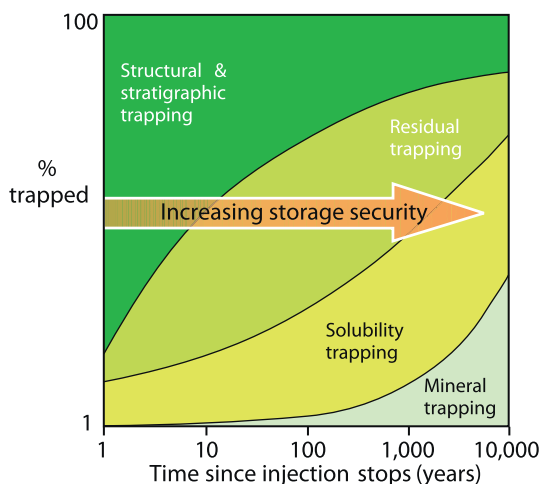


Fig. 2. Diagrammatic illustration of the proportions of a CO₂ plume trapped by residual, dissolution and mineral trapping as a function of time (Metz et al., 2005). Note that the relative magnitudes of the three processes and their evolution with time are very poorly known and will depend on the physical state and mineralogy of the reservoir, and the complex coupling of fluid–flow and fluid–rock reaction.

porosity by capillary forces (Hesse et al., 2008) and 5) formation pressures and two phase flow effects in less permeable reservoirs may require injection pressures sufficiently high so as to induce brittle deformation facilitating CO₂ escape (Rutqvist et al., 2007).

Supercritical CO₂ at reservoir conditions is less dense and an order-of-magnitude less viscous than brines. The flow of supercritical CO₂ into brine filled pore-space will depend on capillary pressure and phenomena related to the relative permeability of brine filled pores to CO₂ and the brine-CO₂ viscosity contrast and interfacial tension (Fig. 3; e.g. Bachu and Bennion, 2008). Generally, the brine-CO₂ viscosity contrast and CO₂-brine interfacial tension decrease with increasing pressure, and increase with increasing temperature and salinity such that a given brine-saturated rock becomes more permeable to CO₂ at higher pressures, or lower temperatures and salinity (Bachu and Bennion, 2009). These relative permeability phenomena strongly influence the amount of residual CO₂ trapping; with higher permeability to CO₂ tending to lead to higher residual CO₂ saturation and greater amounts of residually trapped CO₂. However, these multiphase flow processes are complex and this description is a simplified one, and ultimately the overall amount of residually trapped CO₂ will be dependent on the macroscopic structure of the growing CO₂ plume.

Injected CO₂ will rise through reservoirs until it reaches impermeable horizons, where it will flow laterally and the CO₂ front will tend to finger (Homsy, 1987). In geological reservoirs the innate heterogeneity of reservoir permeabilities will undoubtedly dominate and accentuate the structure of the resulting fingering. The overall flow of the light supercritical CO₂ from injection wells will be dominated by viscous and buoyancy forces that drive the spread of CO₂ as a gravity current and these have been modelled by a range of approaches including a variety of analytical solutions (Lyle et al., 2005; Nordbotten et al., 2005; Vella and Huppert, 2006; Golding et al., 2011) to full numerical simulations (Pruess, 2004; Chadwick and Noy, 2010).

Seismic reflection images of the CO₂ injection operation at Sleipner illustrate the characteristics of the flow of injected CO₂ and the complexities which arise from reservoir heterogeneity (Arts et al., 2004; Chadwick et al., 2008). Here the CO₂ was injected near the base of the

~200 m thick permeable Utsira Sand which contains a number of thin and probably discontinuous ~1 m thick mudstones, and is overlain by the several hundred metres thick Nordland Shale. The thin mudstones were predicted to retard the flow of the injected CO₂ (Zweigel et al., 2000) and seismic reflection profiles taken periodically since injection started in 1996 nicely illustrate this, with 8 horizons retarding CO₂ flow within the reservoir (Fig. 4).

Analytical modelling of sharp-interface axisymmetric gravity flows (Lyle et al., 2005) predicts that the CO₂ will rise and spread out under impermeable caprocks and that the radius of an axisymmetric accumulation will increase as the square-root of time. This relationship is preserved in models which allow for capillarity (Golding et al., 2011). Although the layer radii derived from seismic reflection surveys at Sleipner in 1999, 2001 and 2002 satisfy such a relationship (Bickle et al., 2007), with planforms moderated by topographic infilling (Singh et al., 2010; Boait et al., 2012), subsequent surveys show that lower layers apparently start to shrink and dim by 2004 and the seismic dimming extends to the upper layers by 2008 (Fig. 4b; Boait et al., 2012). Shrinkage of the lower layers maybe due to increased migration of the CO₂ through the lower layers as CO₂ completely penetrates the thin mudstones and migration rates increase markedly due to expulsion of the more viscous water, increased CO₂ saturation and removal of the capillary pressure at the CO₂-brine interface (Chadwick and Noy, 2010; Boait et al., 2012). However, Boait et al. (2012) argue that much of the dimming results from a reduction in seismic velocity contrast between the CO₂ plumes and brine which contains widely dispersed residually trapped CO₂. Irrespective of the precise cause of the layer dimming it likely reflects either a flow or trapping process that has increased CO₂-brine contact area and therefore dissolution rates.

Dissolution of CO₂ into formation brine is an important stabilising mechanism, as saturated brines with between 2 and 5 wt.% CO₂ (depending on pressure, temperature and salinity) have negative buoyancy, compared to CO₂-poor brines. Where CO₂ dissolves at the base of a trapped CO₂ plume, sinking plumes of the denser brine set up convective circulation (Ennis-King and Paterson, 2005; Riaz et al., 2006), that can lead to enhanced rates of CO₂ dissolution (Ennis-King and Paterson, 2005; Yang and Gu, 2006; Neufeld et al., 2010). Neufeld et al. (2010) have shown that the rate of convective circulation and dissolution of CO₂ is governed principally by the velocity of the sinking plumes. In the high permeability Utsira Sand at Sleipner, Neufeld et al. (2010) estimate that 10% of the annually injected mass of CO₂ was being dissolved six years after injection commenced, a fraction that should increase with time as the CO₂ plumes spread.

Diffusion of CO₂ in brine is a relatively sluggish process and after a year CO₂ would only penetrate ~25 cm into static brine (Fig. 5). However, Taylor dispersion (Taylor, 1953) at high flow rates may lead to broadening of the diffusive fringe and to an increase in the effective diffusion coefficient up to 15 times that of molecular diffusion (Backhaus et al., 2011). In addition, a combination of complex macroscopic flow paths, such as in the Sleipner example, sub-metre bedding-scale heterogeneities in permeability and flow, and convective circulation of the denser, CO₂-saturated brines are all expected to cause large increases in the surface area of CO₂ in contact with brine, enhancing dissolution (MacMinn et al., 2011). The nine CO₂ layers in Sleipner increase the basal contact areas between CO₂ and brine by about an order-of-magnitude over that occupied by a single layer at the top of the reservoir. Bedding-scale heterogeneities of flow and pore-scale complexities arising from capillarity will further increase the contact areas but without a better constraint on these processes it is impossible to quantify this increase.

Whilst important information about the macroscopic flow of CO₂ can be gained from experiments like Sleipner, further small-scale CO₂ injection experiments are required to test models, theories and predications about the complexities of flow. In-situ geophysical and geochemical observation of the growth and development of fingering,

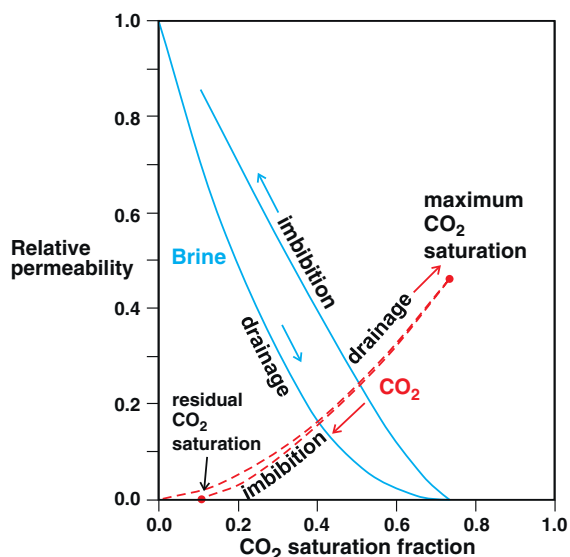


Fig. 3. Schematic brine-CO₂ relative permeability curves illustrating a) two phase flow in high and low permeability rocks and the strong dependence of CO₂ permeability on its relative saturation to brine and b) drainage and imbibition curves showing the relative permeability of brine and CO₂ during flow of CO₂ into the pore volume and then during return flow of brine as the CO₂ plume migrates. The return to a finite residual saturation of CO₂ reflects non-wetting CO₂ trapped in the pore space by capillary forces.

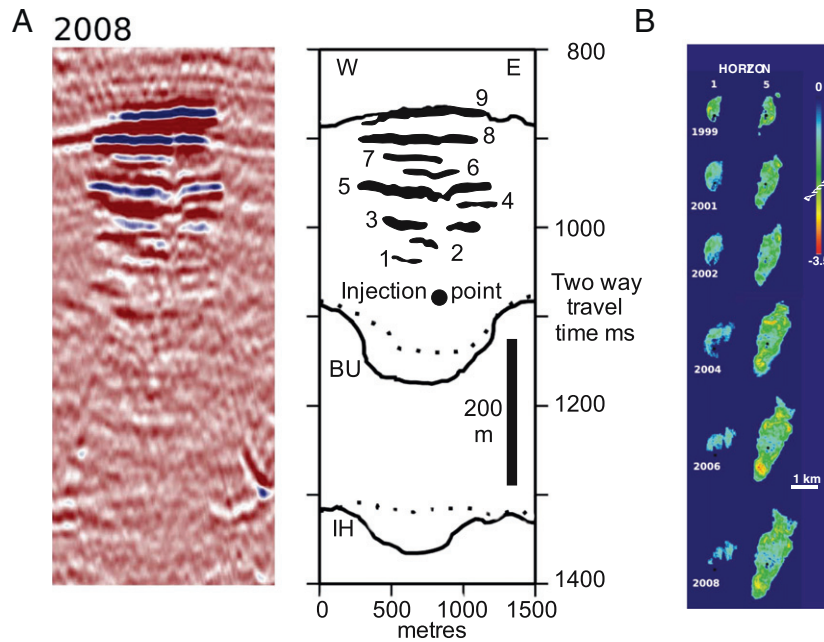


Fig. 4. A) Vertical seismic section from the 2008 Sleipner survey after Boait et al. (2012). Left shows seismic amplitudes with high amplitudes (blue) from CO₂ layers. Right is a line drawing with CO₂ accumulations numbered, CO₂ injection point labelled and solid lines denote formation contacts. The top of Utsira Sand coincides with the top of Layer 9, BU, base of Utsira Sand, and IH, intra Hordland formation. Dotted lines show location on pre-injection 1994 survey where the difference in 2008 reflects 'push down' due to low velocity CO₂ in the reservoir. B) Plan form seismic amplitude maps of the lower and middle CO₂ layers from the 1999–2008 seismic surveys showing i) initial growth and then shrinkage of the lower layer due to filling of the upper layers and ii) sustained growth of the middle layer with plan form moderated by asymmetric buoyant flow of the CO₂ and topographic filling. Redrawn after Boait et al. (2012).

the brine–CO₂ interface and mobility of dense CO₂-saturated brines is critical to predict the subsequent rates of fluid–fluid and fluid–mineral reactions that determine the long-term fate of the CO₂.

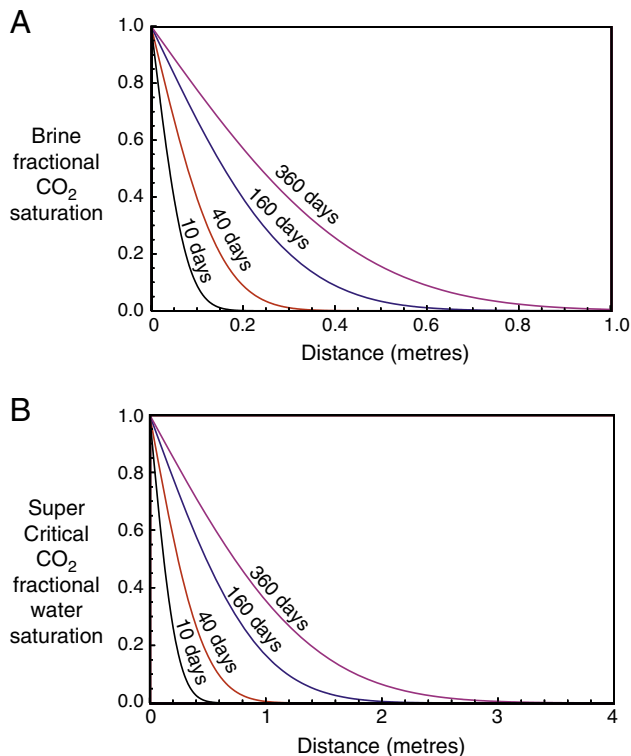
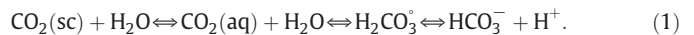


Fig. 5. Diffusion of A) CO₂ into brine and B) H₂O into CO₂ calculated as a function of time for diffusivities of $2 \times 10^{-9} \text{ m}^2 \text{ s}^{-1}$ and $2 \times 10^{-8} \text{ m}^2 \text{ s}^{-1}$ given as fraction of CO₂ and H₂O concentration at saturation. This calculation ignores the tortuosity of pore structure which might retard the diffusion distance by ~30% of the linear calculation.

2.2. Controls on fluid–fluid and fluid–rock reactions

2.2.1. CO₂–brine phase relationships

CO₂ will be injected in a supercritical state to minimise storage volume. The critical point of CO₂ is at 7.4 MPa and 31 °C and injection at depths below ~800 m will maintain this phase stability. Suitable storage sites may occupy reservoirs significantly beneath this depth, creating a diverse range of pressure and temperature conditions suitable for CO₂ storage. The solubility of the injected CO₂ in the formation brine depends on the temperature, pressure and fluid salinity (Fig. 6, Dubacq et al., 2013) and the competing effects of pressure with temperature and salinity lead to solubility maxima for CO₂ at depths of between 0.7 and 1 km for typical geothermal gradients, pore fluid pressures and basin scale pore salinity profiles (Fig. 7). The dissolution of supercritical CO₂, and its subsequent speciation, occurs via a series of pressure and temperature sensitive, linked reversible reactions:



Some fraction of the dissolved CO₂ (~0.3%; Drever, 1982) will hydrate to produce carbonic acid, with a maximum acid dissociation constant at ~55 °C which increases with pressure, and this acidity will promote fluid–rock reaction, leading to the production of bicarbonate ions. The fluid–rock interactions in CO₂ injection sites can be divided into three categories: CO₂–wellbore interactions, CO₂–rock interactions and CO₂–fluid–rock reactions.

2.2.2. CO₂–wellbore interactions

During injection of supercritical CO₂, interactions will occur between the dry CO₂ and materials comprising the wellbore casing and cement, and the rock volume within the near wellbore region. The injected CO₂ will be at surface temperatures and thus cool relative to the surrounding rock volume. Thermal and dehydration effects are predicted to lead to the precipitation of salt from formation brine, within the local pore volume (Zeidouni et al., 2009; Ott et al., 2011), with impacts

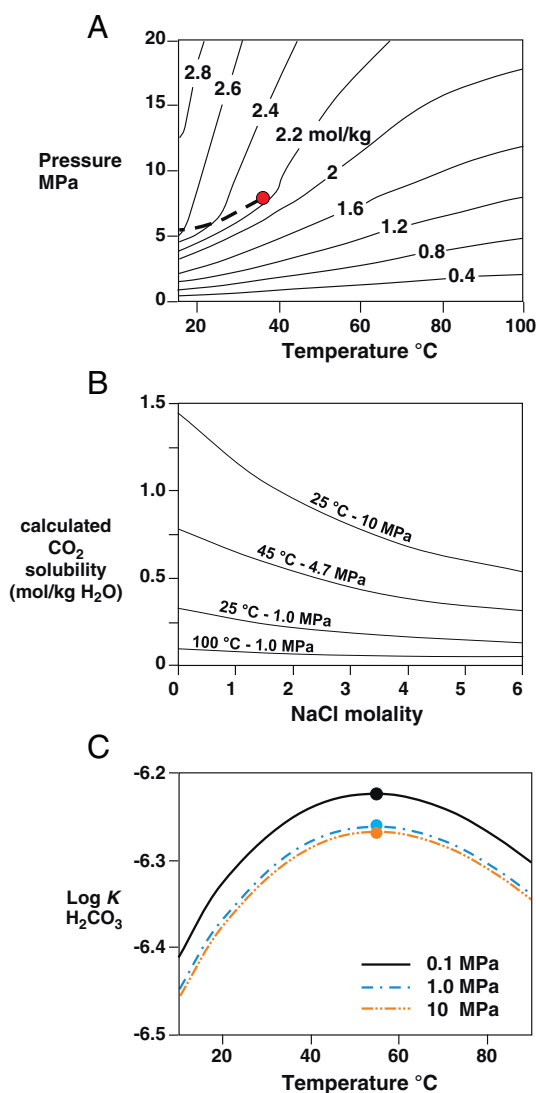


Fig. 6. A) CO₂ solubility in pure water as a function of pressure and temperature, redrawn from Dubacq et al., (2013); B) reduction in CO₂ solubility as a function of increasing fluid salinity, redrawn from Dubacq et al. (2013) and C) temperature dependent dissociation constant for H₂CO₃ showing maxima at ~55 °C and weak dependence on pressure, calculated using SUPCRT92 (Johnson et al., 1992). Above and below ~55 °C the log K decreases such that an initially weak acid becomes increasingly weaker.

for formation permeability (Peysson et al., 2011) and pressure build-up (Pruess and Müller, 2009; Okwen et al., 2011; Kim et al., 2012a). Joule-Thomson expansion of the CO₂ phase as it migrates from the site of injection to shallower depths will lead to cooling of the surrounding fluid and rock volume, which may influence mineral reactivity (Oldenburg, 2007; André et al., 2010; Han et al., 2012). The solubility of water in supercritical CO₂ is relatively limited (between 0.1 and 0.5 wt.%; Spycher et al., 2003; Dubacq et al., 2013) and the zone dried by the CO₂ (which depends on the multiphase flow properties of the reservoir) will occupy only about 5% of the total volume filled by CO₂ and residual water (Spycher and Pruess, 2005). The diffusivity of H₂O in supercritical CO₂ (2×10^{-8} m².s⁻¹ to 2×10^{-7} m².s⁻¹; Espinoza and Santamarina, 2010) is one to two orders of magnitude faster than the diffusivity of CO₂ in water ($\sim 2 \times 10^{-9}$ m².s⁻¹; Mutoru et al., 2010). Thus an initially dry CO₂ plume will hydrate, and the water content will homogenise relatively quickly.

Interaction of the CO₂ stream with wellbore cements is predicted to lead to mineral dissolution (Kutchko et al., 2007) and the development of carbonation fronts coupled to the penetration of CO₂ and porosity development (Corvisier et al., 2010; Gherardi et al., 2012; Huerta et al.,

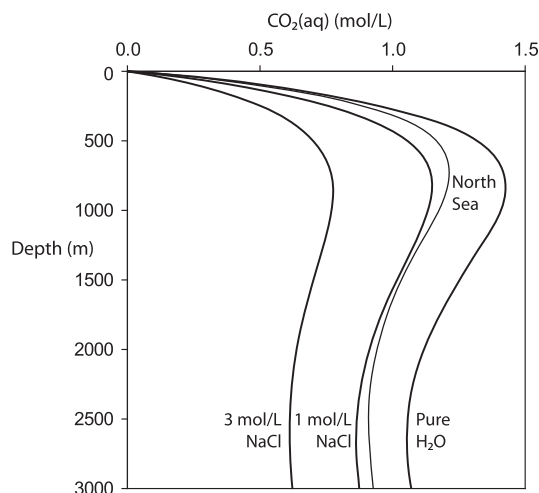


Fig. 7. CO₂ solubility as a function of depth below surface. Solubility profiles calculated using equations from Duan et al. (2006), considering typical geothermal gradients of 25 °C/km and hydrostatic pressure gradients, in pure water and fluid salinities of 1 mol/L and 3 mol/L NaCl. An example for a typical North Sea geothermal gradient of 25 °C/km and pore salinity profile of 25,000 ppm/km (Bjørlykke and Gran, 1994) is also shown.

2012; Jacquemet et al., 2012; Rochelle and Milodowski, 2012). Such reaction fronts may lead to the development of fluid pathways that would allow CO₂ or CO₂-charged fluid to escape into overlying formations or to the surface (Tao et al., 2011), but the development of armouring carbonate mineral coatings may limit the extent of reaction and these pathways may ultimately self-seal through mineral precipitation (Carroll et al., 2011; Huerta et al., 2012). Observations from field studies suggest the interfaces between cement, casing and the surround rock volume are likely to represent sites for focused fluid movement and reaction (Carey et al., 2007), and critical sites for potential CO₂ leakage (Dusseault et al., 2000; Deremble et al., 2011).

2.2.3. Supercritical CO₂-rock reactions

The reactions between supercritical CO₂ and minerals in the reservoir have not been studied extensively. Dry CO₂ may dehydrate hydrous minerals but as the solubility of water in CO₂ is limited, CO₂ penetrating reservoirs or caprocks will rapidly become water saturated. Laboratory experimental studies have documented the mobilisation of trace metals by dry supercritical CO₂ (Rempel et al., 2011), the relatively rapid carbonation of silicate minerals by water-bearing supercritical CO₂ (McGrail et al., 2009; Loring et al., 2012; Schaefer et al., 2013) and some carbonation by dry CO₂ (Regnault et al., 2009), but the mechanisms and rates of these reactions are not well known (e.g. Lin et al., 2008; Lea et al., 2011). The partitioning experiments of Rempel et al. (2011) demonstrate trace element solubility in supercritical CO₂ of up to 0.6 ppm for Fe and 39 ppm for Na, providing an initial evaluation of mineral solubility in supercritical CO₂, although much more data is needed. Interaction of CO₂ with mineral surfaces may also cause dewetting which will reduce capillary entry pressure, alter quantities of residually trapped CO₂ and relative permeability, and enhance CO₂ penetration into low permeability rock (Kim et al., 2012b).

Mineral-fluid reactions involving supercritical CO₂ are still poorly understood and should form a concerted focus of research. Much experimental work is still needed to evaluate the reactivity of hydrated supercritical CO₂, and its impacts on the transport properties of reservoirs and caprocks. Specifically the long-term impacts of supercritical CO₂ on reservoir caprocks are of concern and scientific drilling of deep natural CO₂ reservoirs would provide invaluable information to test these impacts.

2.2.4. CO₂-fluid-rock reactions

Most interest centres on the rates of CO₂ dissolution in formation brines and the nature and rates of reaction of the acid CO₂-saturated

brines with reservoir and caprock minerals. Acidity produced during the dissolution of CO₂ will promote mineral dissolution reactions and desorption of exchangeable or mineral surface bound ions that will modify the reservoir fluid chemistry.

Modelling (Knauss et al., 2005; Xu et al., 2007) and field observations (Kharaka et al., 2006a; Kampman et al., 2009) suggest that CO₂-charged brines flowing through a reservoir rapidly dissolve and become saturated in carbonate and Fe-oxyhydroxide minerals near their source, followed by more sluggish reactions with silicate and phyllosilicate minerals that further raise the pH and cause precipitation of clays and carbonates in the more distal regions (Fig. 8). A similar set of chemical reactions is predicted for caprocks, that is initial dissolution of carbonate followed by precipitation of carbonate driven by the pH increase consequent on the more sluggish reactions with phyllosilicate minerals (Gaus et al., 2005) (Fig. 9). In general transport of CO₂ into caprocks will be by diffusion as rates of advective transport drop below diffusion rates at low permeabilities ($<10^{-14}$ m²) even if the capillary entry pressures do not exclude the CO₂ phase.

Several aspects of modelling these fluid–mineral reactions are problematic. 1) The impact of injected CO₂ on the host rock may be moderated by mineral dissolution and/or precipitation. The reactions are kinetically limited and experimental data on mineral dissolution rate constants for crucial endmember mineral phases, and in complex solid-solutions, over a wide range of pressures, temperatures and fluid compositions are generally lacking. 2) The equilibrium thermodynamics of the mineral–fluid reactions may be uncertain, especially in high ionic strength brines and where experimental equilibrium constants are lacking. 3) The reaction paths may involve metastable reaction products which are not accounted for by equilibrium thermodynamic models. 4) The controls on fluid–mineral reaction kinetics are complex, with rates measured in field sites frequently orders-of-magnitude slower than far-from-equilibrium laboratory-derived rates (White and Brantley, 2003) and the rate limiting steps may be either mineral surface dissolution, secondary mineral precipitation, CO₂ dissolution and diffusion or fluid transport. 5) The relative flows of CO₂ and brine are governed by the complexities arising from two-phase flow and the intrinsic heterogeneities in geological reservoirs. The nature of these flows governs the dissolution of CO₂ into the brines, and the subsequent geochemical evolution of the brines is controlled by the coupling of

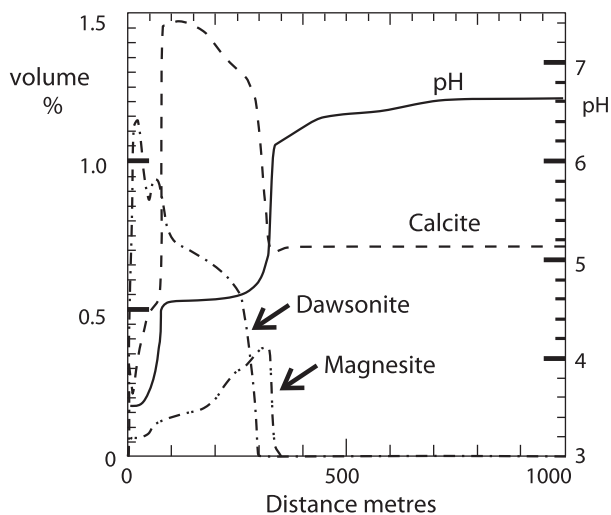


Fig. 8. Modelled mineral abundances as a function of distance along a radial flow path away from an injector of brine in equilibrium with 8.4 MPa CO₂ into an arkosic sandstone. Note that close to the injector the acid fluids (pH ~3.5) dissolve calcite but that further out more evolved fluids have reacted with silicate minerals which increases their pH to ~4.5 and causes precipitation of carbonate. Modelled precipitation of dawsonite, the carbonate NaAlCO₃(OH)₂, is uncertain because dawsonite is rare in nature and its equilibrium thermodynamics and precipitation rate constants are uncertain. Redrawn after Knauss et al., (2005).

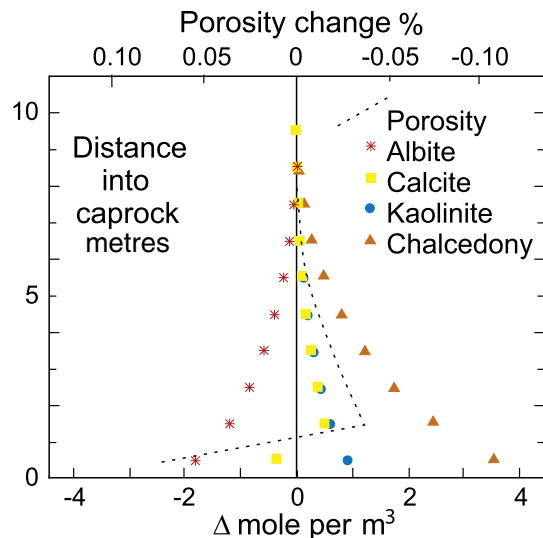


Fig. 9. Alteration at the base of caprock by supercritical CO₂, calculated from reactive transport modelling (redrawn after Gaus et al., 2005). Changes in mineral modes reflect dissolution of albite and precipitation of kaolinite and chalcedony throughout the profile, and dissolution of calcite at the base of the profile but precipitation greater than ~1 m above the base. Note the net decrease in porosity except at the very base of the profile. Redrawn after Gaus et al. (2005).

CO₂ diffusion and fluid–rock reactions. Most reactive-flow modelling experiments have modelled flow of an initially CO₂-saturated brine in one or two dimension with grid sizes that are typically larger than the length-scales of geological heterogeneities, and have simplified or ignored two-phase flow phenomena and the potential for additional inputs of CO₂ along the flow path (Knauss et al., 2005; Xu et al., 2005; Audigane et al., 2007). Modelling the kinetics of fluid–mineral reactions in the context of CO₂ storage is reviewed in Hellevang et al. (2013). Such simplifications of the modelling efforts are necessary for the treatment of these computationally intensive processes but without capturing the underlying physics of flow, geochemical model predictions are undermined.

2.2.4.1. Laboratory versus field-scale reaction rates. In natural CO₂ reservoirs, the rates of the silicate dissolution reactions (e.g. feldspars), that may ultimately promote CO₂ trapping or leakage, have been shown to differ by several orders of magnitude (10^2 to 10^5) from those rates determined experimentally (Kampman et al., 2009). Growing evidence suggests that the apparent rate discrepancy between laboratory and field-scale rates may be due to the decrease in mineral dissolution rates near equilibrium (Kampman et al., 2009; Maher et al., 2009), with consequent transport-control of reaction rates (White et al., 2009; Maher, 2010).

Laboratory studies on quartz (Berger et al., 1994), feldspars (e.g. Burch et al., 1993; Schott and Oelkers, 1995; Taylor et al., 2000; Beig and Lüttge, 2006; Hellmann and Tisserand, 2006) and phyllosilicate minerals (Nagy et al., 1991; Cama et al., 2000) confirm theoretical predictions (e.g. Lasaga, 1984) that dissolution rates are independent of saturation state far from equilibrium (but see Oelkers et al., 1994) and decrease in a transition region as equilibrium is approached, with a critical step in the dependence close to equilibrium as the mechanism of dissolution changes (see Hellmann and Tisserand, 2006; Arvidson and Luttge, 2010). In addition, the dissolution rates of many important rock forming silicate minerals (e.g. feldspars) are highly sensitive to processes occurring at or close to the dissolving mineral surface including; the rate of secondary mineral precipitation (Maher et al., 2009; Moore et al., 2012); interfacial dissolution–reprecipitation phenomena (see Hellmann et al., 2012 and references therein), such as the development of silica surface layers (Amrhein and Suarez, 1992; Hellmann et al., 2003, 2012) and the carbonation of mineral surfaces (Béarat et al., 2006; Daval

et al., 2009), which may be passivating (e.g. Daval et al., 2011, 2013); and the slow transport of insoluble metal species e.g. Al^{3+} (e.g. Muir and Nesbitt, 1991). Silicate mineral dissolution rates are further influenced by properties of the bulk solution including concentrations of carbonate ions (e.g. Berg and Banwart, 2000), organic acids (e.g. Drever and Stillings, 1997) and ligands (e.g. Blake and Walter, 1999). In addition the $\text{CO}_2(\text{aq})$ ion itself may have an impact on the rates and mechanism of dissolution, not least through its impacts on surface charge and complexation, although such processes are not yet well understood (Carroll and Knauss, 2005; Hünchen et al., 2006; Hellmann et al., 2010). The role of mineral-surface processes during mineral dissolution is reviewed in Brown and Calas (2012). This myriad of complications is generally not treated in most reactive transport models, and further attempts to integrate such processes into modelling studies are needed.

In CO_2 reservoirs the nature of silicate mineral–fluid reactions is likely to range from surface-reaction controlled where brines are far-from-equilibrium with minerals and not limited by the supply of acidity, to transport-controlled where rates depend on the input of acidity close-to-equilibrium. Indeed where reactions take place close-to-equilibrium, reaction rates will adjust to balance the surface reaction-rate against transport controls. Conversely, the dissolution of carbonate, oxide and oxyhydroxide minerals with rapid kinetics is likely to be transport controlled by propagation of the dissolved CO_2 and acidity front moving ahead of the injected CO_2 plume.

This variability in the controls on natural reaction rates creates substantial complexities for the modelling of brine-mineral reactions during CO_2 injection. Kinetically slow silicate and phyllosilicate mineral dissolution reactions are likely to preside over the long-term fate of the CO_2 and the rate of these reactions will depend on the state of fluid-mineral thermodynamic disequilibrium, itself controlled by reaction progress, diffusion of CO_2 into the brine phase and transport of the brine (Wigley et al., 2013a). In the far-from-equilibrium conditions of dilute acidic CO_2 -rich solutions, feldspar dissolution rates are rapid enough to cause significant porosity increases over short time-scales (see for example Sorai et al., 2005), with consequent impacts for permeability in sandstones, which have extreme porosity–permeability relationships (e.g. Nelson, 1994). However, as reaction progress drives changes in solution composition and equilibrium is approached, pores may become clogged by clay and carbonate deposition (e.g. Bertier et al., 2006), most extremely illustrated by experiments on peridotite (e.g. Hövelmann et al., 2012). In natural systems the approach to equilibrium is complicated by the presence of multiple mineral phases which react and buffer solution chemistry at different rates, most notably soluble carbonates, sulphates, sulphides and oxides which rapidly consume acidity and the much slower reaction rates of most silicate minerals. On the short-term, the dissolution of soluble minerals may be transport-controlled following complete consumption of the reactant, or attainment of fluid–mineral equilibrium, over the length scale under consideration, such that aqueous transport is the rate-limiting factor. If the system is transport-controlled, kinetic rate constants and mineral surface areas determine the geometry of the reaction front, but these parameters do not have a substantial influence on the propagation of the reaction front or the net transformation rate. However, factors that affect thermodynamic departure from equilibrium of the dissolving phase(s), such as the rates of CO_2 dissolution, pH buffering, secondary mineral precipitation reactions, and the evolution of porosity/permeability and fluid flow rate will determine the rate at which reaction fronts propagate.

2.2.4.2. Secondary mineral precipitation. The subsequent growth of clay and carbonate phases within the reservoir will be controlled by these reactive fluid transport processes, buffering of fluid pH and the availability of metal cations from the slow dissolution of silicate minerals which, in the long-term, is likely to form a rate limiting step. Several authors have emphasised that clay mineral precipitation rates can also be important in controlling silicate mineral dissolution rates

(e.g., Maher et al., 2009; Zhu and Lu, 2013). Growth of clay and carbonate minerals may be linked to the availability of nucleation sites and precursor seed phases, which may exert a control on the stable growing phase, its growth rate and mechanism (e.g. Fernandez-Martinez et al., 2013; Fritz et al., 2013).

The acid hydrolysis of silicate minerals in natural fluids is largely incongruent being balanced by the precipitation of clay minerals, typified by kaolinite (Maher et al., 2009). The low solubilities of Al^{3+} and $\text{SiO}_2(\text{aq})$ at the temperatures and pressure conditions relevant to CO_2 storage preclude significant mass transport of these constituents from the surface of the dissolving silicate mineral. Since Al solubility is very small, clay mineral precipitation rates must essentially balance feldspar dissolution rates. Observations from natural CO_2 reservoirs (Kampman et al., 2009) suggest the thermodynamic undersaturation of the silicate minerals is balanced by the thermodynamic overstep in clay mineral saturation and that clay mineral precipitation rates vary with, and as consequence of, silicate mineral dissolution rates (Bickle et al., 2013).

The chemistry and mineralogy of the clay mineral precipitates is highly sensitive to temperature, fluid pH and solute activities. Experimental and model predictions include the growth of illite, illite–smectite, smectite, kaolinite and Al-hydroxide minerals (e.g. Creodoz et al., 2009; Kohler et al., 2009; Munz et al., 2012). Neutral $\text{SiO}_2(\text{aq})$ concentrations are likely to be dependent on the supply from feldspar dissolution only on short times-scales as silica mineral solubilities are independent of pH, and natural fluids already contain (equilibrium) concentrations of dissolved silica. Observations from natural CO_2 reservoirs (Kampman et al., 2009) and produced fluids from oil-fields (Houston et al., 2007) suggest that silica concentrations can be rapidly buffered by reaction with silica phases such as quartz and chalcedony, with the equilibrium concentrations being highly dependent on temperature and the time taken to return to equilibrium concentrations being dependent on the kinetics of the buffering reactions.

The growth of carbonate minerals in CO_2 -brine-rock systems has been observed in a large number of experiments, including the carbonation of silicate mineral surfaces at high temperature (e.g. Munz et al., 2012). The stable growing phase(s) vary widely, being governed by the thermodynamic considerations of pressure, temperature and solute chemistry and by the activities of constituent species in the fluid phase. The mineralogy of carbonate cements formed in natural CO_2 reservoirs provides an indication of the phases that may be stable in CO_2 storage sites (see the review in Section 5.2) and this varies from the relatively soluble pure calcite end-member to more insoluble Fe–Mg–Ca carbonate minerals, including dolomite ($\text{CaMg}(\text{CO}_3)_2$), ankerite ($\text{Ca}(\text{Fe},\text{Mg},\text{Mn})(\text{CO}_3)_2$) and siderite (FeCO_3). Calcite cements typically precipitate in natural CO_2 -reservoir sandstones poor in detrital Fe- and Mn-bearing minerals, or from fluids with high oxygen fugacities. In Fe-rich sediments, such as in red-bed aeolian sandstones, in contact with reducing formation fluids, the high activities of Fe^{2+} and Mn^{2+} in solution can lead to the formation of siderite and in the presence of Mg^{2+} rich fluids, ankerite and/or Fe-bearing dolomite. Predicting the stable carbonate phase in CO_2 reservoirs is frustrated by the limited experimental data on the thermodynamic stability, nucleation, growth and kinetics of the more complex Ca–Mg–Fe carbonate minerals, and such data is necessary for accurate model predictions. Recent modelling studies predict the growth of dolomite, in CO_2 reservoirs at low temperature (37 °C), which would not be predicated from classic nucleation theory (Hellevang et al., 2013). Such predictions are supported by observations from natural CO_2 reservoirs where dolomite is often the stable carbonate phase. Clearly an improved understanding of carbonate nucleation and growth is required to predict the long-term mineralisation of CO_2 in storage reservoirs.

Ultimately a significant source of uncertainty in interpreting or predicting the various fluid–mineral reactions in injection experiments or natural systems is accurate assessment of the evolution of dissolved CO_2 and in-situ pH, crucial in determining the thermodynamic state of

fluid–mineral disequilibrium, secondary mineral saturation and the rates of the controlling fluid–mineral reactions.

3. CO₂–fluid–rock interactions in CO₂ injection experiments

3.1. CO₂ injection experiments and CO₂-EOR projects

Given the complex reservoir structures, flow paths and controls on reactive-transport processes involved, the progress of CO₂ dissolution in brines and fluid–rock reactions can be best studied by direct sampling of anthropogenic CO₂ injection projects or natural CO₂ accumulations. Anthropogenic CO₂ injection experiments which have attempted this are listed in Table 1. Fluid sampling in these projects was conducted over a period of a few days to several months, typically from single observation wells, using in-situ sampling methods (see below). The Frio-I (Hovorka et al., 2006; Kharaka et al., 2006a) and Frio-II (Daley et al., 2007a,b) Brine Pilot injection experiments are notable for the high temporal resolution of the sampling and quality of the resulting analyses. However the lack of spatially distributed sample points, the proximity of the injection and sampling well, and the averaging of fluid samples over significant vertical intervals in the reservoirs complicates the analysis of geochemical processes, given the expected decimetric-scale variability of flows of the CO₂ and brine.

CO₂ injection for enhanced oil recovery (CO₂-EOR) projects provides an additional source of fluid samples relevant to subsurface CO₂ injection (Table 2). These projects are reviewed in Alvarado and Manrique (2010). These CO₂-EOR projects provide a high spatial density of sampling due to the presence of multiple production and monitoring wells and allow mapping spatial changes in solute chemistry related to flow and dissolution of the CO₂ and the CO₂-induced fluid–rock reactions over periods of months to years. However, interpreting the results from CO₂-EOR projects is complicated by the complex fluid injection history of old oil fields, the complex dynamic pressure and flow fields resulting from the interactions of numerous injection and production wells and the presence of an oil phase.

Geochemical sampling of the injection experiments has the potential to provide key information that supplements, or is not available from, other monitoring techniques:

- The amount of CO₂ dissolved in sampled brine;
- The time CO₂ arrives at the sample well;
- The progress of fluid–mineral dissolution or precipitation reactions;
- A constraint on the heterogeneity of flow paths;

- The CO₂ saturation in the reservoir interval sampled;
- The amount of CO₂ retained by capillary trapping.

Remote and downhole geophysical monitoring may be able to map the location of the supercritical CO₂ plume and measure CO₂ saturation but has neither the resolution to map heterogeneities of CO₂ and brine flow on the ~30 cm scale critical to CO₂–brine interactions, nor the ability to measure the amount of CO₂ dissolved in the brine.

The magnitude of CO₂ dissolution in brine may be monitored from analysis of dissolved CO₂ concentrations at in-situ pressures and temperatures or estimated from analyses of oxygen isotopic compositions that reflect isotope exchange between the injected CO₂ and formation water. These measurements will also reveal the timing of CO₂ arrival at the sample well. The changes in brine chemistry and isotopic compositions provide a monitor of the progress of the mineral dissolution and precipitation reactions. Injection and analysis of inert (e.g. SF₆), reactive (e.g. esters), and noble gas isotopic (e.g. ³He/⁴He, ¹²⁹Xe) tracers can provide important additional information on CO₂–brine interactions including estimates of field-scale capillary trapping (Zhang et al., 2011; Zhou et al., 2011; Myers et al., 2012). Perhaps the most critical information from geochemical sampling is the magnitude and impact of the small-scale heterogeneities that control the flow paths of CO₂ and brine and dissolution of CO₂ in brine. Pore-space CO₂ saturation may be estimated by direct measurement of CO₂ and brine volumes at surface or from the density of the brine-CO₂ mixture measured in-situ. However, measurements of the relative volumes of CO₂ and brine which flow into the sampling well may over-estimate the CO₂ fraction due to the contrast in viscosity and flow rate of the two phases.

Measurements of in-situ dissolved CO₂ concentrations and pH are crucial to quantify the progress of these trapping mechanisms. However, such measurements are not easily achieved because of the rapid degassing of CO₂-rich fluids at surface pressures. Accurate determination of dissolved CO₂ concentrations and pH requires specialist downhole equipment that allows either in-situ determination or the recovery and containment of fluid samples at reservoir pressure, on which measurements can be made at surface.

3.2. Sampling CO₂ injection experiments

A range of specialist downhole sampling tools have been devised to sample reservoir fluids, including commercially available wireline samplers (Kuster Flow Through Sampler[®], Leuter Bottom Hole Positive Displacement Sampler[®] and Cased Hole Dynamics Tester[®]), experimental

Table 1
CO₂-injection experiments.

Project name	Frio-I brine pilot experiment	Frio-II brine pilot experiment	Ketzin CO ₂ SINK project	CO ₂ CRC Otway project	Nagaoka injection project
Location	Texas, USA	Texas, USA	Ketzin, Germany	Otway, Australia	Nagaoka, Japan
Start date	Oct. 2004	Sept. 2006	June 2008	April 2008	July 2003
Injection duration	11 days	4 days	2 years	17 months	18 months
CO ₂ injected (tonnes)	1600	360	60,000	65,000 (CO ₂ -CH ₄)	10,400
Reservoir formation	Upper Frio Formation	Lower Frio Formation	Stuttgart		
Facies	Waarre C Sandstone	Haizume			
Lithology	Fluvial	Fluvial	Fluvial	Shoreface	Shlw. Marine
Arenite	Feldspathic litharenites	Feldspathic litharenites	Feldspathic litharenites	Quartz	
Porosity (%)	Argillaceous sandstones				
Permeability (D)	32	34	23	15	22.5
Depth (m)	2–3	3–4	0.5–1	0.01–1	0.01–0.03
Temperature (°C)	1500	1650	650	2000	1100
Pressure (bar)	50	55	36	85	48
Fluid type	150	165	70–80	180–190	110
Salinity (mol/L NaCl)	Na–Ca–Cl	Na–Ca–Cl	Na–Ca–Cl	Na–Cl	Na–Br
Hydrocarbons	1.35	1.60	3.90	0.1	0.3
References	CH ₄ gas			CH ₄ gas	
	Doughty et al. (2008), Kharaka et al. (2006a)	Daley et al. (2007a)	Förster et al. (2006), Giese et al. (2009), Schilling et al. (2009)	Boreham et al. (2011), Freifeld (2009), Underschlutz et al. (2011)	Kikuta et al. (2005), Mito et al. (2008)

Table 2
CO₂-EOR projects.

Project name	Pembina-Cardium CO ₂ -EOR pilot	Weyburn-Midale CO ₂ -EOR project	Salt Creek CO ₂ -EOR project	SECARB Cranfield project
Location	Alberta, Canada	Saskatchewan, Canada	Wyoming, USA	Mississippi, USA
Start date	March 2005	September 2000	January 2004	July 2008
Injection duration	3–5 years	25–30 years	25–30 years	1.5 years
CO ₂ Injected (tonnes)	79 tonnes/day	~5000 tonnes/day	~7500 tonnes/day	2,100,000
Reservoir formation	Upper Cretaceous Cardium Formation	Mississippian Charles Formation.	Late Cretaceous Frontier Formation	Tuscaloosa Formation
Facies	Shallow marine	Shallow marine	Shoreface	Fluvial
Lithology	Subarkose	Carbonates and evaporites	Arkose	Quartzite
Porosity (%)	15	14	16	25
Permeability (Darcys)	0.01–0.03	0.1–1	0.01–0.2	0.1
Depth (m)	1650	1300–1500	750	3000
Temperature (°C)	50	62	35	125
Pressure (bar)	190	150	80	320
Fluid type	Na–Cl	Na–K–Cl	Na–Cl	Na–Ca–Cl
Salinity (mol/L NaCl)	0.1	1.3	0.1	2.00
Hydrocarbons	Oil	Oil	Oil	Oil
References	Dashtgard et al. (2008), Lawton (2009), Shevalier et al. (2009)	Emberley et al. (2004, 2005), Quattrocchi et al. (2006), White and Johnson (2009), Whittaker et al. (2011)	Kampman et al. (2011)	Hovorka et al. (2011), Lu et al. (2012)

piston samplers (Alfredsson et al., 2011), the U-tube in-situ sampling lines for wellbore fluids (Freifeld et al., 2005) and passive samplers of dissolved gases (Zimmer et al., 2011).

The U-tube in-situ multiphase fluid samplers comprise a stainless steel sampling U-tube, with check valve fluid entry ports, and two stainless steel lines that run to surface, through which pressurised nitrogen can be pumped to drive the sample to the surface at pressure. The U-tube sampling line can also be combined with inline pH sensors for determination of downhole fluid pH (Daley et al., 2007a), from which dissolved CO₂ concentrations can be estimated, where measurements of fluid alkalinity are available. A newly developed variant of the U-tube sampler has been developed and trialled at the Ketzin injection experiment (Zimmer et al., 2011). This Gas Membrane Sensor utilises phase separating membranes mounted in a perforated protective stainless steel housing to passively separate dissolved gas from the contacting reservoir fluid, which is then driven to surface by pressurised argon pumped through stainless steel capillaries (Zimmer et al., 2011).

U-tube sampling lines are frequently integrated with other monitoring tools including geophones and distributed temperature, pressure and fluid density sensors (Freifeld et al., 2005, 2008; Giese et al., 2009) and connected to portable quadrupole mass spectrometers for real time gas composition analysis (Freifeld and Trautz, 2006; Zimmer et al., 2011). Such in-situ sampling lines provide a convenient and low cost method for repeatedly sampling two-phase formation fluid in on-going injection experiments. However, the sampling methods and surface sample processing employed to-date do not allow direct determination of dissolved CO₂ concentrations. Such in-situ sampling methods are also prone to corrosion of the sampling lines and housing by reactive CO₂-rich fluids (Daley et al., 2007a; Zimmer et al., 2011).

To date there are no published analyses of dissolved CO₂ concentrations in CO₂ reservoirs sampled using wireline, although they have been widely used by the oil and gas industries to sample hydrocarbon reservoirs. Kampman et al., 2013-in this issue—a,b show how reservoir pH and dissolved CO₂ concentrations can be determined at surface on pressurised fluids sampled by wireline, using high pressure pH probes and by the addition of an excess of base to convert dissolved CO₂ to CO₃²⁻, whose concentration can then be measured by titration.

3.3. Monitoring of CO₂ dissolution and CO₂ saturation

Dissolved CO₂ concentrations in brines may be measured directly in samples recovered at formation conditions as discussed above or estimated from partition of conservative tracer concentrations or isotopic ratios. CO₂ saturation may be measured directly in the vicinity of observation wells by several geophysical techniques; neutron capture, resistivity and distributed thermal perturbation sensors (Freifeld et al.,

2009). Attempts have also been made to infer CO₂ saturation and residual trapping from geochemical measurements but interpretation of these is complex as discussed below.

3.3.1. Direct measurements of dissolved CO₂ and CO₂ saturation

Direct observations of the progress of CO₂ dissolution during CO₂ injection are limited because of the complexities associated with in-situ measurements or the recovery of reservoir fluids with high dissolved gas loads. The U-tube sampler is capable of returning fluids to surface without decompression. In the Frio II experiment, combined measurements of pH at formation pressure and alkalinity allowed brine CO₂ concentrations to be reconstructed (Daley et al., 2007a). In the Ketzin CO₂ injection experiment, Zimmer et al. (2011) obtained in-situ dissolved CO₂ concentrations from measurements made using downhole gas membrane sensors installed at ~150 m within two ~750 m deep observation wells, sited ~50 and ~100 m up-dip from the injection well. CO₂ breakthrough at the proximal observation well was observed after sixteen days and the breakthrough of the CO₂ phase was accompanied by reservoir fluids with measured dissolved CO₂ concentrations at saturation (0.63 mol/L using the gas membrane sensors and 0.65 mol/L using a wireline downhole fluid sampler, slightly above the expected CO₂ solubility of ~0.52 mol/L at reservoir temperature, pressure and salinity) suggesting that reservoir fluids in contact with the propagating CO₂ plume quickly saturate.

3.3.2. Indirect estimation of dissolved CO₂ concentrations and CO₂-gas saturation

The degree of CO₂-saturation in under-saturated brines has been estimated by using the concentrations or isotopic compositions of conservative tracers for which the relative exchange rates between CO₂ and brine are known. Once the supercritical CO₂ plume extends to the sample well, both CO₂ and CO₂ saturated brine are sampled. The relative fractions of CO₂ and brine can be estimated from the partition of tracer concentrations or isotopic ratios between the CO₂ and brine.

The most effective conservative tracers of CO₂-brine interactions are likely to be the 5 stable noble gases which have 22 isotopes between them (Nimz and Hudson, 2005; Zhang et al., 2011; Holland and Gilfillan, 2012). To date most indirect estimates of CO₂ saturation have exploited the marked difference between the oxygen isotopic composition of the injected CO₂ and formation brines in for example the Frio-I and Pembina injection experiments (Kharaka et al., 2006a; Johnson et al., 2011a).

For the Frio-I experiment (Fig. 10) Kharaka et al. (2006a) used a simple mass-balance calculation, constrained by measurements of the oxygen-isotope exchange between the injected CO₂ and formation brine, to calculate residual CO₂ saturation in the reservoir interval

sampling as [Friedfield et al. \(2005\)](#) infer, these compositions might be preserved. Whether the oxygen-isotopic compositions of either the brine or CO₂ are modified by exchange before the CO₂ enters the sampled pore space will depend on the time-scales and flow paths. The samples taken at Frio-I within a few days of injection had limited time for exchange and it is likely that the CO₂ was little modified in composition. Monitoring of arrival times of CO₂ and injected tracer gases (PFT's, SF₆, Xe and Kr) over the few days of CO₂ injection showed that the more soluble Kr was retarded compared with the other tracers ([Freifeld et al., 2005](#)) but given the likely solubility of Kr (inferred from the air–water Henry's law constant; [Wilhelm et al., 1977](#)), average Kr concentrations were only ~3% of saturation implying limited CO₂–brine diffusive exchange. The samples taken 5 months later may have had a more complex history.

Measurements of the sampled fluid density in the U-tube give a ratio of CO₂ to brine >80% after CO₂ breakthrough which [Friedfield et al. \(2005\)](#) and [Hovorka et al. \(2006\)](#) ascribe to the higher mobility (lower viscosity) of CO₂ than brine. The similarly high values of CO₂ saturation calculated from the oxygen-isotope shifts ([Fig. 12](#)) are probably the result of diffusive exchange before or during sampling and not accounted for in the modelling.

[Johnson et al. \(2011a\)](#) calculate CO₂ dissolution and CO₂ saturation in the Pembina EOR injection experiment from shifts in the oxygen isotopic compositions of the produced brines. They model the shift in the oxygen isotopic composition of brine with a mass balance equation that assumes that the δ¹⁸O of the CO₂ remains constant and that oxygen isotopic shifts of the brine result from addition of dissolved CO₂ to the brine. The mass balance equation which relates the final oxygen isotopic composition of the brine (δ¹⁸O_{H₂O}^f) to the initial oxygen isotopic composition of the brine (δ¹⁸O_{H₂O}ⁱ), the oxygen isotopic composition of

the CO₂ (δ¹⁸O_{CO₂}), and the fraction of O in the system sourced from CO₂ (X_{CO₂}⁰), ([Johnson et al., 2011a](#), Eq. (4)) is

$$\delta^{18}\text{O}_{\text{H}_2\text{O}}^f = \delta^{18}\text{O}_{\text{H}_2\text{O}}^i(1 - X_{\text{CO}_2}^0) + X_{\text{CO}_2}^0(\delta^{18}\text{O}_{\text{CO}_2} - \varepsilon) \quad (2)$$

where ε is the CO₂(g)–H₂O fractionation factor ([Bottinga and Craig, 1968](#)); 35‰ at Pembina reservoir conditions). The Pembina brine saturates with 1.3 mol/L CO₂ that would shift the δ¹⁸O of the brine only 0.4‰. The observed isotopic shifts at Pembina (up to 4‰) are much in excess of the expected shift due to oxygen transported by the CO₂ needed to saturate the brine and this must reflect diffusional exchange between the brine and CO₂. Eq. (1) does not model this and also doesn't allow for the corresponding changes in the δ¹⁸O_{CO₂}. [Fig. 11](#) illustrates the more complex reality where exchange of oxygen isotopes is controlled primarily by diffusion in the brine phase of the oxygen isotope signal carried by H₂O that has exchanged with CO₂ with or at the plume interface.

The Frio and Pembina experiments demonstrate the fundamental problems of estimating CO₂ saturation. The large mobility difference between CO₂ and brine biases direct sampling, and geochemical measurements average over a range of saturations and are influenced by CO₂–brine interactions along the flow path to the sample site and at the sample site.

3.3.3. Fluid–rock interactions inferred from CO₂ injection experiments

Injection experiments provide real-time constraints on the rate of fluid–mineral reactions. Perhaps the most important observation from all the injection experiments is the rapidity with which the brines saturate with CO₂ and then with exchangeable ions and carbonate and

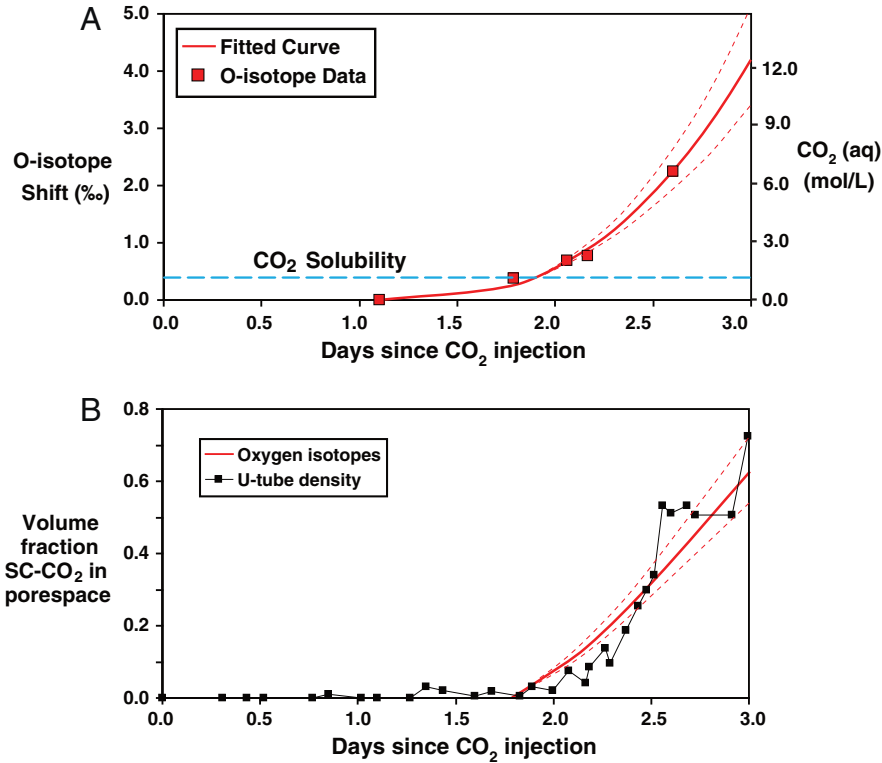


Fig. 12. O-isotope shifts in produced water from the Frio-I Brine Pilot injection experiment ([Kharaka et al., 2006a](#)). A) Best fit line to shifts in O-isotopic composition (left-hand axis) of sampled brine (red squares). O-isotopic exchange between CO₂ and brine rapidly modifies the isotopic composition of the brine. In-situ dissolved CO₂ concentrations (right-hand axis) were calculated from the O-isotopic composition of H₂O using equations of [Johnson et al. \(2011a\)](#). B) Fraction of CO₂ occupying the total pore volume at the observation well as determined by fluid density changes sampled by the U-tube sampler, compared to estimates from the O-isotope shift in [Fig. 11A](#) ([Hovorka et al., 2006](#)). Note that the U-tube sampler preferentially samples CO₂ (geophysical RST measurements indicate only 20 to 30% saturation and a flow model based on arrival times ~16%) and the correspondence between the estimates from oxygen isotopes and the U-tube densities probably reflects diffusive exchange in the reservoir or during sampling.

Fe-oxyhydroxide minerals. The Frio brine pilot injection experiments employed the most detailed fluid sampling programs published to date (Hovorka et al., 2006; Kharaka et al., 2006a,b, 2009) (Figs. 10, 13).

At Frio-I the arrival of the supercritical CO₂ plume at the observation well at 52 h is tracked primarily by the step change in fluid composition in the U-tube samples (Fig. 13A) as well as injected PFT tracers (Freifeld et al., 2005). Small changes in fluid density and gas phase composition ~31 h after the start of injection accompanied by shifts in the O-isotopic composition of the produced fluid are interpreted to reflect arrival of thin CO₂ fingers ahead of the main CO₂ plume at

52 h. pH measured at surface starts dropping 30 h after injection starts and continues dropping, with a reversal when the pumps were serviced, until CO₂ breakthrough. Alkalinity and the concentrations of divalent metal cations (Ca, Sr, Fe, Mn), Si and some trace metals (Zn, Pb, Cr) increase rapidly at CO₂ breakthrough (Fig. 13B–F).

The pH measurements at surface pressures will be increased by CO₂-degassing as the fluids were decompressed. If the fluids are saturated in CO₂ at reservoir conditions just prior to the arrival of the CO₂ plume the pH would drop to 3.5 (calculated using PHREEQC, Parkhurst and Appelo, 1999), c.f. Xu et al., 2010). The subsequent rise in alkalinity of ~50 mmol

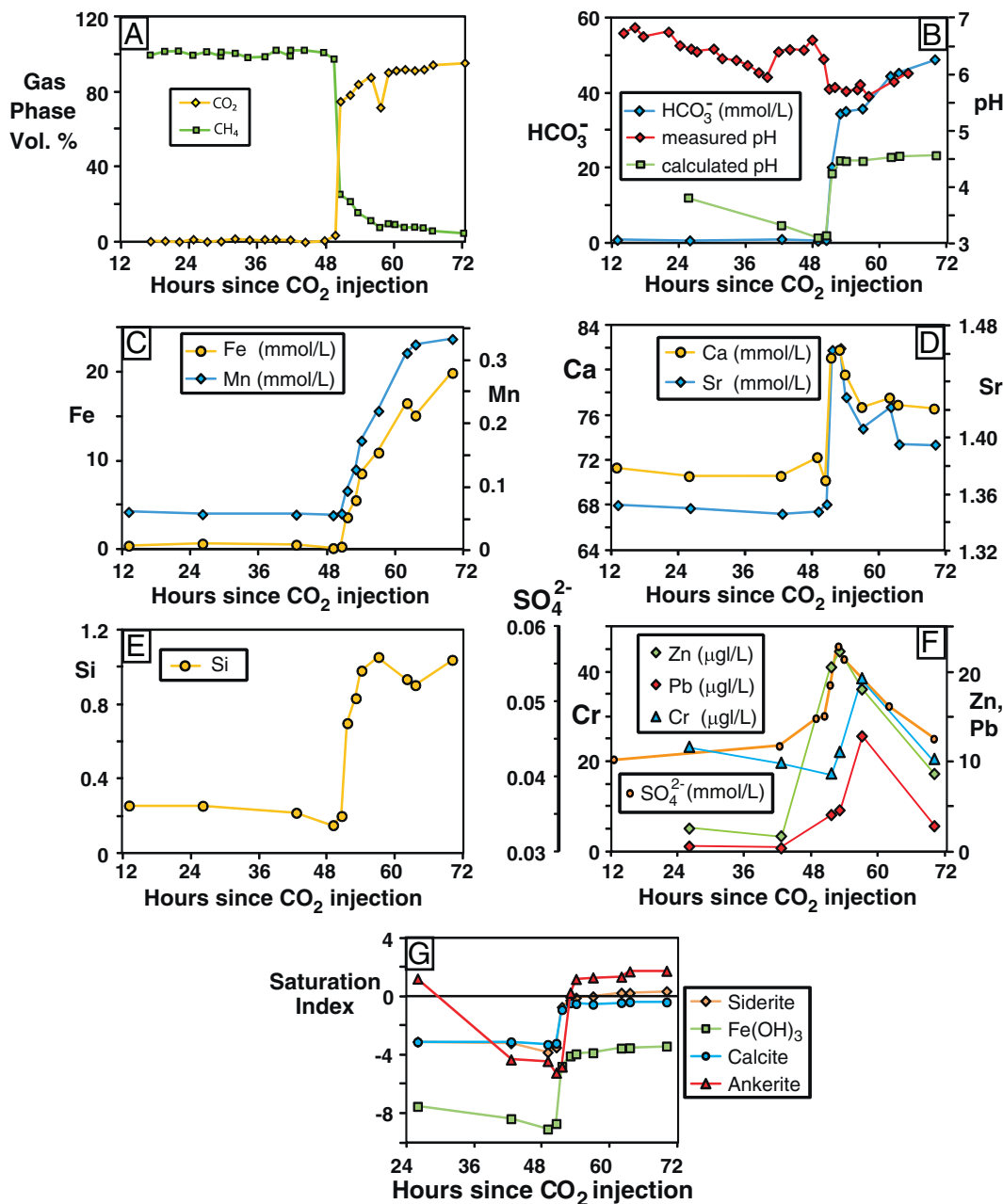
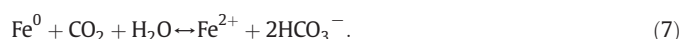
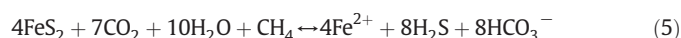
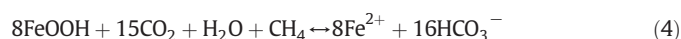
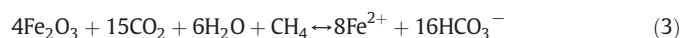


Fig. 13. Frio-I fluid chemistry redrawn after Kharaka et al., 2006a,b and analyses provided by Kharaka (pers. comm. 2012). A) Arrival of the CO₂ plume at the observation well is observed in the changes in the gas composition measured on gases produced from the U-tube sampler. B) Arrival of the CO₂ plume is preceded by a low pH front of fluid containing dissolved CO₂, pH measured at surface is consistently two pH units higher than in-situ pH recalculated using O-isotope data suggesting degassing of samples brought to surface P,T. Arrival of the main CO₂ front is accompanied by a rapid increase in fluid alkalinity due to fluid–rock reaction, which rapidly buffers pH. C) Alkalinity is generated by the rapid dissolution of Fe-bearing minerals, D) and the dissolution of calcite, releasing Ca and Sr to solution. E) Increases in silica concentrations most likely reflect dissolution of phyllosilicate minerals. F) Changes in major element chemistry are accompanied by a spike in trace metal concentrations most likely sourced from pH driven desorption and dissolution metal oxides. G) Mineral saturation index calculations using PHREEQC (Parkhurst and Appelo, 1999) based on calculated pH and measured fluid compositions imply that the properties of the fluid are buffered by reaction with a Fe-carbonate phase. As CO₂ arrives at the observation well the fluid rapidly moves to equilibrium with siderite, whilst Fe-oxide phases remain undersaturated.

corresponds to an increase in Ca of 10 mmol/L and Fe of 20 mmol/L, and if the brine remains CO₂ saturated, raises the calculated pH to ~4.6 at 3 days since CO₂ injection (Fig. 13G, c.f. Xu et al., 2010).

The lag between the drop in pH and increase in alkalinity reflects the time taken for reactions to increase alkalinity, and is therefore controlled by the kinetics of those reactions. Ca and Sr concentrations increase concurrently (Fig. 13D) and the constant Sr/Ca molar ratio are consistent with carbonate mineral dissolution. Concentrations of Fe, Mn and Si increase more slowly reflecting the more sluggish dissolution of Fe-oxide, Fe-oxyhydroxide and/or Fe-sulphide, and silicate or phyllosilicate minerals.

The pulse of increased concentrations of Zn, Pb and Cr most likely reflect pH-driven desorption from mineral grain surfaces (Xu et al., 2010), see Section 3.3.4). Increases in alkalinity are mainly balanced by increases in Ca and Fe. Xu et al. (2010) model the increase in Fe from an unknown Fe-bearing mineral or minerals, or surface adsorption. The Fe:alkalinity ratio of 1:2, after subtraction for alkalinity sourced from calcite dissolution, is consistent with dissolution of Fe-oxide or Fe-oxyhydroxide, with a methane reductant (Eqs. (3) & (4); c.f. Wigley et al., 2012). The important role of CO₂ in this acid-reduction is reflected in the reaction stoichiometry. Potential iron dissolution reactions from haematite, iron oxyhydroxides, pyrite, siderite and steel drill pipe are:



Several lines of evidence indicate derivation of the Fe from Fe-oxides, Fe-oxyhydroxides or pyrite; 1) Kharaka et al. (2006a) noted Fe-rich grain coatings on clays in the core, 2) pyrite is the dominant diagenetic Fe-bearing phase (McGuire, 2009) reflecting the reducing nature of the methane-rich groundwater (Kharaka et al., 2006a), 3) no siderite was observed in the core (McGuire, 2009), 4) the fluid Fe and Mn concentrations which exhibit a Mn/Fe molar ratio of 0.016 are similar to the Mn/Fe ratio of 0.015 measured in pyrite grains in core from the injection interval in the Frio C sandstone (McGuire, 2009), and 5) the initial rapid release of Fe is coincident with the small increase in fluid SO₄²⁻, which may reflect oxidation of H₂S released during the acid dissolution of pyrite, although HS⁻ and H₂S concentrations in the fluid were not measured. Determining the origin of the released Fe is complicated by multiple potential sources; use of trace element or isotopic tracers measured in the source minerals, equipment or casing would enable a more definitive assessment.

Calculations of mineral saturation indices during the Frio-I experiment, based on the measured fluid chemistry and at CO₂ saturation, show that release of Ca, Fe and HCO₃⁻ to solution and neutralisation of pH buffers the fluid to equilibrium with siderite and ankerite over 1.5 to 2 days, although calcite and Fe-oxyhydroxides remain undersaturated (Fig. 13G). The continued increase in fluid Fe concentrations whilst maintaining equilibrium with siderite requires coprecipitation of a Fe-carbonate phase over short timescales.

Similar results have been obtained for the Frio-II Brine Pilot injection experiment (Fig. 14), where 360 tonnes of CO₂ were injected at 1650 m into the Blue Sands unit of the Lower Frio Formation (Daley et al., 2007a,b). The arrival of the CO₂ plume at the observation well, 32 m up dip, ~62 h after injection was accompanied by a sharp drop in fluid pH to ~3.5, and by a sharp increase in the concentration of Zn, Pb, Cr and Si at CO₂ breakthrough, followed by two pulses of

alkalinity and Fe, Mn, and Co enriched fluids over a ~2 day period (Fig. 14). Recalculation of dissolved CO₂ concentrations using measured alkalinity and in-line pH indicate that the fluids reach CO₂ saturation with CO₂ after 75 h but that this is followed by sampling of undersaturated brines.

Rapid release of Zn, Pb and Cr coincide with a sharp drop in fluid pH and their release is potentially the result of pH driven desorption from metal oxide grain surfaces (see Section 3.3.4). The subsequent double pulse of alkalinity and metal enriched fluid may correspond to the arrival of distinct macroscopic CO₂ fingers at the observation well. The large changes in Fe and HCO₃⁻ concentrations in these alkalinity pulses are highly correlated, with an approximate 1:3 molar ratio, suggesting the production of Fe, Mn and Co may originate from the dissolution of Fe-oxide or Fe-oxyhydroxide by acid-reductive dissolution involving reduced sulphur, or from the steel equipment or casing. Changes in Fe and Mn concentrations are highly correlated (R² = 0.96) and the low Mn/Fe ratio (~0.007) of the fluids is consistent with the dissolution of sedimentary Fe-oxides with low wt% Mn (Drever, 1982). As Fe concentrations increase the fluids evolve towards Fe-isotope ratios of ~-0.5‰ (Kharaka and Cole, 2011), which is compatible with either the dissolution of sedimentary Fe-oxides or borehole casing steel that typically have coincident Fe-isotope ratios of ~-1‰ to 0‰ (Johnson and Beard, 2006).

The reservoir fluids initially present in both the Frio-I and Frio-II contain high concentrations of dissolved methane. Reducing conditions promoted by high concentrations of methane, hydrocarbons, sulphide species and low dissolved oxygen concentrations are a ubiquitous feature of many subsurface reservoirs. The large amount of acidity produced by CO₂ dissolution, in conjunction with the presence of such reducing conditions, allows the acid-reductive dissolution of minerals such as Fe₂O₃ and FeOOH and the conversion of relatively insoluble Fe³⁺ to soluble Fe²⁺. The observations from Frio and natural analogues (Wigley et al., 2012 – see below) suggest this may be ubiquitous in carbon storage sites in impure sandstones. Similar dissolution of carbonates, Fe-oxides and oxyhydroxides has been observed at the Nagaoka CO₂ injection site in Japan (Mito et al., 2008), where fluids sampled from the observation wells one year after completion of injection exhibit high bicarbonate concentrations and increased Ca, Mg, Fe, Mn and Si concentrations (see also Bowker and Shuler, 1991). In contrast, little change was observed in fluid chemistry at the Cranfield CO₂ injection site due the unreactive nature of the quartzite host reservoir (Lu et al., 2012). This highlights the importance of local factors, such as reservoir mineralogy, in determining the likely fluid-rock reactions in CO₂ injection sites.

3.3.4. Trace metal mobilisation

pH driven desorption of trace metals from metal oxide grain surfaces during CO₂ injection is predicted from modelling studies (Apps et al., 2010; Navarre-Sitchler et al., 2012; Siirila et al., 2012; Karamalidis et al., 2013), experiments (Little and Jackson, 2010; Lu et al., 2011; Frye et al., 2012; Payán et al., 2012) and recent field tests (Trautz et al., 2012). Experimental studies have shown that CO₂ can mobilise trace metals at concentrations above US Environmental Protection Agency (EPA) concentration limits (Little and Jackson, 2010); however field experiments have not shown hazardous levels of contamination (Keating et al., 2010; Kharaka et al., 2010; Trautz et al., 2012).

At the Plant Daniel pumped shallow release experiment, injection of CO₂ saturated water at ~50 m depth into the Graham Ferry Formation resulted in the rapid release of divalent metals from the sediment (Trautz et al., 2012). A sharp drop in pH and increase in metal cations (Ca, Mg, Sr, Ba, Fe, Mn and Cr) and alkalinity was observed at the observation well ~5 m from the injection well after 8 to 10 days. Concentrations peaked after 23 to 24 days and gradually returned to or near background concentrations. This pulse release behaviour is attributed to the rapid pH-driven desorption of trace metal from grain surfaces

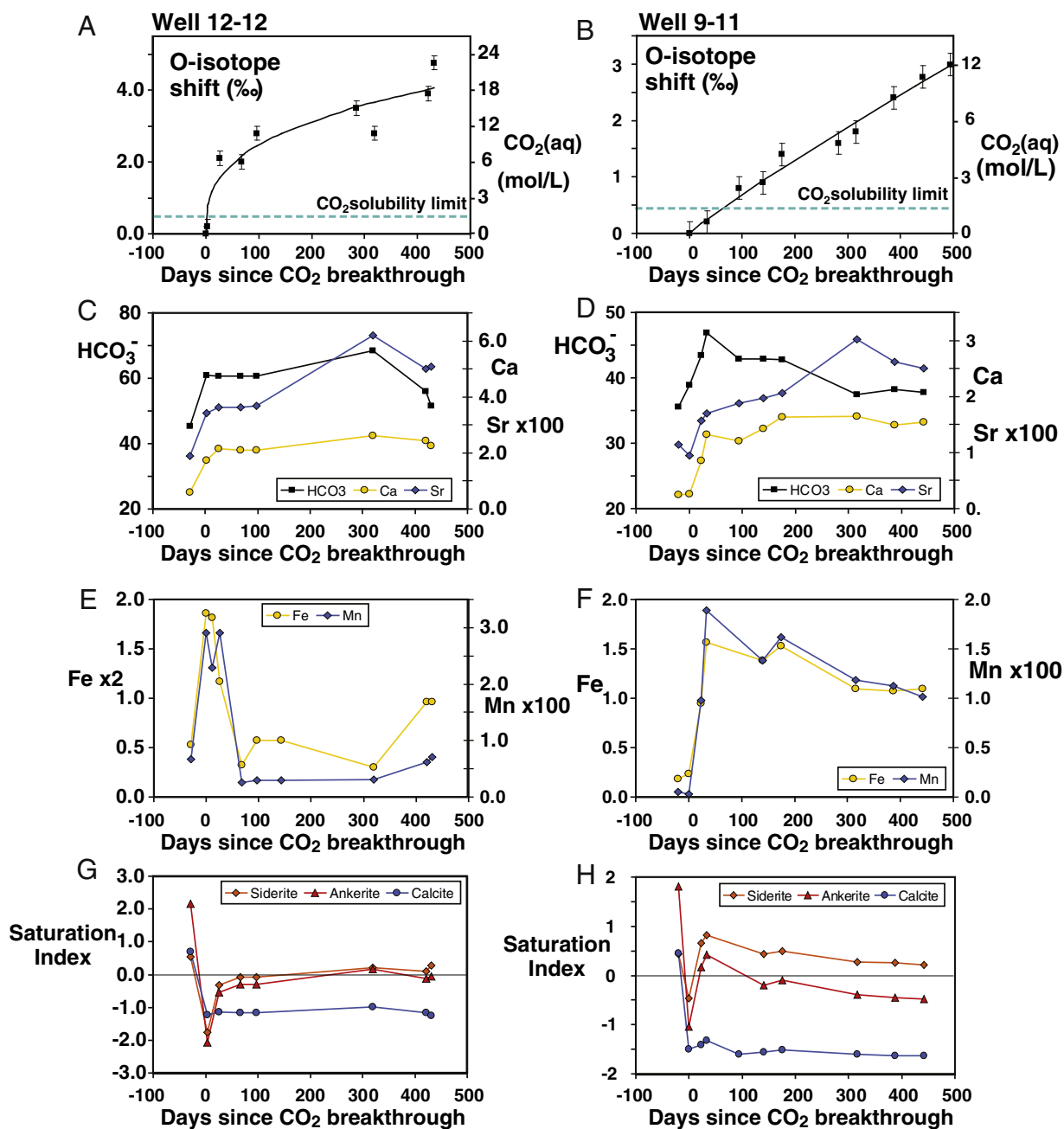


Fig. 14. Pembina-Cardium CO₂-EOR project fluid chemistry, data from Penn West Energy Trust (2007), excluding data with charge imbalance >5% and incomplete fluid chemical analyses (see also Shevalier et al., 2009). A) The O-isotope shift in water from production wells 12–12 and 9–11 since the first arrival of injected CO₂ (after Johnson et al., 2011). The magnitude of the shift implies that waters saturate with CO₂ within several days of the first arrival of CO₂ and continue to undergo diffusive exchange with a free CO₂ phase. B and C) Rapid saturation of the fluid with CO₂ is accompanied by rapid increases in the concentration of Ca and Sr, and Fe and Mn reflecting rapid dissolution of calcite, siderite and Fe-oxides. D) Saturation indices for carbonate minerals present in the formation, calculated using dissolved CO₂ concentrations determined from O-isotope shift and CO₂ saturated concentrations determined using the models of Duan et al., 2006. The fluid is initially saturated in the major carbonate phases; however dissolution and dissociation of the CO₂ drive rapid undersaturation. Calcite and siderite subsequently dissolve driving fluid towards saturation of insoluble Fe–Mg–Ca carbonate. The fluid is then buffered at saturation by the continued dissolution of calcite and reprecipitation of insoluble Fe–Mg–Ca carbonate.

and complete dissolution of finite amounts of Fe-sulphide and dolomite at the low pH plume head, followed by a plume tail that encounters sediment that has been depleted by continuous mobilisation at the plume front (Trautz et al., 2012). Throughout this field experiment the concentrations of potentially hazardous trace metals (e.g. As, Pb, Hg) remained below EPA concentration limits.

The rate of trace metal release by pH-driven desorption will reflect trace metal absorption site density and mineral surface areas, the rate of carbonate and metal oxide dissolution reactions that buffer pH,

the coupling of desorption to the dissolution of trace metal bearing mineral phases (Bearup et al., 2012) and the pre-existing redox state of the fluid. Trace metals may be subsequently removed from solution as pH rises across mineral–fluid reaction fronts (Wigley et al., 2012, 2013b) or by re-adsorption in the presence of compatible mineral phases such as clays (Viswanathan et al., 2012). These observations suggest, that in carbon storage sites, progressive fluid flow and fluid–rock reaction will act to immobilise trace metals previously mobilised by the CO₂.

3.4. Organic contaminants

Subsurface reservoirs, especially depleted oil fields, contain a variety of organic compounds, many of which are toxic and carcinogenic (e.g., BTEX and PAH; Kharaka and Hanor, 2003) and the mobilisation of organic compounds has been observed during some CO₂ injection experiments (Daley et al., 2007a; Kharaka et al., 2009). Fluid samples collected ~20 days after the end of CO₂ injection at the Frio-I injection experiment had dissolved organic carbon (DOC) concentrations ~100 times those in samples collected prior to CO₂ injection, and were enriched in formate, acetate, and toluene, but showed no enrichment in organic acid anions and BTEX compounds (Kharaka et al., 2009). The Frio sandstone is not notably enriched in organic components (Kharaka et al., 2009) and such mobilisation highlights the efficacy of supercritical CO₂ as a solvent for organic compounds and hydrocarbons (Kolak and Burruss, 2006).

Burant et al. (2013) reviewed experimental data on the solubility of organic compounds in supercritical CO₂, and the partitioning of organic compounds between water and CO₂, and suggested that compounds with high volatility and low aqueous solubility will be preferentially mobilised into the CO₂ phase. The solubility of the organic compounds in CO₂ is strongly affected by cosolvency processes, the state of hydration of the CO₂ phase and the salinity of the contacting brine (Burant et al., 2013). The dearth of experimental data on the partitioning of organic compounds between supercritical CO₂ and brine makes assessment and modelling of the subsequent recontamination of the brine phase difficult. The routine measurement of such compounds during CO₂ injection experiments and further experimental studies would improve understanding of the relative partition and efficacy of CO₂ for mobilising organic molecules and contaminating groundwater.

4. Long term fluid–rock interactions in injection experiments and CO₂-EOR studies

4.1. Ionic trapping

Long-term fluid–rock interactions that may stabilise the CO₂ in storage reservoirs include the ionic trapping of CO₂ as bicarbonate ions in solution and precipitation as carbonate minerals, which may impact flow. The results from Frio-I and Frio-II show that rapid dissolution of carbonate minerals and Fe-oxides, Fe-oxyhydroxides and Fe-sulphides lead to the production of ~50 mmol/L alkalinity after only a few days of reaction. Raistrick et al. (2006) and Myrtilinen et al. (2010) examined long-term changes in the $\delta^{13}\text{C}$ of HCO₃⁻ from reservoir fluids at the Weyburn CO₂-EOR project and Ketzin CO₂-injection experiment, respectively. These studies used mass balance calculations, constrained by measurements of alkalinity and the $\delta^{13}\text{C}_{\text{HCO}_3^-}$ in fluids sampled from observation wells to quantify the fraction of bicarbonate originating from the injected CO₂ as opposed to that produced from carbonate mineral dissolution or bacterial sulphate reduction. After 40 months of injection, bicarbonate concentrations at Weyburn and Ketzin respectively increased to between 12 to 24 mmol/L and 12 to 27 mmol/L, and between 65–81% and 69–95% of this newly formed bicarbonate was derived from the injected CO₂ (Eq. (1)) and by reaction with non-carbonate minerals, the remainder being derived from dissolved carbonate minerals.

Production of alkalinity above these concentrations will depend on the relative rates of insoluble silicate mineral dissolution and carbonate mineral precipitation and the time taken to reach carbonate and silicate mineral–fluid equilibrium. The total mass of carbon sequestered by ionic trapping will be limited by the rates of CO₂ flow and dissolution, and CO₂ diffusion and transport of CO₂ in formation brine. The efficacy of ionic trapping is highly dependent on the interaction of the CO₂ with large volumes of water; for example at 30 °C and 100 bar, and a maximum concentration of bicarbonate of ~100 mmol/L, each litre of

CO₂ must interact with 160 l of water for the CO₂ to be completely trapped as bicarbonate ions.

4.2. Carbonate mineral precipitation

Post-injection fluid sampling at the Frio-I injection experiment revealed that Fe concentrations at the observation well had decreased to ~50% of their concentration maximum one month after CO₂ injection stopped (Kharaka et al., 2006a) and close to their initial values after ~6 months (Xu et al., 2010). Xu et al. (2010) reproduced the observed trends using reactive transport modelling and attributing the immobilisation of Fe to the precipitation of ankerite and siderite in the reservoir.

4.2.1. Pembina-Cardium EOR project

Observations from the Pembina-Cardium CO₂-EOR project (Shevalier et al., 2009; Johnson et al., 2011a,b) provide a limited observational database on fluid–rock reactions over a 1.5 year period (Fig. 15). Arrival of CO₂ at the production wells surrounding the CO₂ injection well was accompanied by rapid shifts in oxygen isotopic composition of the brine due to exchange with the CO₂ (Fig. 15A–B; Johnson et al., 2011a) and increases in alkalinity (Fig. 15C–D; up to 40 to 70 mmol/L) and Ca, Sr, Fe and Mn concentrations (Fig. 15C–F) over a period of ~1 to 2 months (data from Penn West Energy Trust, 2007), which is attributed to the rapid dissolution of calcite, siderite and Fe-oxides present in the reservoir. Calculation of dissolved CO₂ concentrations and in-situ pH assuming CO₂ saturated conditions shows that the fluids rapidly become undersaturated in carbonate minerals due to CO₂ dissolution and calcite and siderite dissolves (Fig. 15G–H). The fluids remain undersaturated in calcite whilst moving rapidly to saturation with siderite and ankerite and remain at saturation throughout the 1.5 year sample period, whilst bicarbonate, Fe and Mn concentrations in the fluid decrease. This suggests that the fluid composition is modified by calcite dissolution and reprecipitation of less soluble Fe–Mg–Ca carbonate phases, such as ankerite and siderite.

4.2.2. Salt Creek EOR project

Observations from the large-scale CO₂-EOR project at the Salt Creek Field, Wyoming provide important insights into the progress of fluid rock reactions during CO₂ injection (Fig. 16; Kampman et al., 2011). The 2nd Wall creek sandstone is a feldspathic litharenite and has a reactive mineralogy of abundant plagioclase (~20% An) and mica; it is heavily cemented with calcite at its top and base. The immature nature of the sediment preserves the detrital mica component, with only minor development of illite and kaolinite grain coatings.

Approximately 20 days after CO₂ injection the arrival of significant CO₂ at the up-dip production well was accompanied by a rapid increase in alkalinity corresponding to increases in the concentration of Ca, Sr, Na, K and Si. Changes in alkalinity over the first ~20 days are balanced mainly by changes in Ca in the fluid which, together with the covariance of Ca and Sr and the Ca/Sr ratio, is consistent with calcite dissolution. During this period Na, K and Si concentrations also start to rise, but more slowly, consistent with the sluggish dissolution of silicate minerals in the reservoir. Subsequently, CO₂-rich fluid arrives at the production well and concentrations of K, Na and Si start to rise more rapidly due to the dissolution of biotite and plagioclase in the reservoir. The magnitude of the changes in Si and Al are significantly smaller than those of K and Na reflecting production of silica and clay minerals in the reservoir and possibly exchange of Ca for Na and K on clay minerals. Alkalinity increases from ~65 mmol/L to ~100 mmol/L after ~5 months of reaction which implies the fluids are close to saturation in CO₂.

Simple mass balance calculations, accounting for changes in the evolving fluid composition due to calcite, plagioclase and biotite dissolution, reveal that initial calcite dissolution over 40 days moves to carbonate precipitation as the fluid saturates with carbonate and Ca from

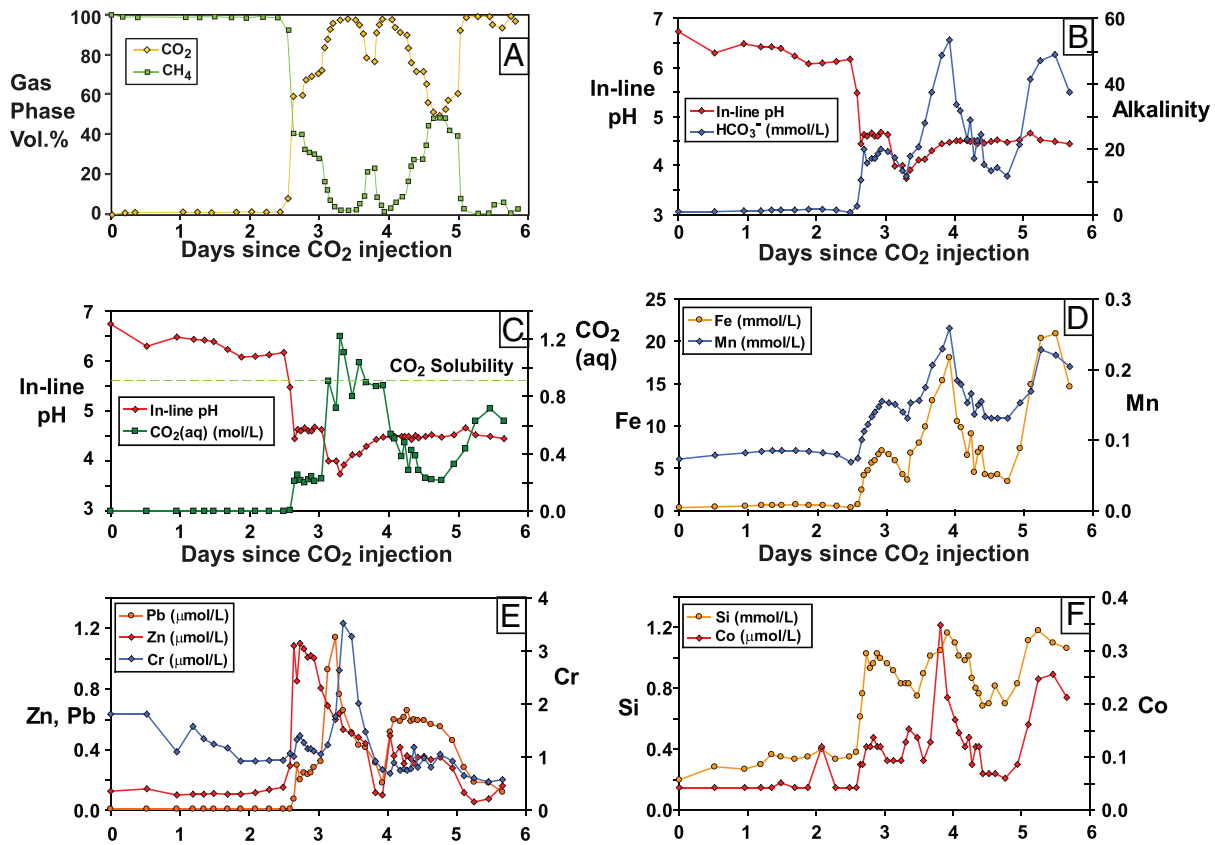


Fig. 15. Frio-II fluid chemistry from Daley et al. (2007a), with CO₂ and CH₄ concentrations changes redrawn after Daley et al. (2007a). A) Proportions of CO₂ and CH₄ in the gas phase at the observation well. B–C) In-line pH measured in U-tube sampler and alkalinity (B) and dissolved CO₂, recalculated in PHREEQC using in-situ pH and alkalinity (C). D) Fe, and Mn concentrations. Changes in these elements are strongly correlated to changes in alkalinity, and are sourced from the dissolution of Fe-oxides. E) Zn, Pb and Cr concentrations. Changes in these elements precede the alkalinity front and coincide with the sharp drop in fluid pH. They are sourced from pH driven desorption from mineral surfaces. F) Si and Co concentrations.

plagioclase dissolution is redeposited as carbonate minerals. The role of ion exchange in this simple illustrative calculation was not assessed. The calculations show that $\sim 1.5\times$ the total mass of carbonate dissolved per litre of fluid is redeposited. The rate of Ca deposition and Na, and K production appears to decline over the 4 month period. This highlights the important role of silicate mineral dissolution as the rate limiting step for carbonate mineral precipitation. The results suggest that silicate mineral dissolution rates can initially be rapid in the mineral-undersaturated acidic conditions following injection.

5. Long term fluid–rock reactions – observations from natural analogues

Natural accumulations of CO₂ provide important insights into the long-term geochemical processes and trapping mechanism operating in CO₂ reservoirs. The study of natural CO₂ reservoirs and their implications for CO₂ storage are reviewed in Bickle et al. (2013). The important questions that may be answered by observations on natural analogues include the rates and significance of the stabilising mechanisms of CO₂ dissolution in brines and carbonate precipitation, the nature of the fluid–mineral reactions and the long-term consequences of interactions between CO₂ and CO₂-saturated brines on caprocks and fault zones. The continued study of such sites is likely to provide important constraints on the coupling of advective-diffusive transport of CO₂ and CO₂-charged brines with mineral dissolution and carbonate precipitation in low permeability rocks, with implications for the long-term integrity of reservoir seals.

There are numerous natural accumulations of CO₂ in geological reservoirs (Allis et al., 2001; Pearce, 2004; Haszeldine et al., 2005; Pearce, 2006). However in most of these, the reservoirs are inadequately

sampled, fluid and gas samples maybe unavailable and details of the age and hydrology of the reservoirs are limited.

In the Colorado Plateau, USA, CO₂ produced by Cenozoic magmatic activity has been stored in a variety of geological reservoir for thousands to many millions of years (Fig. 17; Allis et al., 2001; Gilfillan et al., 2008). CO₂ from several of these reservoirs is exploited for use in enhanced oil recovery (Allis et al., 2001) and therefore samples of CO₂ gas and some core are available. Analyses of travertine deposits (Embaid and Crossey, 2009; Kampman et al., 2012; Burnside et al., 2013) and the noble gas isotopic composition of the CO₂ gas (Ballentine et al., 2001) have put important constraints on the age of the systems, CO₂ mobility (Gilfillan et al., 2011) and CO₂–fluid interactions (Gilfillan et al., 2008, 2009; Dubacq et al., 2012; Zhou et al., 2012). However samples of the reservoir, caprocks and waters are not generally available, the exception being the active leaking system at Green River, Utah, where natural CO₂-driven cold water geysers allow sampling at surface (e.g. Kampman et al., 2009) and a 2012 scientific drilling campaign has sampled core and fluids from the active reservoir. The following sections discuss some of the constraints on long term fluid–fluid and fluid–rock reactions obtained from these natural reservoirs, focusing on the well-studied site at Green River.

5.1. Noble gas constraints on the long term fate of natural CO₂

Changes in the CO₂/³He ratio and $\delta^{13}\text{C}_{\text{CO}_2(\text{g})}$ measured in reservoir gases from multiple wells across ten major CO₂ reservoirs from the Colorado Plateau and elsewhere reveal 40% to 90% of the CO₂ originally emplaced has been lost to solution over geological time-scales (Gilfillan et al., 2009; Zhou et al., 2012), highlighting the important role that dissolution into groundwater has on the long-term stabilisation of CO₂

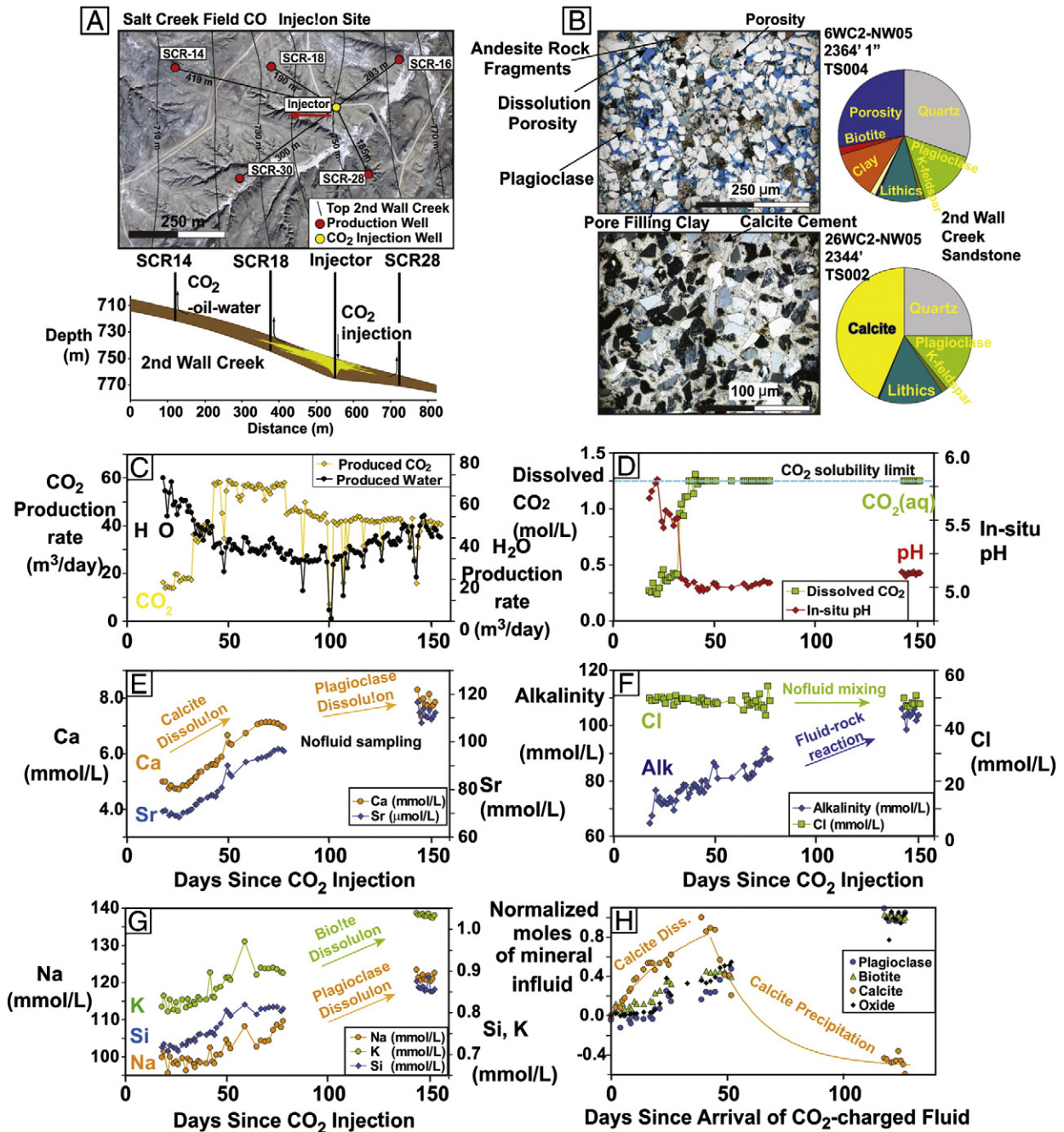


Fig. 16. (A) Surface map from the Salt Creek Field, CO₂-EOR project showing the location of the CO₂-injection well and surrounding production well pattern from which CO₂ and fluids were sampled over a 6 month period, during the noble gas spiked CO₂ injection. Structure contours are the top surface of the Second Wall Creek reservoir into which CO₂ is being injected for enhanced oil recovery. (B) Thin section photomicrographs and mineralogical point counting data for the Second Wall Creek Sandstone from cores from wells 6WC2-NW05 and 26WC2-NW05, drilled adjacent to the CO₂ injection site. These show the abundance of reactive feldspar and diagenetic calcite cements in the injection interval. (C) Water and CO₂ gas production data for Well SCR18 the up dip production well sampled during this project, and the first well to see arrival of the noble gas spiked CO₂. (D) Dissolved CO₂ concentrations in the produced fluid calculated from fluid and gas production volumes using fluid densities calculated at reservoir pressure and temperature conditions. Fluid pH calculated using the calculated CO₂ concentrations and measured alkalinity. (E) Measured Ca and Sr concentrations in the produced fluid showing rapid increases due to the arrival of CO₂ and CO₂-charged fluid at the production well and the dissolution of calcite. Concentrations plateau at day 80 as the fluid saturates with carbonate and calcite dissolution moves to calcite precipitation. (F) Cl and alkalinity concentrations in the produced fluid showing that Cl concentrations are stable, precluding fluid mixing, whilst cation concentrations and alkalinity dramatically increase due to fluid-mineral reactions. (G) Measured Na, K and Si concentrations in the produced fluid reflecting the dissolution of silicate and phyllosilicate minerals in the host reservoir, predominantly plagioclase and biotite. (H) The moles of mineral dissolved in the fluid from mass balance calculations using changes in the measured fluid composition and mineral compositions from electron microprobe analyses. The mass balance modelling shows that the initially rapid dissolution of calcite is followed by the more sluggish dissolution of plagioclase and biotite. The fluid evolves to precipitate carbonate after ~45 days since the arrival of the first CO₂-charged fluids as cation and alkalinity production from fluid-mineral reactions saturate the fluid with carbonate, whilst silicate dissolution reactions continue to produce cations and alkalinity, driving carbonate deposition.

reservoirs. For the young Bravo Dome accumulation, which may be undergoing contemporary CO₂ recharge (Baines and Worden, 2004), fractionation of the CO₂/³He ratio and δ¹³C_{CO2(g)} imply removal of gas from the fluid into solutions with high HCO₃⁻ concentrations, implying that in this dynamic field fluid-rock reaction is an important source of

alkalinity and ionic trapping of the CO₂ (Dubacq et al., 2012). The magnitude of the CO₂ loss in these reservoirs must be related to the hydrodynamics of groundwater flow and diffusive transport processes close to the gas cap-formation water interface. Such transport processes likely produce compositional and isotopic disequilibrium between the gas

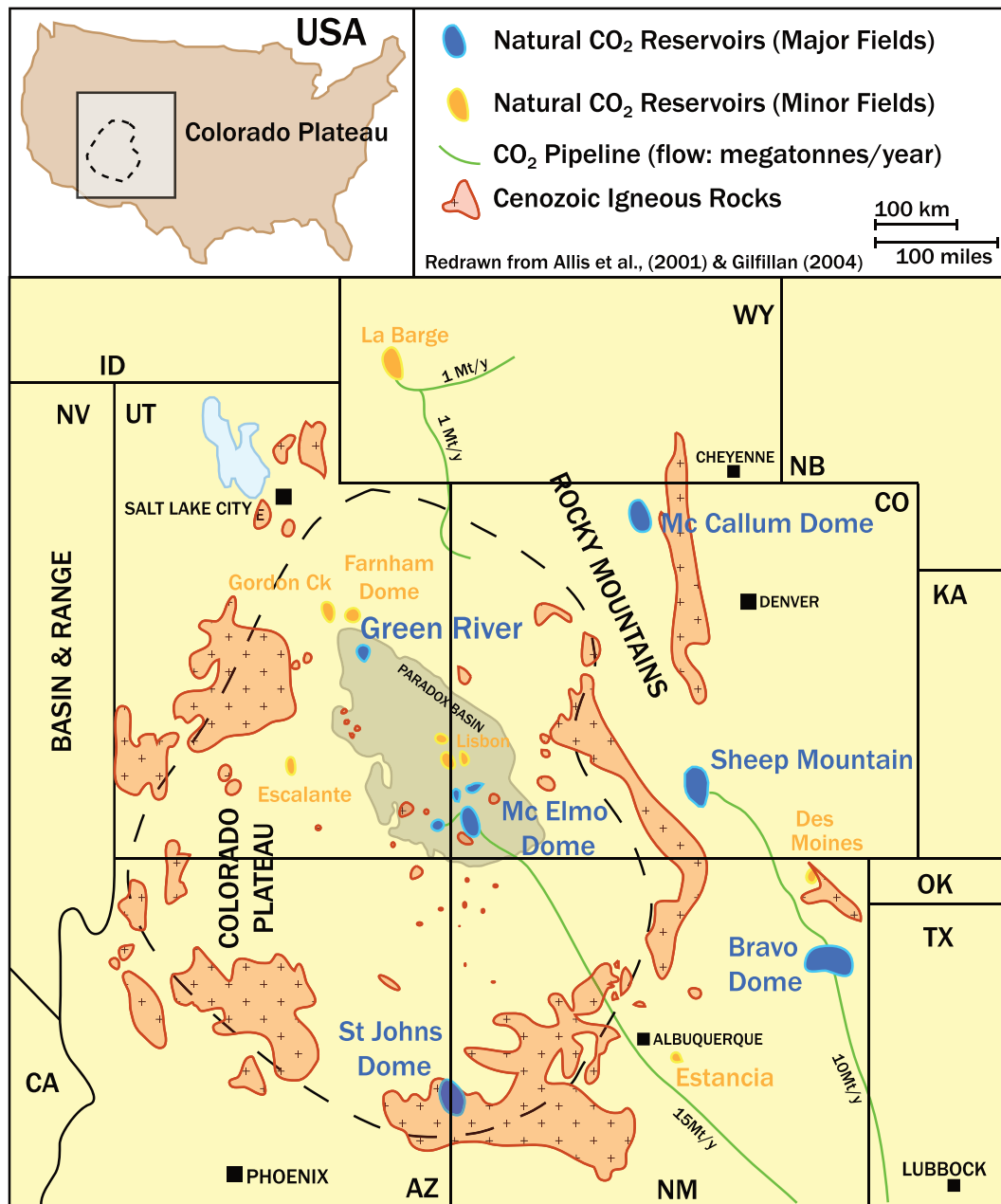


Fig. 17. The Colorado Plateau CO₂ Province is an extensive uplifted region covering portions of Utah, Colorado, Arizona and New Mexico, that contains abundant natural accumulations of CO₂ (redrawn after Allis et al., 2001). Some CO₂ fields, notably Bravo Dome (NM), McElmo and Sheep Mountain (CO), Farnham Dome (UT), Springerville (AZ), and Big Piney-LaBarge (WY) have been exploited for commercial purposes, mainly for enhanced oil recovery and dry ice production. The source of the CO₂ is considered to be dominantly volcanogenic, juvenile CO₂ generated from Cenozoic magmatic activity and mantle degassing (Gilfillan et al., 2008, 2009). The gas reservoirs, usually sandstone or dolomite, lie in four way dip closed or anticlinal structures with mudstone or anhydrite top seals. Fault seals are common along the margins of the reservoirs (Allis et al., 2001; Shipton et al., 2004). The gases from the fields can be >98% CO₂ with trace quantities of N₂ (4%), He (0.1–1%), Ar, and CH₄ (Allis et al., 2001).

cap and the contacting formation water. It is likely that only information about the dissolution of the CO₂ phase into the formation fluid is recorded in the composition of the gas cap, and processes related to subsequent mineralisation of the CO₂ in solution are most likely not recorded, precluding the use of reservoir gases as a measure of subsequent mineral trapping mechanism in the formation fluid.

5.2. Fluid–mineral reactions in natural reservoirs

Petrological studies of natural CO₂ reservoirs reveal a range of degrees of fluid–mineral reaction from minor amounts of carbonate dissolution to complete dissolution of all reactive mineral phases and the deposition of relatively insoluble Fe–Mg–Ca carbonate minerals,

including ankerite, siderite and dolomite (Franks and Forester, 1984; Watson et al., 2004; Wilkinson et al., 2009b; Heinemann et al., 2013), and dawsonite (Baker et al., 1995; Moore et al., 2005; Worden, 2006; Wilkinson et al., 2009b). The impact of CO₂-promoted reactions will differ between sites depending on differences in; 1) pre-existing reservoir mineralogy; 2) CO₂ emplacement mechanism and rates; 3) CO₂ and mineral solubility across the wide range of pressure temperature conditions experienced by natural CO₂ reservoirs and; 4) variable reaction rates due to mineral surface and transport controlled reactions.

Some studies have observed trapping of CO₂ in carbonate minerals (Watson et al., 2004; Moore et al., 2005; Worden, 2006; Pauwels et al., 2007); however the volumes deposited are small as the rate limiting step for carbonate deposition within these reservoirs is alkalinity and

divalent metal cation production from the slow weathering of silicate minerals. The formation of dawsonite is predicted from modelling studies (Hellevang et al., 2005; Xu et al., 2005) but its occurrence in natural CO₂ accumulations is rare (e.g. Moore et al., 2005). The scarcity of natural dawsonite is likely the result of its limited phase stability (Bénézech et al., 2007) in carbon-rich alkaline fluids, and its subordinate stability to other aluminosilicate minerals (e.g. analcime; Kaszuba et al., 2005).

5.2.1. Implications for carbonate mineral deposition

The deposition of carbonate minerals is likely to be a significant process where CO₂ rich fluids diffuse into clay-rich caprocks containing reactive phyllosilicate minerals (Gherardi et al., 2007; Lu et al., 2009) or escape along faults and experience rapid CO₂ degassing (May, 2005; Gratier et al., 2012; Kampman et al., 2012). In both instances the deposition of carbonate is likely to have important long-term impacts on fluid flow and CO₂ leakage rates (McPherson and Heath, 2009). In addition, precipitation of carbonate minerals in faults and fractures may

generate stresses due to the forces of crystallisation sufficient to induce, sustain or enhance leakage (e.g. Iyer et al., 2008; Jamtveit et al., 2009; Gratier et al., 2012; Plümper et al., 2012).

Leaking natural CO₂ reservoirs at St Johns Dome, Arizona (Moore et al., 2003) and Green River, Utah (Shipton et al., 2004, 2005; Dockrill and Shipton, 2010; Kampman et al., 2012; Burnside et al., 2013) both contain significant volumes of surface and fault-hosted carbonate deposits, where degassing of CO₂ during ascent of the fluid has driven carbonate deposition. Studying such deposits provides important insights into the long-term behaviour of fault hosted CO₂ leakage and the important role played by climate driven changes in groundwater hydrology and regional stresses in controlling fault hydraulic behaviour and CO₂ leakage rates over geological time-scales (Kampman et al., 2012).

5.3. Green River, Utah

The CO₂ accumulation at Green River, Utah (Fig. 18) provides important constraints on the nature and rates of the CO₂ promoted

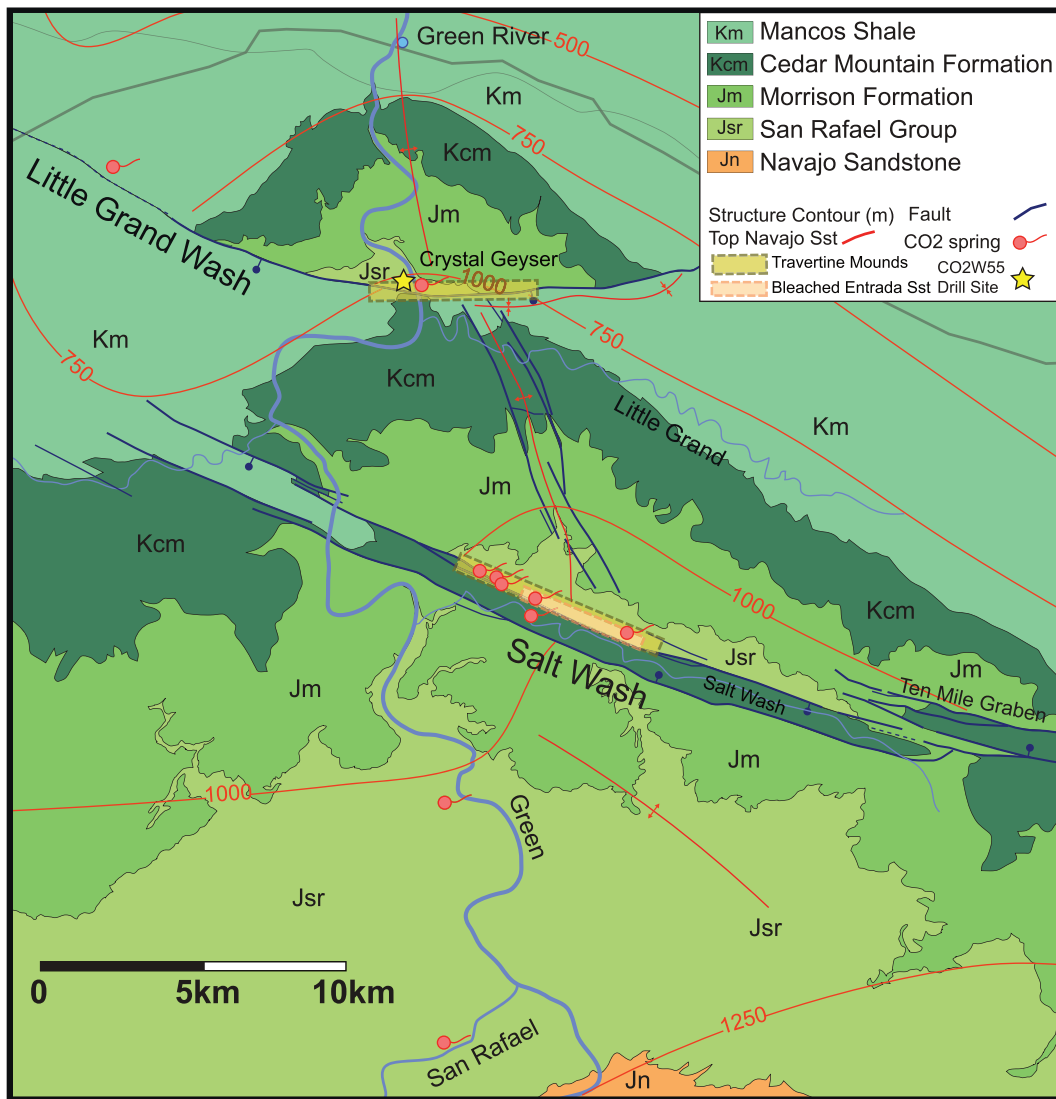


Fig. 18. Geological map of the Green River anticline showing locations of the Little Grand Wash and Salt Wash Graben normal fault systems, CO₂-springs and location of drill hole CO₂W55 (redrawn after Kampman et al., 2009). Supercritical CO₂ is buoyantly accumulated within the White Rim sandstone (>800 m depth) at the anticline crest in traps formed by the faults, which are laterally sealing due to shale and clay gouge cores (Dockrill and Shipton, 2010). The faults contain a damage zone of open fractures that allows CO₂ and CO₂-charged brine to migrate vertically, filling a series of shallow sandstone reservoirs in the Wingate, Navajo and Entrada Sandstones. The CO₂ and CO₂-charged brines mix with meteoric fluids in the sandstone reservoirs and flow parallel to the faults where they are sealing, and to the south where they are transmissive, being driven by the regional gradient in groundwater head (Hood and Patterson, 1984; Kampman et al., 2009). Also shown are the regions of travertine mounds discussed in Kampman et al., 2012 and Burnside et al., 2013, and the sandstone bleaching discussed in Wigley et al., 2012, 2013a,b. Structure contours are for the top surface of the Navajo Sandstone, the major source of CO₂-charged brine escaping at surface.

fluid–mineral reactions. Here the fluid–mineral reaction rates can be constrained both in flowing CO₂-charged groundwaters where fluids have been sampled along flow paths (Kampman et al., 2009), or in the exhumed CO₂-reservoirs where mineralogical profiles across reaction fronts have been measured and fluid transport rates constrained or estimated from hydrological models (Wigley et al., 2013a).

5.3.1. Green River active system

At Green River CO₂-charged fluids flow through the Navajo Sandstone, escape to the surface through a number of abandoned petroleum exploration wells and the fault damage zones of the Little Grand Wash fault and Salt Wash Graben at the apex of the Green River anticline (Fig. 18; Shipton et al., 2004, 2005; Dockrill and Shipton, 2010) where they form a series of natural CO₂ springs (Heath, 2004; Kampman et al., 2009), including the spectacular Crystal Geyser (Gouveia et al., 2005; Gouveia and Friedmann, 2006; Assayag et al., 2009a; Han et al., 2013). The CO₂ and CO₂-charged brines that migrate into the Navajo Sandstone originate from a supercritical reservoir of CO₂ in the White Rim sandstone at depth, and the system is a good analogue for processes occurring during CO₂ migration through the overburden and in shallow CO₂ gas reservoirs. Ancient travertine deposits along the faults attest to leakage of CO₂ from the site for at least the last 400,000 years (Burnside et al., 2013), characterised by successive pulses of CO₂-leakage with a periodicity controlled by climate driven changes in the hydraulic behaviour of the faults (Kampman et al., 2012).

5.3.2. Scientific drilling

Recent scientific drilling at Green River, near the intersection of the apex of the Green River anticline and the Little Grand Wash fault, has sampled core and CO₂-rich fluids to a depth of 322 m from a sequence of sandstone reservoirs (Fig. 19), (Kampman et al., 2013a). At the site of the CO2W55 drillhole, these CO₂-charged reservoirs are juxtaposed against a fault damage zone that has previously hosted CO₂ leakage, being overlain by ancient travertine deposits (Dockrill and Shipton, 2010). CO₂-charged fluid was first encountered at a depth of 50 m in the basal sandstones of the Entrada Sandstone, which is not overlain by a regional caprock in this region, indicating that the thin siltstone layers present in the upper portions of the formation act as a good seal to the CO₂-charged fluids. A second larger reservoir of CO₂-charge fluid was encountered in the Navajo Sandstone, capped by siltstone sequences of the Carmel Formation, and both the reservoir and lower portions of the caprock have been bleached by the CO₂-rich fluids. The core revealed net carbonate precipitation in the reservoir rocks and in the siltstone caprocks around fractures, but mineral dissolution fronts of Fe-oxide grain coatings (c.f. Wigley et al., 2012) and dolomite cements at the caprock reservoir interface (Fig. 20; compare to Wigley et al.,

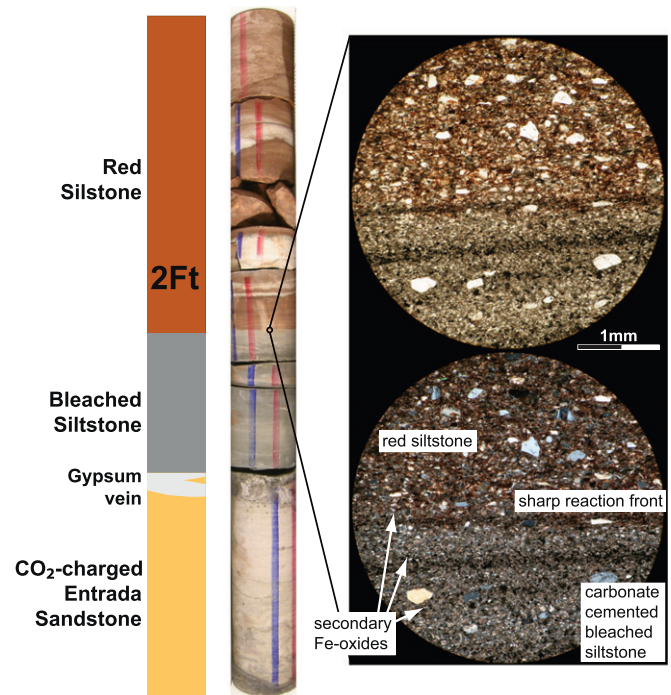


Fig. 20. Core photograph from well CO2W55 showing the contact between CO₂-bearing sandstone of the Entrada Sandstone and siltstone horizons that form internal seals to the CO₂-charged fluids. The lower 10 cm of siltstone has been bleached by removal of Fe-oxide grain coatings by interaction with the CO₂ and micrographs from the bleached-unchanged contact show the mobilised Fe has been redeposited at the reaction front in bands of coarse Fe-oxides, along with abundant carbonate cement throughout the bleached interval. The short distance over which the siltstone has been bleached suggests that the CO₂ has penetrated the siltstone by diffusion and that reactions with the host rock have attenuated the reactivity of the CO₂ over this cm length scale. These observations suggest that fluid–mineral reactions help retard the diffusion distance of the CO₂, potentially aided by the formation of carbonate cement that blocks pores, and that such siltstone layers can form impermeable barriers to the CO₂ and effective seals over 100,000 year time scales.

2013a). Reaction of CO₂(aq) as it diffuses into a caprock will retard the diffusion distance, and limit the extent to which CO₂ penetrates the caprock. Conversely these reactions may generate porosity, further enhancing the penetration depth of the CO₂ and weakening the overall integrity of the caprock. The preliminary observation that the mineral dissolution fronts have penetrated only tens of centimetres into the cored siltstone caprocks in the hundreds of thousands of years

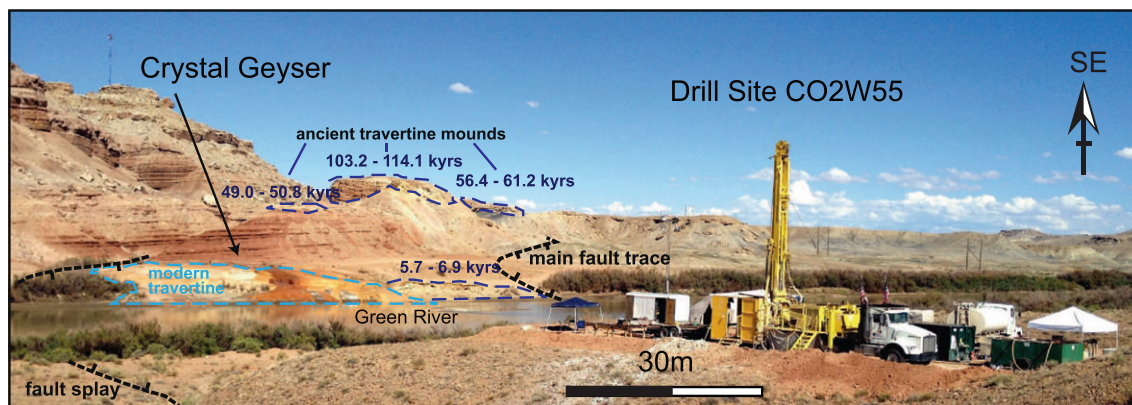


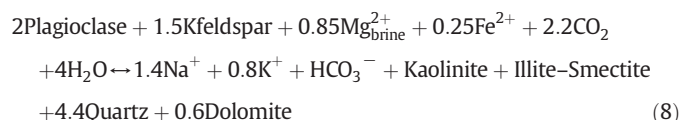
Fig. 19. Field photograph of the drill site of well CO2W55 showing the CS4002 Truck Mounted Core Drill in the foreground and the travertine mound formed by Crystal Geyser on the opposite bank of the Green River. Also shown are the main fault trace of the Little Grand Wash Fault, and the local fault splays. Ancient travertine mounds form away from the main fault trace, within the footwall block of the fault, above the main fault damage zone through which CO₂ and CO₂-charged brine escape to surface. Travertine mound ages from Burnside et al., 2013 are also shown.

of exposure to CO₂ rich fluids suggests limited degradation by the CO₂-charged fluids and attests to the efficiency of the sealing layers.

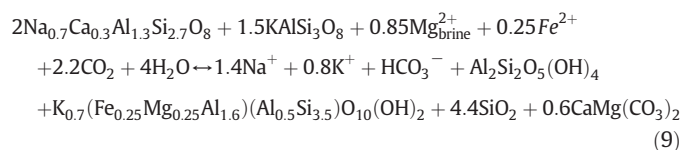
Downhole fluid sampling profiles (Kampman et al., 2013—in this issue —a,b) reveal that the reservoir is being recharged by inflow of CO₂ and CO₂-saturated brines through the fault damage zone, which then flow away from the fault and mix with meteorically derived fluid, and this has previously been inferred from the elemental and isotopic composition of the local CO₂-springs (Kampman et al., 2009; Wilkinson et al., 2009a). Kampman et al. (2012), used U–Th ages calculated by Burnside (2010) combined with isotope ($\delta^{13}\text{C}$, $\delta^{18}\text{O}$ and $^{87}\text{Sr}/^{86}\text{Sr}$) and trace element ratios (Sr/Ca and Ba/Ca) in carbonate veins to show that the reservoir has been periodically recharged over the last 135,000 years by inflow of these CO₂-charged brines through the damage zones of the normal faults. The timing of these CO₂ pulses corresponds to periods of local climatic warming, during the transition from glacial to inter-glacial conditions. They hypothesise that changes in groundwater recharge rates, and in the continental stresses related to unloading of the continental ice sheet and associated draining of nearby pluvial Lake Bonneville, triggered changes in pore-fluid pressure and dilation of fractures in the fault damage zone, thus facilitating enhanced escape of CO₂.

5.3.3. Fluid–rock reaction

Kampman et al. (2009) examined fluid–rock reactions in the Navajo Sandstone that occur as these CO₂-charge fluids flow away from the faults. Mass balance calculations on changes in fluid chemistry along flow paths, flow rates estimated from potentiometric maps, and mineral surface areas estimated from BET measurements were used to show that the dissolution of feldspars in the CO₂-charged groundwater in the Navajo Sandstone are incongruent, being balanced by the deposition of carbonate and clays, and that the dissolution rates are close to, and highly dependent on proximity to thermodynamic equilibrium. CO₂ is introduced to the reservoir by inflow of CO₂-charged brines along two major extensional faults (see below). Following introduction of the CO₂, the release of Na⁺ and K⁺ to solution traces the dissolution of plagioclase and K-feldspar following the reaction;



With the stoichiometry;



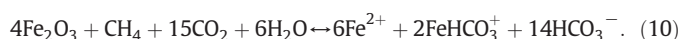
The fluids are undersaturated in the feldspar reactants and oversaturated in dolomite, kaolinite, illite–smectite and silica reaction products. The breakdown of albite is likely the rate limiting step for feldspar dissolution given its insolubility relative to anorthite (c.f. Maher et al., 2009). The feldspar dissolution rates are initially two orders of magnitude slower than far-from equilibrium laboratory rates for feldspars at similar pH and temperature conditions (e.g. Taylor et al., 2000) and decrease over five orders of magnitude as equilibrium is approached. The precipitation rates of carbonate minerals, and thus the rate at which CO₂ is trapped from solution, are consequent on these slow silicate mineral dissolution rates, which are the source of Ca²⁺ and HCO₃⁻ ions.

The incongruent dissolution is reflected in the non-stoichiometric release of Al³⁺ and SiO₂ to solution. Measured Al concentrations (~3–6 μmol/L) are several orders of magnitude below those thought to inhibit feldspar dissolution (e.g. Amrhein and Suarez, 1992). Measured

silica concentrations (~0.1–1 mmol/L) decrease as fluid flows, shallows and cools towards the crest of the anticline and the concentration–temperature relationship is consistent with buffering of silica concentrations by a silica phase with a solubility close to that of chalcedony. Recent laboratory experiments have shown that the growth of silica surface layers during mineral (e.g. Hellmann et al., 2012 and references therein) and glass (see Gin et al., 2008 and references therein) dissolution through interfacial dissolution–reprecipitation can inhibit dissolution rates (Béarat et al., 2006; Daval et al., 2011, 2013), such that the mineral dissolution rate may ultimately be controlled by the saturation state of the fluid with respect to the silica layer, its dissolution rate and passivating properties. Amorphous silica layers have been observed on naturally weathered feldspar surfaces from the Navajo Sandstone (Zhu et al., 2006), but the feldspar dissolution rates of Kampman et al. (2009) are independent of silica saturation state and most likely not determined by the presence of such a silica layer, or at least not in a simple way. This is consistent with the work of Jordan et al. (1999), which suggested that typical feldspar silica surface layers are not passivating (but see Berger et al., 2002) and only become passivating due to the incorporation of trace metals such as Fe³⁺, under fairly oxidising conditions (Daval, pers. comm. 2013). These findings point to the important coupling of fluid–mineral reactions in geological reservoirs. The dependency of silicate mineral dissolution rate on the thermodynamic departure from equilibrium goes some way to explaining the long established discrepancy between fluid–mineral reaction rates measured in the laboratory and those measured in the field (e.g. White and Brantley, 2003), with important implications for the rates of potentially CO₂ stabilising reactions in geological storage sites.

5.3.4. Green River exhumed reservoir

The Entrada Sandstone is exhumed along the Salt Wash Graben at Green River where it exhibits spectacular large-scale bleaching (Fig. 21) which Wigley et al. (2012) interpret to result from the flow of CO₂-rich brines. The evidence for CO₂-rich fluids being involved includes the presence of CO₂ with minor methane in fluid-inclusions, the oxygen and carbon isotopic compositions of secondary carbonates which are similar to those in the active system and markedly different from hydrocarbon related bleaching elsewhere in the Paradox Basin (Chan et al., 2000; Beitler et al., 2005; Eichhubl et al., 2009) and the restriction of the bleaching to the base of the formation consistent with denser CO₂-bearing brines. The flow of the CO₂-charged brines, containing small quantities of CH₄, dissolved haematite grain coatings by a reaction with the stoichiometry (Wigley et al., 2012),



The CO₂ promoted reaction fronts are demarked by sharp mineralogical fronts where haematite and silicate minerals are dissolved from rock that has interacted with the CO₂-rich brine (Fig. 22). The km-scale lenticular topology of the bleached zone reflects propagation of the reaction front laterally by advection of the dense CO₂-saturated brine as a gravity current, driven in the direction of regional groundwater flow parallel to the fault, and propagation of the upper boundary by a rate controlled by the upward diffusion of the CO₂. Wigley et al. (2013a) have shown that haematite dissolution rates were inhibited by, and coupled to, the more sluggish silicate mineral dissolution rates close to thermodynamic equilibrium and at low rates of fluid transport. Wigley et al. (2013b) have shown that as pH was buffered across mineral reaction fronts, potentially harmful trace metals mobilised by the CO₂-charged fluids were subsequently re-deposited in secondary Fe-oxide and Fe-rich dolomite that grow at the reaction front (Fig. 23–24). Such exhumed CO₂ reservoirs (see also Loope et al., 2010; Potter-McIntyre et al., 2013) provide invaluable insight into the coupled nature of fluid transport and mineral reaction and reveal reactive-transport processes not yet considered by modelling studies.

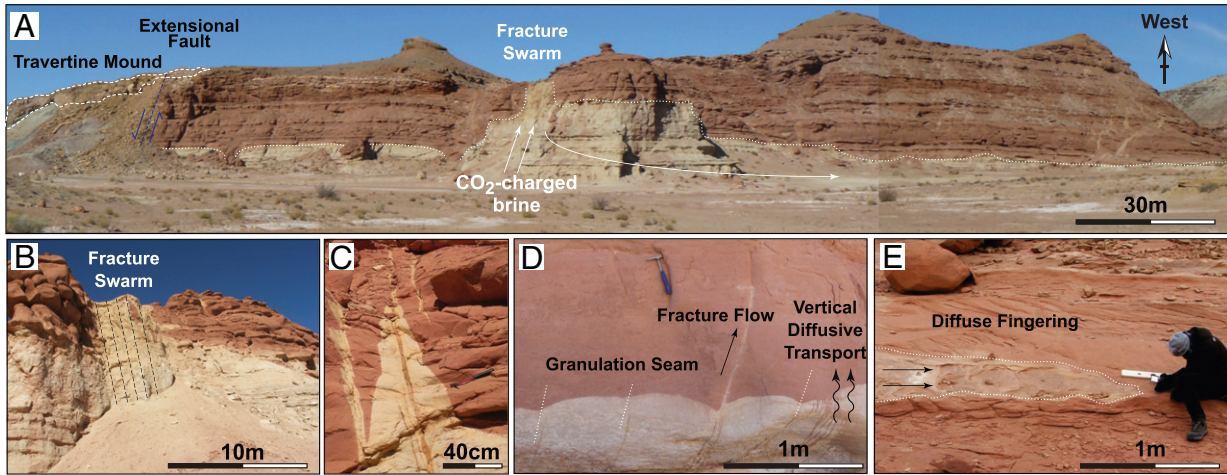


Fig. 21. Field photographs showing bleached portions of the Entrada Sandstone, Salt Wash Graben, Green River, Utah. (A) Shows the outcrop of the northerly major normal fault of the graben, dipping to the south (left of view) and the extensive zone of sandstone bleaching at the base of the Entrada Sandstone. The bleached contact dips steeply to the north and shallowly to the east forming a lenticular zone running parallel to the broadly east–west running fault. The bleached zone was fed by inflow of CO₂-charged fluid through a fracture swarm, close up pictured in (B). (C) The bleached contact is elevated where fluids flow up and along fractures, which frequently contain Fe-oxide remineralisation at their cores. (D) The bleached contact is sharp and the topology of the surface is sensitive to extreme changes in porosity and tortuosity such as those developed in granulation seams and in open fractures. (E) Towards the east the bleached zone dies out in a series of diffuse horizontal fingers of bleached sandstone.

6. Conclusions and future work

Remote imaging of large-scale commercial CO₂ projects attests to the complexities of macroscopic CO₂ flow during geological CO₂ storage but does not provide adequate constraints on the nature or rates of the fluid–fluid and fluid–mineral interactions, required to predict trapping of the injected CO₂. Direct sampling of small-scale CO₂ injection experiments and CO₂-EOR projects provide important constraints on the flow

and dissolution of the CO₂, and the subsequent CO₂–fluid–mineral reactions. Measurements of in-situ dissolved CO₂ concentrations and elemental and isotopic tracers suggest that fluids in contact with the migrating CO₂ plume rapidly saturate with CO₂(aq), and the total mass of CO₂ dissolved is likely enhanced by fingering of the CO₂ front on lengths scales controlled by the geological heterogeneity of the reservoir (i.e. bedding scales of ~10 to 100 cm), and by convective mixing of dense CO₂ saturated brines. The rapid dissolution of carbonate

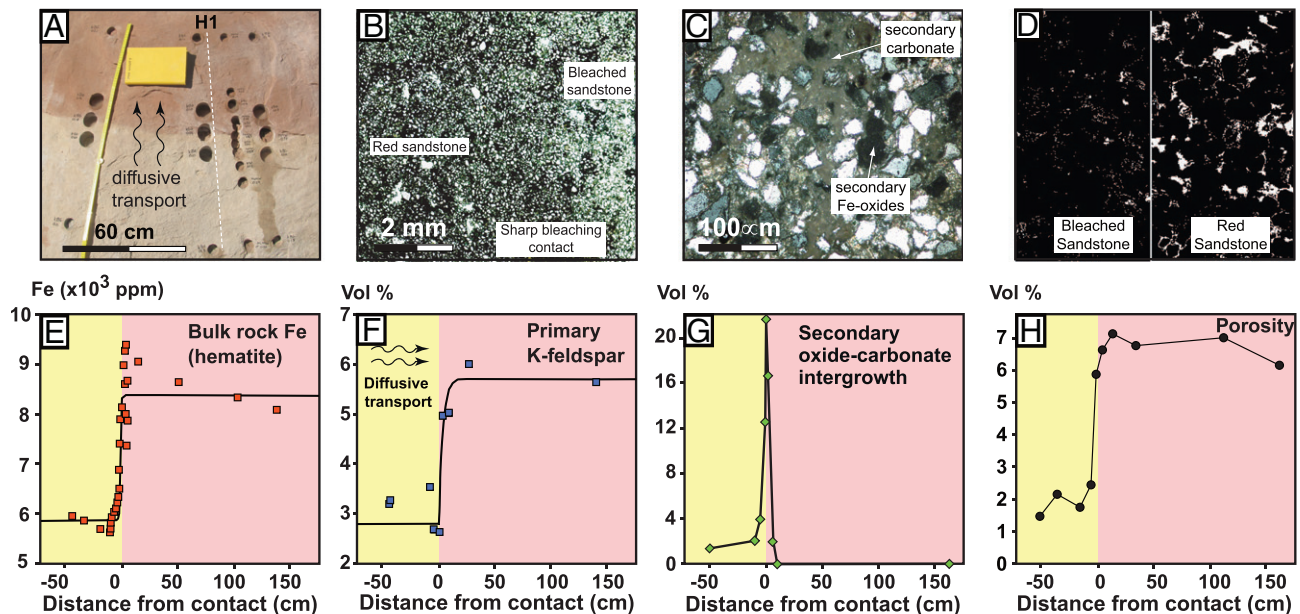


Fig. 22. (A) Field photograph showing sample transect H1 of core plugs drilled from outcrops of the bleached and red Entrada Sandstones, analysed for geochemical and mineralogical profiles. (B) Thin-section micrograph showing removal of haematite grain coatings from the bleached sandstone, and the sharp bleached–unbleached contact. (C) Close-up micrograph showing the precipitation of carbonate and Fe-oxide intergrowths at the bleached–unbleached contact. (D) Rasterised BSE micrographs showing differences in porosity between the bleached and unaltered sediment. Geochemical and mineralogical profiles across the bleached–unbleached sandstone contact showing (E) Mobilisation of Fe³⁺, in the form of haematite grain coatings, from the bleached sandstones and the redeposition of Fe on the reaction, resulting in high Fe contents at the front, relative to the background concentrations in the sediment. (F) Acidity generated from the dissociation of the CO₂ dissolved silicate grains in the sediment, predominantly K-feldspar, resulting in step changes in mineral concentrations across the reaction front. (G) Buffering of fluid pH across the front, and the generation of alkalinity and cations by mineral dissolution produced a spike in carbonate and Fe-oxide mineral saturation at the reaction front driving the precipitation of carbonate and Fe-oxide minerals at the front. (H) The precipitation of clay minerals (kaolinite and illite–smectite) from the incongruent dissolution of feldspars clogs pores and reduces porosity in the bleached sediment. (Redrawn from and using data in Wigley et al., 2013a).

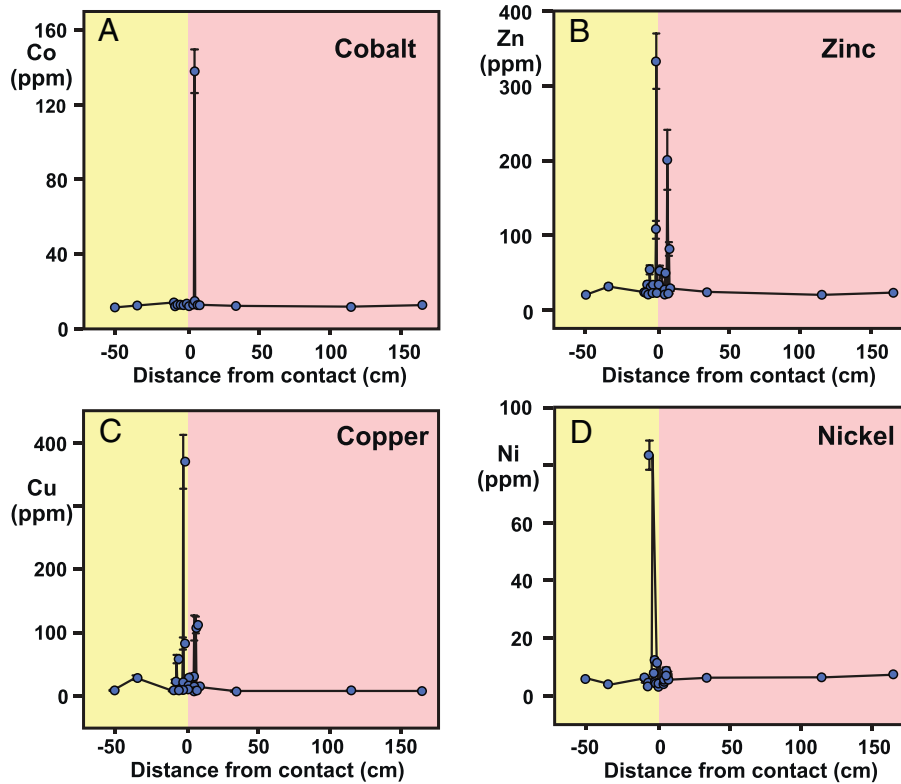


Fig. 23. Geochemical profiles through the bleached-unbleached Entrada Sandstone showing trace element enrichment at the contact where elements mobilised by the CO₂-rich fluids are redeposited into and onto the surface of carbonate and Fe-oxides minerals that grow at the reaction front (Drawn using data in Wigley et al., 2013b). Fluid–mineral reactions buffer pH across the reaction front driving mineral precipitation and lowering the solubility of trace elements which are soluble at acidic pH's but become increasingly insoluble at circum-neutral pH's. The figure shows a selection of the elements (Co, Zn, Cu, Ni) analysed and similar enrichments are observed in other elements including As, Pb and Cd.

and Fe-oxide minerals, in the initially low pH ~3.5 fluid, is observed in many experiments and in a variety of reservoir lithologies. Dissolution of soluble carbonate and oxide minerals buffers fluid to pH ~4.5 and accounts for the majority of early alkalinity production (up to ~50 mmol/L), quickly driving fluids to carbonate mineral saturation. Observations from the Salt Creek EOR project, where the reservoir is rich in feldspars and micas, suggest that dissolution of silicate minerals can generate further alkalinity with total alkalinity approaching ~100 mmol/L. Observations from CO₂-EOR projects and natural CO₂ reservoirs suggest that the fluids remain buffered at carbonate mineral saturation by calcite, oxide and silicate mineral dissolution and the redeposition of less soluble Fe–Ca–Mg carbonates.

In the long-term carbonate mineral deposition may be rate limited by the balance between fluid transport and flow and dissolution of the CO₂, and by sluggish surface-controlled silicate mineral dissolution close to thermodynamic equilibrium. More significant carbonate deposition is likely to occur where CO₂-saturated fluids migrate vertically in faults and fractures, to lower pressures, degassing CO₂ driving carbonate mineral supersaturation and rapid deposition rates, which may ultimately self-seal such leakage pathways. Carbonation of reactive phyllosilicate rich caprocks has been observed during scientific drilling of a natural CO₂ accumulation, where penetration by diffusion of CO₂-rich fluids has generated fluid–mineral reaction fronts which may impact on the long term integrity of the seal.

Laboratory experiments predict the mobilisation of harmful trace element and organic contaminants, which is observed during CO₂ injection experiments but typically not to harmful concentrations and observations from natural analogues suggest trace element contaminants may be immobilised as pH changes across mineral reaction fronts.

Further small-scale CO₂-injection experiments are required to improve understanding of the coupled nature of CO₂ flow, dissolution and mineral–fluid reactions. The mobility of tracers and isotopes depends on two phase flow and fluid–fluid dissolution as well as on diffusive exchange. More detailed studies will enable inversion of such measurements to constrain the complexities of CO₂ flow and the efficacy of CO₂ dissolution and capillary trapping. The results of such studies could then be used to further refine numerical models of two-phase flow processes, such as CO₂-brine fingering, determine the efficacy of CO₂ trapping.

The measurement of in-situ pH and the recovery of samples at reservoir pressure on which pH and CO₂ saturation can be determined at surface, are crucial to successfully measure and interpret the progress of CO₂ dissolution and fluid–mineral reactions. The measurement of

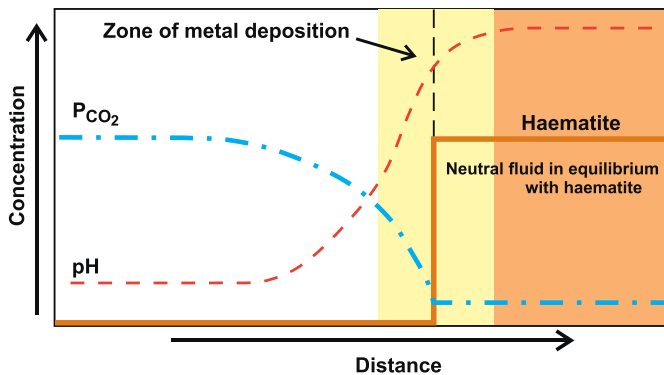


Fig. 24. Conceptual model of the evolution of fluid CO₂ content, bicarbonate concentration and pH across the fluid–mineral reaction fronts and the correspondingly stabilisation of carbonate and Fe-oxide minerals and trace metal redeposition at the reaction front.

in-situ redox state will also be crucial to the successful interpretation and prediction of mineral stability and trace element contaminant mobilisation from mineral dissolution or surface desorption. The measurement of organic and trace element concentrations and partitioning between brine and CO₂ phases during injection experiments is also required to better predict future contaminant mobilisation and transport. Interpreting the results of future fluid sampling projects will be significantly enhanced by detailed studies of reservoir petrology and mineral surface properties (BET; silica coatings etc). Accurate modelling of CO₂–fluid–mineral reactions and the progress of ionic and mineral trapping requires more laboratory measurements of mineral dissolution rate constants and mineral solubilities, especially for Fe–Mn oxides and oxyhydroxides and Fe–Ca–Mg carbonate minerals and their solid solutions. Ultimately, small-scale CO₂-injection experiments and studies of natural CO₂ reservoirs provide the best constraints on the length-scales and the coupling of the crucial physical and geochemical processes that determine the long-term fate of CO₂ in anthropogenic storage sites.

Acknowledgements

Research into Geological Storage in Cambridge is funded by the UK Natural Environment Research Council grant NE/F004699/1 through the CRIUS consortium and the UK Department of Energy and Climate Change. Niko Kampman acknowledges financial support from Shell Global Solutions International. The authors wish to thank the scientists of the CRIUS consortium for many years of useful discussion that greatly improved the quality of this manuscript. This manuscript benefited considerably from insightful comment and review from Bruce Yardley and Damien Daval, for which the authors are grateful. The authors would like to thank Susan Hovorka and Youssef Kharaka for supplying the Frio data.

References

- Alfredsson, H.A., Wolff-Boenisch, D., Stefánsson, A., 2011. CO₂ sequestration in basaltic rocks in Iceland: development of a piston-type downhole sampler for CO₂ rich fluids and tracers. *Energy Procedia* 4, 3510–3517.
- Allis, R., Bergfeld, D., Moore, J., McClure, K., Morgan, C., Chidsey, T., Heath, J., McPherson, B., 2001. Natural CO₂ reservoirs on the Colorado Plateau and Southern Rocky Mountains: candidates for CO₂ sequestration. *Proc. nat. conf. on carbon sequestration*.
- Alvarado, V., Manrique, E., 2010. Enhanced oil recovery: an update review. *Energ.* 3, 1529–1575.
- Amrhein, C., Suarez, D., 1992. Some factors affecting the dissolution kinetics of anorthite at 25 °C. *Geochim. Cosmochim. Acta* 56 (5), 1815–1826.
- André, L., Azaroual, M., Menjot, A., 2010. Numerical simulations of the thermal impact of supercritical CO₂ injection on chemical reactivity in a carbonate saline reservoir. *Transp. Porous Media* 82 (1), 247–274.
- Apps, J.A., Zheng, L., Zhang, Y., Xu, T., Birkholzer, J.T., 2010. Evaluation of potential changes in groundwater quality in response to CO₂ leakage from deep geologic storage. *Transp. Porous Media* 82 (1), 215–246.
- Arts, R., Eiken, O., Chadwick, A., Zweigel, P., Van der Meer, L., Zinszner, B., 2004. Monitoring of CO₂ injected at Sleipner using time-lapse seismic data. *Energy* 29 (9–10), 1383–1392.
- Arvidson, R.S., Lutge, A., 2010. Mineral dissolution kinetics as a function of distance from equilibrium – new experimental results. *Chem. Geol.* 269 (1–2), 79–88.
- Assayag, N., Bickle, M., Kampman, N., Becker, J., 2009a. Carbon isotopic constraints on CO₂ degassing in cold-water Geysers, Green River, Utah. *Energy Procedia* 1 (1), 2361–2366.
- Assayag, N., Matter, J., Ader, M., Goldberg, D., Agrinier, P., 2009b. Water–rock interactions during a CO₂ injection field-test: implications on host rock dissolution and alteration effects. *Chem. Geol.* 262, 406–414.
- Audigane, P., Gaus, I., Czernichowski-Lauriol, I., Pruess, K., Xu, T., 2007. Two-dimensional reactive transport modeling of CO₂ injection in a saline aquifer at the Sleipner site, North Sea. *Am. J. Sci.* 307 (7), 974–1008.
- Bachu, S., Bennion, D.B., 2008. Effects of in-situ conditions on relative permeability characteristics of CO₂–brine systems. *Environ. Geol.* 5 (8), 1707–1722.
- Bachu, S., Bennion, D.B., 2009. Dependence of CO₂–brine interfacial tension on aquifer pressure, temperature and water salinity. *Energy Procedia* 1 (1), 3157–3164.
- Backhaus, S., Turitsyn, K., Ecke, R., 2011. Convective instability and mass transport of diffusion layers in a Hele–Shaw geometry. *Phys. Rev. Lett.* 106 (10), 104501.
- Baines, S.J., Worden, R.H., 2004. The long-term fate of CO₂ in the subsurface: natural analogues for CO₂ storage. *Geol. Soc. Lond. Spec. Publ.* 233 (1), 59–85.
- Baker, J.C., Bai, G.P., Hamilton, P.J., Golding, S.D., Keene, J.B., 1995. Continental-scale magmatic carbon dioxide seepage recorded by dawsonite in the Bowen–Gunnedah–Sydney basin system, eastern Australia. *J. Sediment. Res.* 65 (3).
- Ballentine, C.J., Schoell, M., Coleman, D., Cain, B.A., 2001. 300-Myr-old magmatic CO₂ in natural gas reservoirs of the west Texas Permian basin. *Nature* 409 (6818), 327–331.
- Béarat, H., Mckelvy, M.J., Chizmeshya, A.V.G., Gormley, D., Nunez, R., Carpenter, R.W., Squires, K., Wolf, G.H., 2006. Carbon sequestration via aqueous olivine mineral carbonation: role of passivating layer formation. *Environ. Sci. Technol.* 40 (15), 4802–4808.
- Bearup, L.A., Navarre-Sitchler, A.K., Maxwell, R.M., McCray, J.E., 2012. Kinetic metal release from competing processes in aquifers. *Environ. Sci. Technol.* 46 (12), 6539–6547.
- Beig, M., Lüttge, A., 2006. Albitic dissolution kinetics as a function of distance from equilibrium: implications for natural feldspar weathering. *Geochim. Cosmochim. Acta* 70 (6), 1402–1420.
- Beitler, B., Parry, W., Chan, M., 2005. Fingerprints of fluid flow: chemical diagenetic history of the Jurassic Navajo Sandstone, southern Utah, USA. *J. Sediment. Res.* 75 (4), 547.
- Bénézet, P., Palmer, D.A., Anovitz, L.M., Horita, J., 2007. Dawsonite synthesis and reevaluation of its thermodynamic properties from solubility measurements: implications for mineral trapping of CO₂. *Geochim. Cosmochim. Acta* 71 (18), 4438–4455.
- Berg, A., Banwart, S., 2000. Carbon dioxide mediated dissolution of Ca-feldspar: implications for silicate weathering. *Chem. Geol.* 163 (1–4), 25–42.
- Berger, G., Cadore, E., Schott, J., Dove, P.M., 1994. Dissolution rate of quartz in lead and sodium electrolyte solutions between 25 and 300 °C: effect of the nature of surface complexes and reaction affinity. *Geochim. Cosmochim. Acta* 58 (2), 541–551.
- Berger, G., Beaufort, D., Lachapagne, J.C., 2002. Experimental dissolution of sanidine under hydrothermal conditions: mechanism and rate. *Am. J. Sci.* 302 (8), 663–685.
- Bertier, P., Swennen, R., Laenen, B., Lagrou, D., Dreesen, R., 2006. Experimental identification of CO₂–water–rock interactions caused by sequestration of CO₂ in Westphalian and Buntsandstein sandstones of the Campine Basin (NE-Belgium). *J. Geochem. Explor.* 89 (1), 10–14.
- Bickle, M., Chadwick, A., Huppert, H.E., Hallworth, M., Lyle, S., 2007. Modelling carbon dioxide accumulation at Sleipner: implications for underground carbon storage. *Earth Planet. Sci. Lett.* 255 (1–2), 164–176.
- Bickle, M., Kampman, N., Wigley, M., 2013. Natural analogues. *Rev. Mineral. Geochem.* 77 (1), 15–71.
- Bildstein, O., Kervévan, C., Lagneau, V., Delaplace, P., Crédoz, A., Audigane, P., Jullien, M., 2010. Integrative modeling of caprock integrity in the context of CO₂ storage: evaluation of transport and geochemical properties and impact on performance and safety assessment. *Oil Gas Sci. Technol.–Revue de l'Institut Français du Pétrole* 65 (3), 485–502.
- Bjørlykke, K., Gran, K., 1994. Salinity variations in North Sea formation waters: implications for large-scale fluid movements. *Mar. Pet. Geol.* 11 (1), 5–9.
- Blake, R., Walter, L., 1999. Kinetics of feldspar and quartz dissolution at 70–80 °C and near-neutral pH: effects of organic acids and NaCl. *Geochim. Cosmochim. Acta* 63 (13–14), 2043–2059.
- Boait, F.C., White, N.J., Bickle, M.J., Chadwick, R.A., Neufeld, J.A., Huppert, H.E., 2012. Spatial and temporal evolution of injected CO₂ at the Sleipner Field, North Sea. *J. Geophys. Res.* 117 (B3), B03309.
- Boreham, C., Underschlutz, J., Stalker, L., Kirste, D., Freifele, B., Jenkins, C., Ennis-King, J., 2011. Monitoring of CO₂ storage in a depleted natural gas reservoir: gas geochemistry from the CO2CRC Otway Project, Australia. *Int. J. Greenhouse Gas Control* 5, 1039–1054.
- Bottinga, Y., Craig, H., 1968. High temperature liquid–vapor fractionation factors for H₂O–HDO–H₂O¹⁸. *Trans. Am. Geophys. Union* 49 (1), 356–360.
- Bowker, K.A., Shuler, P., 1991. Carbon dioxide injection and resultant alteration of the Weber Sandstone, Rangely Field, Colorado (1). *AAPG Bull.* 75 (9), 1489–1499.
- Brown, G.E., Calas, G., 2012. Section 16 Mineral weathering as a molecular-level mineral-surface process. *Geochem. Perspect.* 1 (4–5), 650–662.
- Burant, A., Lowry, G.V., Karamalidis, A.K., 2013. Partitioning behavior of organic contaminants in carbon storage environments: a critical review. *Environ. Sci. Technol.* 47 (1), 37–54.
- Burch, T., Nagy, K., Lasaga, A., 1993. Free energy dependence of albitic dissolution kinetics at 80 °C and pH 8.8. *Chem. Geol.* 105 (1), 137–162.
- Burnside, N., 2010. U–Th Dating of Travertine on the Colorado Plateau: Implications for the Leakage of Geologically Stored CO₂. University of Glasgow, UK.
- Burnside, N., Shipton, Z., Dockrill, B., Ellam, R.M., 2013. Man-made versus natural CO₂ leakage: a 400 k.y. history of an analogue for engineered geological storage of CO₂. *Geology* 41, 471–474.
- Cama, J., Ganor, J., Ayora, C., Lasaga, C.A., 2000. Smectite dissolution kinetics at 80 °C and pH 8.8. *Geochim. Cosmochim. Acta* 64 (15), 2701–2717.
- Carey, J.W., Wigand, M., Chipera, S.J., WoldeGabriel, G., Pawar, R., Lichtner, P.C., Guthrie Jr., G.D., 2007. Analysis and performance of oil well cement with 30 years of CO₂ exposure from the SACROC Unit, West Texas, USA. *Int. J. Greenhouse Gas Control* 1 (1), 75–85.
- Carroll, S.A., Knauss, K.G., 2005. Dependence of labradorite dissolution kinetics on CO₂(aq), Al(aq), and temperature. *Chem. Geol.* 217, 213–225.
- Carroll, S., McNab, W., Torres, S., 2011. Experimental study of cement–sandstone/shale–brine–CO₂ interactions. *Geochem. Trans.* 12 (1), 9.
- Chadwick, R.A., Noy, D.J., 2010. History-matching flow simulations and time-lapse seismic data from the Sleipner CO₂ plume. Geological Society, London, Petroleum Geology Conference series, 7, pp. 1171–1182.
- Chadwick, A., Arts, R., Bernstone, C., May, F., Thibeau, S., Zweigel, P., 2008. Best practice for the storage of CO₂ in saline aquifers—observations and guidelines from the SACS and CO2STORE projects. British Geological Survey, Keyworth, Nottingham, Occasional Publication 14, 267 p.
- Chan, M., Parry, W., Bowman, J., 2000. Diagenetic hematite and manganese oxides and fault-related fluid flow in Jurassic sandstones, southeastern Utah. *AAPG Bull.* 84 (9), 1281.

- Corvisier, J., Brunet, F., Fabbri, A., Bernard, S., Findling, N., Rimmelé, G., Goffé, B., 2010. Raman mapping and numerical simulation of calcium carbonates distribution in experimentally carbonated Portland-cement cores. *Eur. J. Mineral.* 22 (1), 63–74.
- Creodo, A., Bildstein, O., Jullien, M., Raynal, J., Pétronin, J.-C., Lillo, M., Pozo, C., Geniaut, G., 2009. Experimental and modeling study of geochemical reactivity between clayey caprocks and CO₂ in geological storage conditions. *Energy Procedia* 1, 3445–3452.
- Daley, T., Freifeld, B., Ajo-Franklin, J.B., Doughty, C., Benson, S.M., 2007a. Frio II Brine Pilot: Report on GEOSEQ Activities. Lawrence Berkeley National Lab.
- Daley, T.M., Solbau, R.D., Ajo-Franklin, J.B., Benson, S.M., 2007b. Continuous active-source seismic monitoring of injection in a brine aquifer. *Geophysics* 72 (5), A57–A61.
- Dashtgard, S.E., Buschkuehle, M.B.E., Fairgrieve, B., Berhane, H., 2008. Geological characterization and potential for carbon dioxide (CO₂) enhanced oil recovery in the Cardium Formation, central Pembina Field. Alberta. *Bull. Can. Petrol. Geol.* 56 (2), 147–164.
- Daval, D., Martinez, I., Guigner, J.M., Hellmann, R., Corvisier, J., Findling, N., Guyot, F., 2009. Mechanism of wollastonite formation deduced from micro- to nanometer length scale observations. *Am. Mineral.* 94 (11–12), 1707–1726.
- Daval, D., Sissmann, O., Menguy, N., Saldi, G.D., Guyot, F., Martinez, I., Hellmann, R., 2011. Influence of amorphous silica layer formation on the dissolution rate of olivine at 90 °C and elevated pCO₂. *Chem. Geol.* 284 (1–2), 193–209.
- Daval, D., Hellmann, R., Saldi, G.D., Wirth, R., Knauss, K.G., 2013. Linking nm-scale measurements of the anisotropy of silicate surface reactivity to macroscopic dissolution rate laws: new insights based on diopside. *Geochim. Cosmochim. Acta* 0.
- DECC (UK Department of Energy and Climate Change), 2012. CCS Roadmap Storage Strategy. <http://www.decc.gov.uk/en/content/cms/emissions/ccs/ccs.aspx>.
- Deremble, L., Loizzo, M., Huet, B., Lecampion, B., Quesada, D., 2011. Stability of a leakage pathway in a cemented annulus. *Energy Procedia* 4, 5283–5290.
- Dockrill, B., Shipton, Z.K., 2010. Structural controls on leakage from a natural CO₂ geologic storage site: Central Utah, U.S.A. *J. Struct. Geol.* 32 (11), 1768–1782.
- Doughty, C., Freifeld, B.M., Trautz, R.C., 2008. Site characterization for CO₂ geologic storage and vice versa: the Frio brine pilot, Texas, USA as a case study. *Environ. Geol.* 54, 1635–1656.
- Drever, J.L., 1982. *Geochemistry of Natural Waters*. Prentice-Hall, Inc, Englewood Cliffs New Jersey 388.
- Drever, J., Stillings, L., 1997. The role of organic acids in mineral weathering. *Colloids Surf. A Physicochem. Eng. Asp.* 120 (1), 167–181.
- Duan, Z., Sun, R., Zhu, C., Chou, I., 2006. An improved model for the calculation of CO₂ solubility in aqueous solutions containing Na⁺, K⁺, Ca²⁺, Mg²⁺, Cl⁻, and SO₄²⁻. *Mar. Chem.* 98 (2–4), 131–139.
- Dubacq, B., Bickle, M.J., Wigley, M., Kampman, N., Ballentine, C.J., Sherwood Lollar, B., 2012. Noble gas and carbon isotopic evidence for CO₂-driven silicate dissolution in a recent natural CO₂ field. *Earth Planet. Sci. Lett.* 341–344, 10–19.
- Dubacq, B., Bickle, M.J., Evans, K.A., 2013. An activity model for phase equilibria in the H₂O–CO₂–NaCl system. *Geochim. Cosmochim. Acta* 110, 229–252.
- Dusseault, M., Gray, M., Nawrocki, P., 2000. Why oilwells leak: cement behaviour and long-term consequences. Society of Petroleum Engineers International Oil and Gas Conference: Beijing (<http://www.onepetro.org/mslib/servlet/onepetroreview?id=00064733>).
- Eichhubl, P., Davatz, N.C., Becker, S.P., 2009. Structural and diagenetic control of fluid migration and cementation along the Moab fault, Utah. *AAPG Bull.* 93 (5), 653–681.
- Emberley, S., Hutcheon, I., Shevalier, M., Durocher, K., Perkins, E., 2004. Geochemical monitoring of Xuid-rock interaction and CO₂ storage at the Weyburn CO₂-injection enhanced oil recovery site, Saskatchewan, Canada. *Energy* 29, 1393–1401.
- Emberley, S., Hutcheon, I., Shevalier, M., Durocher, K., Mayer, B., Gunter, W.B., Perkins, E.H., 2005. Monitoring of fluid-rock interaction and CO₂ storage through produced fluid sampling at the Weyburn CO₂-injection enhanced oil recovery site, Saskatchewan, Canada. *Appl. Geochem.* 20, 1131–1157.
- Embid, E., Crossey, L., 2009. U-series dating, geochemistry, and geomorphic studies of travertines and springs of the Springville area, east-central Arizona, and tectonic implications. (PhD Thesis) University of New Mexico, Albuquerque.
- Ennis-King, J., Paterson, L., 2005. Role of convective mixing in the long-term storage of carbon dioxide in deep saline formations. *SPE J.* 10 (3).
- Espinoza, D.N., Santamarina, J.C., 2010. Water–CO₂-mineral systems: interfacial tension, contact angle, and diffusion—implications to CO₂ geological storage. *Water Resour. Res.* 46 (7), W07537.
- Fernandez-Martinez, A., Hu, Y., Lee, B., Jun, Y.-S., Waychunas, G.A., 2013. In situ determination of interfacial energies between heterogeneously nucleated CaCO₃ and quartz substrates: thermodynamics of CO₂ mineral trapping. *Environ. Sci. Technol.* 47, 102–109.
- Förster, A., Norden, B., Zinck-Jørgensen, K., Frykman, P., Kulenkampff, J., Spangenberg, E., Erzinger, J., Zimmer, M., Kopp, J., Borm, G., Juhlin, C., Cosma, C., Hurter, S., 2006. Baseline characterization of the CO₂SINK geological storage site at Ketzin, Germany. *Environ. Geosci.* 13 (3), 145–161.
- Franks, S.G., Forester, R.W., 1984. Relationships among secondary porosity, pore-fluid chemistry and carbon dioxide, Texas Gulf Coast Clastic diagenesis. *AAPG Mem.* 37, 63–79.
- Freifeld, B.M., Trautz, R.C., 2006. Real-time quadrupole mass spectrometer analysis of gas in borehole fluid samples acquired using the U-tube sampling methodology. *Geofluids* 6 (3), 217–224.
- Freifeld, B.M., Trautz, R.C., Kharaka, Y.K., Phelps, T.J., Myer, L.R., Hovorka, S.D., Collins, D.J., 2005. The U-tube: a novel system for acquiring borehole fluid samples from a deep geologic CO₂ sequestration experiment. *J. Geophys. Res.* 110 (B10), B10203.
- Freifeld, B.M., Finsterle, S., Onstott, T.C., Toole, P., Pratt, L.M., 2008. Ground surface temperature reconstructions: using in situ estimates for thermal conductivity acquired with a fiber-optic distributed thermal perturbation sensor. *Geophys. Res. Lett.* 35 (14), L14309.
- Freifeld, B.M., Daley, T.M., Hovorka, S.D., Hennings, J., Underschlutz, J., Sharma, S., 2009. Recent advances in well-based monitoring of CO₂ sequestration. *Energy Procedia* 1 (1), 2277–2284.
- Fritz, B., Clement, A., Montes-Hernandez, G., Noguera, C., 2013. Calcite formation by hydrothermal carbonation of portlandite: complementary insights from experiment and simulation. *CrystEngComm.* 15, 3392–3401.
- Frye, E., Bao, C., Li, L., Blumsack, S., 2012. Environmental controls of cadmium desorption during CO₂ leakage. *Environ. Sci. Technol.* 46 (8), 4388–4395.
- Gaus, I., 2010. Role and impact of CO₂–rock interactions during CO₂ storage in sedimentary rocks. *Int. J. Greenhouse Gas Control* 4, 73–89.
- Gaus, I., Azaroual, M., Czernichowski-Lauriol, I., 2005. Reactive transport modelling of the impact of CO₂ injection on the clayey cap rock at Sleipner (North Sea). *Chem. Geol.* 217 (3–4), 319–337.
- Gherardi, F., Xu, T., Pruess, K., 2007. Numerical modeling of self-limiting and self-enhancing caprock alteration induced by CO₂ storage in a depleted gas reservoir. *Chem. Geol.* 244 (1–2), 103–129.
- Gherardi, F., Audigane, P., Gaucher, E.C., 2012. Predicting long-term geochemical alteration of wellbore cement in a generic geological CO₂ confinement site: tackling a difficult reactive transport modeling challenge. *J. Hydrol.* 420–421, 340–359.
- Giese, R., Hennings, J., Lüth, S., Morozova, D., Schmidt-Hattenberger, C., Würdemann, H., Juhlin, C., 2009. Monitoring at the CO₂ SINK site: a concept integrating geophysics, geochemistry and microbiology. *Energy Procedia* 1 (1), 2251–2259.
- Gilfillan, S., Ballentine, C.J., Holland, G., Blagburn, D., Lollar, B.S., Stevens, S., Cassidy, M., 2008. The noble gas geochemistry of natural CO₂ gas reservoirs from the Colorado Plateau and Rocky Mountain provinces, USA. *Geochim. Cosmochim. Acta* 72 (4), 1174–1198.
- Gilfillan, S.M.V., Lollar, B.S., Holland, G., Blagburn, D., Stevens, S., Schoell, M., Cassidy, M., Ding, Z., Zhou, Z., Lacrampe-Couloume, G., Ballentine, C.J., 2009. Solubility trapping in formation water as dominant CO₂ sink in natural gas fields. *Nature* 458 (7238), 614–618.
- Gilfillan, S., Wilkinson, M., Haszeldine, R.S., Shipton, Z.K., Nelson, S.T., Poreda, R.J., 2011. He and Ne as tracers of natural CO₂ migration up a fault from a deep reservoir. *Int. J. Greenhouse Gas Control* 5, 1507–1516.
- Guin, S., Jégou, C., Frugier, P., Minet, Y., 2008. Theoretical consideration on the application of the Aagaard–Helgeson rate law to the dissolution of silicate minerals and glasses. *Chem. Geol.* 255 (1–2), 14–24.
- Gislason, S.R., Wolff-Boenisch, D., Stefansson, A., Oelkers, E.H., Gunnlaugsson, E., Sigurdardottir, H., Fridriksson, T., 2010. Mineral sequestration of carbon dioxide in basalt: a pre-injection overview of the CarbFix project. *Int. J. Greenhouse Gas Control* 4 (3), 537–545.
- Golding, M.J., Neufeld, J.A., Hesse, M.A., Huppert, H.E., 2011. Two-phase gravity currents in porous media. *J. Fluid Mech.* 678 (1), 248–270.
- Gouveia, F., Friedmann, S., 2006. Timing and Prediction of CO₂ Eruptions from Crystal Geyser UT. United States. Dept. of Energy.
- Gouveia, F., Johnson, M., Leif, R., Friedmann, S., 2005. Aerometric measurement and modeling of the mass of CO₂ emissions from Crystal Geyser, Utah. UCRL-TR-211870, Lawrence Livermore National Lab. Livermore, CA (USA).
- Gratier, J.P., Frery, E., Deschamps, P., Royne, A., Renard, F., Dysthe, D., Hamelin, B., 2012. How travertine veins grow from top to bottom and lift the rocks above them: the effect of crystallization force. *Geology* 40 (11), 1015–1018.
- Han, W.S., Kim, K.Y., Park, E., McPherson, B.J., Lee, S.Y., Park, M.H., 2012. Modeling of spatiotemporal thermal response to CO₂ injection in saline formations: interpretation for monitoring. *Transp. Porous Media* 93 (3), 381–399.
- Han, W.S., Lu, M., McPherson, B.J., Keating, E.H., Moore, J., Park, E., Watson, Z.T., Jung, N.-H., 2013. Characteristics of CO₂-driven cold-water geyser, Crystal Geyser in Utah: experimental observation and mechanism analyses. *Geofluids* 13 (3), 283–297.
- Hanchen, M., Prigiobbe, V., Storti, G., Seward, T.M., M., M., 2006. Dissolution kinetics of forsterite olivine at 90–150 °C. *Geochim. Cosmochim. Acta* 70, 4403–4416.
- Haszeldine, R.S., Quinn, O., England, G., Wilkinson, M., Shipton, Z.K., Evans, J.P., Graham, C.M., 2005. Natural geochemical analogues for carbon dioxide storage in deep geological porous reservoirs, a United Kingdom perspective. *Oil Gas Sci. Technol.* 60 (1), 33–49.
- Heath, J., 2004. Hydrogeochemical Characterization of Leaking Carbon Dioxide-Charged Fault Zones in East-Central Utah. Utah State University, USA.
- Heinmann, N., Wilkinson, M., Haszeldine, S., Fallick, A., Pickup, G., 2013. CO₂ sequestration in a UK North Sea analogue for geological carbon storage. *Geology* 41 (4).
- Hellevang, H., Aagaard, P., Oelkers, E.H., Kvamme, B., 2005. Can dawsonite permanently trap CO₂? *Environ. Sci. Technol.* 39 (21), 8281–8287.
- Hellevang, H., Pham, V.T., Aagaard, P., 2013. Kinetic modelling of CO₂–water–rock interactions. *Int. J. Greenhouse Gas Control* 15, 3–15.
- Hellmann, R., Tisserand, D., 2006. Dissolution kinetics as a function of the Gibbs free energy of reaction: an experimental study based on albite feldspar. *Geochim. Cosmochim. Acta* 70 (2), 364–383.
- Hellmann, R., Pénissot, J., Hervig, R., Thomassin, J., Abrioux, M., 2003. An EFTEM/HRTEM high-resolution study of the near surface of labradorite feldspar altered at acid pH: evidence for interfacial dissolution–reprecipitation. *Phys. Chem. Miner.* 30 (4), 192–197.
- Hellmann, R., Daval, D., Tisserand, D., 2010. The dependence of albite feldspar dissolution kinetics on fluid saturation state at acid and basic pH: progress towards a universal relation. *Compt. Rendus Geosci.* 342 (7–8), 676–684.
- Hellmann, R., Wirth, R., Daval, D., Barnes, J.P., Pénissot, J.M., Tisserand, D., Hervig, R.L., 2012. Unifying natural and laboratory chemical weathering with interfacial dissolution–

- reprecipitation: a study based on the nanometer-scale chemistry of fluid-silicate interfaces. *Chem. Geol.* 294–295, 203–216.
- Hendriks, C., Graus, W., Van Bergen, F., 2004. Global Carbon Dioxide Storage Potential and Costs.
- Hesse, M., Orr, F., Tchelepi, H., 2008. Gravity currents with residual trapping. *J. Fluid Mech.* 611 (1), 35–60.
- Holland, G., Gilfillan, S., 2012. Application of noble gases to the viability of CO₂ storage. *The Noble Gases as Geochemical Tracers*. Springer (177 pp.).
- Homsy, G., 1987. Viscous fingering in porous media. *Annu. Rev. Fluid Mech.* 19 (1), 271–311.
- Hood, J., Patterson, D., 1984. Bedrock aquifers in the northern San Rafael Swell area. Utah, with special emphasis on the Navajo Sandstone. State of Utah Department of Natural Resources Technical, Publication, 78, p. 128.
- Hosa, A., Esentia, M., Stewart, J., Haszeldine, S., 2011. Injection of CO₂ into saline formations: benchmarking worldwide projects. *Chem. Eng. Res. Des.* 89 (9), 1855.
- Houston, S., Yardley, B., Smalley, C., Collins, I., 2007. Rapid fluid–rock interactions in oilfield reservoirs. *Geology* 35, 1143–1146.
- Hövelmann, J., Austrheim, H., Jamtveit, B., 2012. Microstructure and porosity evolution during experimental carbonation of a natural peridotite. *Chem. Geol.* 334, 254–265.
- Hovorka, S.D., Benson, S.M., Doughty, C., Freifeld, B.M., Sakurai, S., Daley, T.M., Kharaka, Y.K., Holtz, M., Trautz, R.C., Nance, S., Myer, L.R., Knauss, K.G., 2006. Measuring permanence of CO₂ storage in saline formations: the Frio experiment. *Environ. Geosci.* 13 (2), 105.
- Hovorka, S.D., Meckel, T.A., Trevino, R.H., Lu, J., Nicot, J.-N., Choi, J.-W., David, Freema, D., Cook, P., Daley, T.M., Ajo-Franklin, J.B., Freifeld, B.M., Doughty, C., Carrigan, C.R., La Brecque, D., Kharaka, Y.K., Thordsen, J.J., Phelps, T.J., Yang, C., Romanak, K.D., Zhang, T., Holt, R.M., Lindler, J.S., Butsch, R.J., 2011. Monitoring a large volume CO₂ injection: year two results from SECARB project at Denbury's Cranfield, Mississippi, USA. *Energy Procedia* 4, 3478–3485.
- Huerta, N.J., Hesse, M.A., Bryant, S.L., Strazisar, B.R., Lopano, C.L., 2012. Experimental evidence for self-limiting reactive flow through a fractured cement core: implications for time-dependent wellbore leakage. *Environ. Sci. Technol.* 47 (1), 269–275.
- Iyer, K., Jamtveit, B., Mathiesen, J., Malthe-Sorensen, A., Feder, J., 2008. Reaction-assisted hierarchical fracturing during serpentinization. *Earth Planet. Sci. Lett.* 267 (3–4), 503–516.
- Jacob, B., 1972. *Dynamics of Fluids in Porous Media* (New York).
- Jacquemet, N., Pironon, J., Lagneau, V., Saint-Marc, J., 2012. Armouring of well cement in H₂S–CO₂ saturated brine by calcite coating – experiments and numerical modelling. *Appl. Geochem.* 27 (3), 782–795.
- Jamtveit, B., Putnis, C., Malthe-Sorensen, A., 2009. Reaction induced fracturing during replacement processes. *Contrib. Mineral. Petrol.* 157 (1), 127–133.
- Johnson, C.M., Beard, B.L., 2006. Fe isotopes: an emerging technique for understanding modern and ancient biogeochemical cycles. *GSA TODAY* 16 (11), 4.
- Johnson, J.W., Oelkers, E.H., Helgeson, H.C., 1992. Supcrt92 – A software package for calculating the standard molal thermodynamic properties of minerals, gases, aqueous species, and reactions from 1–bar to 5000–bar and 0–degrees-c to 1000–degrees-c. *Comput. Geosci.* 18 (7), 899–947.
- Johnson, G., Mayer, B., Nightingale, M., Shevalier, M., Hutcheon, I., 2011a. Using oxygen isotope ratios to quantitatively assess trapping mechanisms during CO₂ injection into geological reservoirs: the Pembina case study. *Chem. Geol.* 283 (3–4), 185–193.
- Johnson, G., Mayer, B., Shevalier, M., Nightingale, M., Hutcheon, I., 2011b. Tracing the movement of CO₂ injected into a mature oilfield using carbon isotope abundance ratios: the example of the Pembina Cardium CO₂ Monitoring project. *Int. J. Greenhouse Gas Control* 5 (4), 933–941.
- Jordan, G., Higgins, S.R., Eggleston, C.M., Swapp, S.M., Janney, D.E., Knauss, K.G., 1999. Acidic dissolution of plagioclase: in-situ observations by hydrothermal atomic force microscopy. *Geochim. Cosmochim. Acta* 63 (19–20), 3183–3191.
- Kampman, N., Bickle, M., Becker, J., Assayag, N., Chapman, H., 2009. Feldspar dissolution kinetics and Gibbs free energy dependence in a CO₂-enriched groundwater system, Green River, Utah. *Earth Planet. Sci. Lett.* 284 (3–4), 473–488.
- Kampman, N., Bickle, M., Galy, A., Chapman, H., Zhou, Z., Dubacq, B., Wigley, M., Warr, O., Sirkittputtisak, T., Ballentine, C., 2011. Short-term CO₂–fluid–mineral interactions in a CO₂ injection experiment, Wyoming. *Mineral. Mag.* 75 (3), 1149.
- Kampman, N., Burnside, N.M., Shipton, Z.K., Chapman, H.J., Nicholl, J.A., Ellam, R.M., Bickle, M.J., 2012. Pulses of carbon dioxide emissions from intracrustal faults following climatic warming. *Nat. Geosci.* 5 (5), 352–358.
- Kampman, N., Maskell, A., Bickle, M.J., Evans, J.P., Schaller, M., Purser, G., Zhou, Z., Gattacceca, J., Peitre, E.S., Rochelle, C.A., Ballentine, C.J., Busch, A., scientists of the GRDP, 2013a. Scientific drilling and downhole fluid sampling of a natural CO₂ reservoir, Green River, Utah. *Sci. Drill.* 1 (1), 1–11.
- Kampman, N., et al., 2013. Drilling and fluid sampling a natural CO₂ reservoir: implications for fluid flow and CO₂–fluid–rock reaction during CO₂ migration through the overburden. *Chem. Geol.* 369, 51–82 (in this issue).
- Karamalidis, A.K., et al., 2013. Trace metal source terms in carbon sequestration environments. *Environ. Sci. Technol.* 47 (1), 322–329.
- Kaszuba, J.P., Janeky, D.R., Snow, M.G., 2005. Experimental evaluation of mixed fluid reactions between supercritical carbon dioxide and NaCl brine: relevance to the integrity of a geologic carbon repository. *Chem. Geol.* 217 (3–4), 277–293.
- Keating, E.H., Fessenden, J., Kanjorski, N., Koning, D.J., Pawar, R., 2010. The impact of CO₂ on shallow groundwater chemistry: observations at a natural analog site and implications for carbon sequestration. *Environ. Earth Sci.* 60 (3), 521–536.
- Kelemen, P.B., Matter, J., 2008. In situ carbonation of peridotite for CO₂ storage. *Proc. Natl. Acad. Sci. U. S. A.* 105 (45), 17295–17300.
- Kharaka, Y.K., Cole, D.R., 2011. Geochemistry of geological sequestration of carbon dioxide. In: Harmon, R., Parker, A. (Eds.), *Frontiers in Geochemistry: Contributions of Geochemistry to the Study of the Earth*. Wiley, Oxford, pp. 135–174.
- Kharaka, Y., Hanor, J., 2003. Deep fluids in the continents: I Sedimentary basins. *Treatise on Geochem.* 5, 499–540.
- Kharaka, Y.K., Cole, D.R., Hovorka, S.D., Gunter, W.D., Knauss, K.G., Freifeld, B.M., 2006a. Gas–water–rock interactions in Frio Formation following CO₂ injection: implications for the storage of greenhouse gases in sedimentary basins. *Geology* 34 (7), 577–580.
- Kharaka, Y.K., Cole, D.R., Thordsen, J.J., Kakouros, E., Nance, H.S., 2006b. Gas–water–rock interactions in sedimentary basins: CO₂ sequestration in the Frio Formation, Texas, USA. *J. Geochem. Explor.* 89 (1–3), 183–186.
- Kharaka, Y.K., Thordsen, J.J., Hovorka, S.D., Seay Nance, H., Cole, D.R., Phelps, T.J., Knauss, K.G., 2009. Potential environmental issues of CO₂ storage in deep saline aquifers: geochemical results from the Frio-I Brine Pilot test, Texas, USA. *Appl. Geochem.* 24 (6), 1106–1112.
- Kharaka, Y.K., Thordsen, J.J., Kakouros, E., Ambats, G., Herkelrath, W.N., Beers, S.R., Gullickson, K.S., 2010. Changes in the chemistry of shallow groundwater related to the 2008 injection of CO₂ at the ZERT field site, Bozeman, Montana. *Environ. Earth Sci.* 60 (2), 273–284.
- Kikuta, K., Hongo, S., Tanase, D., Ohsumi, T., 2005. Field test of CO₂ injection, Nagaoko, Japan. *Proceedings of the 7th SEGJ International Symposium*, Sendai, Japan.
- Kim, K.-Y., Han, W., Oh, J., Kim, T., Kim, J.-C., 2012a. Characteristics of salt-precipitation and the associated pressure build-up during CO₂ storage in saline aquifers. *Transp. Porous Media* 92 (2), 397–418.
- Kim, Y., Wan, J., Kneafsey, T.J., Tokunaga, T.K., 2012b. Dewetting of silica surfaces upon reactions with supercritical CO₂ and brine: pore-scale studies in micromodels. *Environ. Sci. Technol.* 46 (7), 4228–4235.
- Knauss, K., Johnson, J., Steefel, C., 2005. Evaluation of the impact of CO₂, co-contaminant gas, aqueous fluid and reservoir rock interactions on the geologic sequestration of CO₂. *Chem. Geol.* 217 (3–4), 339–350.
- Kohler, E., Parra, T., Vidal, O., 2009. Clayey cap-rock behavior in H₂O–CO₂ media at low pressure and temperature conditions: an experimental approach. *Clay Clay Miner.* 57, 616–637.
- Kolak, J.J., Burruss, R.C., 2006. Geochemical investigation of the potential for mobilizing non-methane hydrocarbons during carbon dioxide storage in deep coal beds. *Energy Fuel* 20 (2), 566–574.
- Kutchko, B.G., Strazisar, B.R., Dzombak, D.A., Lowry, G.V., Thaulow, N., 2007. Degradation of well cement by CO₂ under geologic sequestration conditions. *Environ. Sci. Technol.* 41 (13), 4787–4792.
- Lasaga, A.C., 1984. Chemical kinetics of water–rock interactions. *J. Geophys. Res.* 89 (B6), 4009–4025.
- Lawton, D.C., 2009. Time-lapse seismic analysis. In: Hitchon, B. (Ed.), *Pembina Cardium CO₂ Monitoring Pilot: A CO₂-EOR Project*. Geoscience Publishing, Alberta Canada, pp. 201–249.
- Lea, A.S., Higgins, S.R., Knauss, K.G., Rosso, K.M., 2011. A high-pressure atomic force microscope for imaging in supercritical carbon dioxide. *Rev. Sci. Instrum.* 82 (4).
- Lin, H., Fujii, T., Takisawa, R., Takahashi, T., Hashida, T., 2008. Experimental evaluation of interactions in supercritical CO₂/water/rock minerals system under geologic CO₂ sequestration conditions. *J. Mater. Sci.* 43 (7), 2307–2315.
- Little, M.G., Jackson, R.B., 2010. Potential impacts of leakage from deep CO₂ geosequestration on overlying freshwater aquifers. *Environ. Sci. Technol.* 44 (23), 9225–9232.
- Loope, D.B., Kettler, R.M., Weber, K.A., 2010. Follow the water: connecting a CO₂ reservoir and bleached sandstone to iron-rich concretions in the Navajo Sandstone of south-central Utah, USA. *Geology* 38 (11), 999–1002.
- Loring, J.S., Schaeff, H.T., Turcu, R.V., Thompson, C.J., Miller, Q.R., Martin, P.F., Rosso, K.M., 2012. In situ molecular spectroscopic evidence for CO₂ intercalation into montmorillonite in supercritical carbon dioxide. *Langmuir* 28 (18), 7125–7128.
- Lu, J., Wilkinson, M., Haszeldine, R.S., Fallick, A.E., 2009. Long-term performance of a mudrock seal in natural CO₂ storage. *Geology* 37 (1), 35–38.
- Lu, P., Fu, Q., Seyfried Jr., W., Hereford, A., Zhu, C., 2011. Navajo Sandstone–brine–CO₂ interaction: implications for geological carbon sequestration. *Environ. Earth Sci.* 62 (1), 101–118.
- Lu, J., Kharaka, Y.K., Thordsen, J.J., Horita, J., Karamalidis, A., Griffith, C., Hovorka, S.D., 2012. CO₂–rock–brine interactions in Lower Tuscaloosa Formation at Cranfield CO₂ sequestration site, Mississippi, USA. *Chem. Geol.* 291, 269–277.
- Lyle, S., Huppert, H.E., Hallworth, M., Bickle, M., Chadwick, A., 2005. Axisymmetric gravity currents in a porous medium. *J. Fluid Mech.* 543, 293–302.
- MacMinn, C., Szulczewski, M., Juanes, R., 2011. CO₂ migration in saline aquifers. Part 2. Capillary and solubility trapping. *J. Fluid Mech.* 688, 321.
- Maher, K., 2010. The dependence of chemical weathering rates on fluid residence time. *Earth Planet. Sci. Lett.* 294 (1–2), 101–110.
- Maher, K., Steefel, C.L., White, A.F., Stonestrom, D.A., 2009. The role of reaction affinity and secondary minerals in regulating chemical weathering rates at the Santa Cruz Soil Chronosequence, California. *Geochim. Cosmochim. Acta* 73 (10), 2804–2831.
- May, F., 2005. Alteration of wall rocks by CO₂-rich water ascending in fault zones: natural analogues for reactions induced by CO₂ migrating along faults in siliciclastic reservoir and cap rocks. *Oil Gas Sci. Technol.* 60 (1), 19–32.
- McGrail, B.P., Schaeff, H.T., Glezakou, V.A., Dang, L.X., Owen, A.T., 2009. Water reactivity in the liquid and supercritical CO₂ phase: has half the story been neglected? *Energy Procedia* 1 (1), 3415–3419.
- McGuire, K.A., 2009. CO₂ Injection and Reservoir Characterization: An Integrated Petrographic and Geochemical Study of the Frio Formation, Texas. Masters Thesis Ball State University, Muncie, Indiana (115 pp.).
- McPherson, B.J., Heath, J., 2009. Self-sealing of faults by CO₂-rich fluids. *Geochim. Cosmochim. Acta Suppl.* 73, 861.
- Metz, B., Davidson, O., De Coninck, H., Loos, M., Meyer, L., 2005. IPCC, 2005: IPCC Special Report on Carbon Dioxide Capture and Storage. Prepared by Working Group III

- of the Intergovernmental Panel on Climate Change. Cambridge University Press, Cambridge, United Kingdom and New York, NY, USA.
- Mito, S., Xue, Z., Ohsumi, T., 2008. Case study of geochemical reactions at the Nagaoka CO₂ injection site, Japan. *Int. J. Greenhouse Gas Control* 2 (3), 309–318.
- Moore, J., Adams, M., Allis, R., Lutz, S., Rauzi, S., 2003. CO₂ mobility in natural reservoirs beneath the Colorado Plateau and southern Rocky Mountains: an example from the Springerville–St. Johns Field, Arizona and New Mexico. *Proceedings of the Second Annual Conference on Carbon Sequestration*, pp. 5–8.
- Moore, J., Adams, M., Allis, R., Lutz, S., Rauzi, S., 2005. Mineralogical and geochemical consequences of the long-term presence of CO₂ in natural reservoirs: an example from the Springerville–St. Johns Field, Arizona, and New Mexico, USA. *Chem. Geol.* 217 (3), 365–385.
- Moore, J., Lichtner, P.C., White, A.F., Brantley, S.L., 2012. Using a reactive transport model to elucidate differences between laboratory and field dissolution rates in regolith. *Geochim. Cosmochim. Acta* 93, 235–261.
- Muir, I., Nesbitt, H., 1991. Effects of aqueous cations on the dissolution of labradorite feldspar. *Geochim. Cosmochim. Acta* 55, 3181–3189.
- Munz, I., Brandvoll, O., Haug, T., Iden, K., Smeets, R., Kihle, J., Johansen, H., 2012. Mechanisms and rates of plagioclase carbonation reactions. *Geochim. Cosmochim. Acta* 77, 27–51.
- Mutoro, J.W., Leahy Dios, A., Firoozabadi, A., 2010. Modeling infinite dilution and Fickian diffusion coefficients of carbon dioxide in water. *AIChE J* 57 (6), 1617–1627.
- Myers, M., Stalker, L., Ross, A., Dyt, C., Ho, K.B., 2012. Method for the determination of residual carbon dioxide saturation using reactive ester tracers. *Appl. Geochem.* 27 (10), 2148–2156.
- Myrntinen, A., Becker, V., Van Geldern, R., Würdemann, H., Morozova, D., Zimmer, M., Barth, J.A.C., 2010. Carbon and oxygen isotope indications for CO₂ behaviour after injection: first results from the Ketzin site (Germany). *Int. J. Greenhouse Gas Control* 4 (6), 1000–1006.
- Nagy, K., Blum, A., Lasaga, A., 1991. Dissolution and precipitation kinetics of kaolinite at 80 °C and pH 3: the dependence on solution saturation state. *Am. J. Sci.* 291 (7), 649–686.
- Navarre-Sitchler, A.K., Maxwell, R.M., Siirila, E.R., Hammond, G.E., Lichtner, P.C., 2012. Elucidating geochemical response of shallow heterogeneous aquifers to CO₂ leakage using high-performance computing: implications for monitoring of CO₂ sequestration. *Adv. Water Resour.* 53, 45–55.
- Nelson, P.H., 1994. Permeability–porosity relationships in sedimentary rocks. *Log Anal.* 35, 38–38.
- Neufeld, J.A., Hesse, M.A., Riaz, A., Hallworth, M.A., Tchelepi, H.A., Huppert, H.E., 2010. Convective dissolution of carbon dioxide in saline aquifers. *Geophys. Res. Lett.* 37 (22), L22404.
- Nimz, G., Hudson, G., 2005. The use of noble gas isotopes for monitoring leakage of geologically stored CO₂. Carbon dioxide capture for storage in deep geologic formations, 2, pp. 1113–1130.
- Nordbotten, J.M., Celia, M.A., Bachu, S., 2005. Injection and storage of CO₂ in deep saline aquifers: analytical solution for CO₂ plume evolution during injection. *Transp. Porous Media* 58 (3), 339–360.
- Oelkers, E., Schott, J., Devidal, J., 1994. The effect of aluminum, pH, and chemical affinity on the rates of aluminosilicate dissolution reactions. *Geochim. Cosmochim. Acta* 58, 2011–2024.
- Okwen, R.T., Stewart, M.T., Cunningham, J.A., 2011. Temporal variations in near-wellbore pressures during CO₂ injection in saline aquifers. *Int. J. Greenhouse Gas Control* 5 (5), 1140–1148.
- Oldenburg, C.M., 2007. Joule–Thomson cooling due to CO₂ injection into natural gas reservoirs. *Energy Convers. Manag.* 48 (6), 1808–1815.
- Ott, H., de Kloe, K., Marcelis, F., Makurat, A., 2011. Injection of supercritical CO₂ in brine saturated sandstone: pattern formation during salt precipitation. *Energy Procedia* 4, 4425–4432.
- Parkhurst, D., Appelo, C., 1999. User's guide to PHREEQC (version 2)—a computer program for speciation, batch-reaction, one-dimensional transport, and inverse geochemical calculations. US Geological Survey Water-Resources Investigations Report, 99(4259), p. 310.
- Pauwels, H., Gaus, I., le Nindre, Y.M., Pearce, J., Czernichowski-Lauriol, I., 2007. Chemistry of fluids from a natural analogue for a geological CO₂ storage site (Montmiral, France): lessons for CO₂–water–rock interaction assessment and monitoring. *Appl. Geochem.* 22 (12), 2817–2833.
- Payán, M.C., Galan, B., Coz, A., Vandecasteele, C., Viguri, J.R., 2012. Evaluation through column leaching tests of metal release from contaminated estuarine sediment subject to CO₂ leakages from Carbon Capture and Storage sites. *Environ. Pollut.* 171, 174–184.
- Pearce, J., 2004. Natural analogues for the geological storage of CO₂ Final report of the Nascent project. *Brit. Geol. Surv. Tech. Rep.* 122.
- Pearce, J., 2006. What can we learn from natural analogues? *Advances in the Geological Storage of Carbon Dioxide*. 127–139.
- Penn West Energy Trust, 2007. Pembina Cardium 'A' Lease CO₂ Pilot Project Annual Report, Alberta Energy.
- Peysson, Y., Bazin, B., Magnier, C., Kohler, E., Youssef, S., 2011. Permeability alteration due to salt precipitation driven by drying in the context of CO₂ injection. *Energy Procedia* 4, 4387–4394.
- Plumper, O., Roynce, A., Magraso, A., Jamtveit, B., 2012. The interface-scale mechanism of reaction-induced fracturing during serpentinization. *Geology* 40 (12), 1103–1106.
- Potter-McIntyre, S., et al., 2013. Iron precipitation in a natural CO₂ reservoir: Jurassic Navajo Sandstone in the northern San Rafael Swell, UT, USA. *Geofluids* 13, 82–92.
- Pruess, K., 2004. Numerical simulation of CO₂ leakage from a geologic disposal reservoir, including transitions from super- to subcritical conditions, and boiling of liquid CO₂. *SPE J.* 9 (2), 237–248.
- Pruess, K., Müller, N., 2009. Formation dry-out from CO₂ injection into saline aquifers: 1. Effects of solids precipitation and their mitigation. *Water Resour. Res.* 45 (3), W03402.
- Pruess, K., Freifeld, B., Kennedy, M., Oldenburg, C., Phelps, T.J., van Soest, M.C., 2005. Use of gas phase tracers for monitoring CO₂ injection at the Frio test site. Fourth Annual Conference on Carbon Capture and Sequestration, Alexandria, VA.
- Quattrocchi, F., Barbieri, M., Bencini, R., Cinti, D., Durocher, K., Galli, G., Pizzino, L., Shevalier, M., Voltattorni, N., 2006. Strontium isotope (⁸⁷Sr/⁸⁶Sr) chemistry in produced oilfield waters: the IEAWeyburn CO₂ monitoring and storage project. In: Lombardi, S., Altunina, K.L., Beaubien, S.E. (Eds.), *Advances in Geological Storage of Carbon Dioxide*. NATO Science Series. Springer Publishing, Berlin, pp. 243–259.
- Raistrick, M., Mayer, B., Shevalier, M., Perez, R.J., Hutcheon, I., Perkins, E., Gunter, B., 2006. Using chemical and isotopic data to quantify ionic trapping of injected carbon dioxide in oil field brines. *Environ. Sci. Technol.* 40 (21), 6744–6749.
- Regnault, O., Lagneau, V., Schneider, H., 2009. Experimental measurement of portlandite carbonation kinetics with supercritical CO₂. *Chem. Geol.* 265 (1), 113–121.
- Rempel, K.U., Liebscher, A., Heinrich, W., Schettler, G., 2011. An experimental investigation of trace element dissolution in carbon dioxide: applications to the geological storage of CO₂. *Chem. Geol.* 289 (3–4), 224–234.
- Riaz, A., Hesse, M., Tchelepi, H.A., Orr, F.M., 2006. Onset of convection in a gravitationally unstable diffusive boundary layer in porous media. *J. Fluid Mech.* 548, 87–111.
- Rochelle, C.A., Milodowski, A.E., 2012. Carbonation of borehole seals: comparing evidence from short-term laboratory experiments and long-term natural analogues. *Appl. Geochem.* 30, 161–177.
- Rutqvist, J., Birkholzer, J., Cappa, F., Tsang, C.F., 2007. Estimating maximum sustainable injection pressure during geological sequestration of CO₂ using coupled fluid flow and geomechanical fault-slip analysis. *Energy Convers. Manag.* 48 (6), 1798–1807.
- Schaeff, H.T., McGrail, B.P., Loring, J.L., Bowden, M.E., Arey, B.W., Rosso, K.M., 2013. Forsterite [Mg₂SiO₄] carbonation in wet supercritical CO₂: an in situ high-pressure X-ray diffraction study. *Environ. Sci. Technol.* 47 (1), 174–181.
- Schilling, F., Borm, G., Würdemann, H., Möller, F., Kühn, M., 2009. Status report on the first European on-shore CO₂ storage site at Ketzin (Germany). *Energy Procedia* 1 (1), 2029–2035.
- Schott, J., Oelkers, E., 1995. Dissolution and crystallization rates of silicate minerals as a function of chemical affinity. *Pure Appl. Chem.* 67 (6), 903–910.
- Shevalier, M., Nightingale, M., Johnson, G., Mayer, B., Perkins, E., Hutcheon, I., 2009. Monitoring the reservoir geochemistry of the Pembina Cardium CO₂ monitoring project, Drayton Valley, Alberta. *Energy Procedia* 1 (1), 2095–2102.
- Shipton, Z.K., Evans, J.P., Dockrill, B., Heath, J., Williams, A., Kirchner, D., Kolesar, P.T., 2004. Analysis of CO₂ leakage through 'low-permeability' faults from natural reservoirs in the Colorado Plateau, east-central Utah. *Geol. Soc. Lond. Spec. Publ.* 233 (43).
- Shipton, Z.K., Evans, J.P., Kirchner, D., Kolesar, P.T., Williams, A.P., Heath, J., 2005. Natural leaking CO₂-charged systems as analogs for failed geologic storage reservoirs. The CO₂ Capture and Storage Project (CCP).
- Siirila, E.R., Navarre-Sitchler, A.K., Maxwell, R.M., McCray, J.E., 2012. A quantitative methodology to assess the risks to human health from CO₂ leakage into groundwater. *Adv. Water Resour.* 36, 146–164.
- Singh, V., Cavanagh, A., Hansen, H., Nazarian, B., Iding, M., Ringrose, P., 2010. Reservoir modeling of CO₂ plume behavior calibrated against monitoring data from Sleipner, Norway. SPE Annual Technical Conference, 19–22 September, Florence, Italy.
- Sorai, M., Ohsumi, T., Ishikawa, M., 2005. Nanoscale surface observation of feldspar dissolved under supercritical CO₂–water–mineral system. *Energy* 30 (11–12), 2334–2343.
- Spycher, N., Pruess, K., 2005. CO₂–H₂O mixtures in the geological sequestration of CO₂. II. Partitioning in chloride brines at 12–100 °C and up to 600 bar. *Geochim. Cosmochim. Acta* 69 (13), 3309–3320.
- Spycher, N., Pruess, K., Ennis-King, J., 2003. CO₂–H₂O mixtures in the geological sequestration of CO₂. I. Assessment and calculation of mutual solubilities from 12 to 100 °C and up to 600 bar. *Geochim. Cosmochim. Acta* 67, 3015–3031. [http://dx.doi.org/10.1016/S0016-7037\(03\)00273-4](http://dx.doi.org/10.1016/S0016-7037(03)00273-4).
- Tao, Q., Checkai, D., Huerta, N., Bryant, S.L., 2011. An improved model to forecast CO₂ leakage rates along a wellbore. *Energy Procedia* 4, 5385–5391.
- Taylor, G., 1953. Dispersion of soluble matter in solvent flowing slowly through a tube. *Proc. R. Soc. Lond. A. Math. Phys. Sci.* 219 (1137), 186–203.
- Taylor, A., Blum, J., Lasaga, A., MacInnis, I., 2000. Kinetics of dissolution and Sr release during biotite and phlogopite weathering. *Geochim. Cosmochim. Acta* 64 (7), 1191–1208.
- Trautz, R.C., et al., 2012. Effect of dissolved CO₂ on a shallow groundwater system: a controlled release field experiment. *Environ. Sci. Technol.* 47 (1), 298–305.
- Underschultz, J., Boreham, C., Dance, T., Stalker, L., Freifeld, B., Kirste, D., Jonathan, Ennis-King, J., 2011. CO₂ storage in a depleted gas field: An overview of the CO₂CRC Otway Project and initial results. *Int. J. Greenhouse Gas Control* 5, 922–932.
- Vella, D., Huppert, H.E., 2006. Gravity currents in a porous medium at an inclined plane. *J. Fluid Mech.* 555, 353–362.
- Viswanathan, H., Dai, Z., Lopano, C., Keating, E., Hakala, J.A., Scheckel, K.G., Pawar, R., 2012. Developing a robust geochemical and reactive transport model to evaluate possible sources of arsenic at the CO₂ sequestration natural analog site in Chimayo, New Mexico. *Int. J. Greenhouse Gas Control* 10, 199–214.
- Watson, M.N., Zwingmann, N., Lemon, N.M., 2004. The Ladbrooke Grove–Katnook carbon dioxide natural laboratory: a recent CO₂ accumulation in a lithic sandstone reservoir. *Energy* 29 (9–10), 1457–1466.
- White, A., Brantley, S., 2003. The effect of time on the weathering of silicate minerals: why do weathering rates differ in the laboratory and field? *Chem. Geol.* 202 (3–4), 479–506.
- White, D.J., Johnson, J.W., 2009. Integrated geophysical and geochemical research programs of the IEA GHG Weyburn–Midale CO₂ monitoring and storage project. *Energy Procedia* 1 (1), 2349–2356.

- White, A.F., Schulz, M.S., Stonestrom, D.A., Vivit, D.V., Fitzpatrick, J., Bullen, T.D., Blum, A.E., 2009. Chemical weathering of a marine terrace chronosequence, Santa Cruz, California. Part II: Solute profiles, gradients and the comparisons of contemporary and long-term weathering rates. *Geochim. Cosmochim. Acta* 73 (10), 2769–2803.
- Whittaker, S., Rostron, B., Hawkes, C., Gardner, C., White, D., Johnson, J., Chalaturny, R., Seeburger, D., 2011. A decade of CO₂ injection into depleting oil fields: monitoring and research activities of the IEA GHG Weyburn-Midale CO₂ Monitoring and Storage Project. *Energy Procedia* 4, 6069–6076.
- Wigley, M., Kampman, N., Dubacq, B., Bickle, M., 2012. Fluid–mineral reactions and trace metal mobilisation in an exhumed natural CO₂ reservoir, Green River, Utah. *Geology* 40 (6), 555–558.
- Wigley, M., Dubacq, B., Kampman, N., Bickle, M., 2013a. Controls of sluggish, CO₂-promoted, hematite and K-feldspar dissolution kinetics in sandstones. *Earth Planet. Sci. Lett.* 362, 76–87.
- Wigley, M., Kampman, N., Chapman, H., Dubacq, B., Bickle, M., 2013b. In-situ re-deposition of trace metals mobilized by CO₂-charged fluids. *Geochem. Geophys. Geosyst.* 12 (5), 1321–1332.
- Wilhelm, E., Battino, R., Wilcock, R.J., 1977. Low-pressure solubility of gases in liquid water. *Chem. Rev.* 77 (2), 219–262.
- Wilkinson, M., Gilfillan, S.V.M., Haszeldine, R.S., Ballentine, C.J., 2009a. Plumbing the depths: testing natural tracers of subsurface CO₂ origin and migration, Utah. In: Grobe, M., Pashin, J.C., Dodge, R.L. (Eds.), *Carbon Dioxide Sequestration in Geological Media – State of the Science*. AAPG Studies in Geology, pp. 619–634.
- Wilkinson, M., Haszeldine, R.S., Fallick, A.E., Odling, N., Stoker, S.J., Gatliff, R.W., 2009b. CO₂–mineral reaction in a natural analogue for CO₂ storage—implications for modeling. *J. Sediment. Res.* 79 (7), 486–494.
- Worden, R.H., 2006. Dawsonite cement in the Triassic Lam Formation, Shabwa Basin, Yemen: a natural analogue for a potential mineral product of subsurface CO₂ storage for greenhouse gas reduction. *Mar. Pet. Geol.* 23 (1), 61–77.
- Xu, T., Apps, J., Pruess, K., 2005. Mineral sequestration of carbon dioxide in a sandstone–shale system. *Chem. Geol.* 217 (3–4), 295–318.
- Xu, T., Apps, J., Pruess, K., Yamamoto, H., 2007. Numerical modeling of injection and mineral trapping of CO₂ with H₂S and SO₂ in a sandstone formation. *Chem. Geol.* 242 (3–4), 319–346.
- Xu, T., Kharaka, Y.K., Doughty, C., Freifeld, B.M., Daley, T.M., 2010. Reactive transport modeling to study changes in water chemistry induced by CO₂ injection at the Frio-I Brine Pilot. *Chem. Geol.* 271 (3–4), 153–164.
- Yang, C., Gu, Y., 2006. Accelerated mass transfer of CO₂ in reservoir brine due to density-driven natural convection at high pressures and elevated temperatures. *Ind. Eng. Chem. Res.* 45 (8), 2430–2436.
- Zeidouni, M., Pooladi-Darvish, M., Keith, D., 2009. Analytical solution to evaluate salt precipitation during CO₂ injection in saline aquifers. *Int. J. Greenhouse Gas Control* 3 (5), 600–611.
- Zhang, Y., Freifeld, B., Finsterle, S., Leahy, M., Ennis-King, J., Paterson, L., Dance, T., 2011. Single-well experimental design for studying residual trapping of supercritical carbon dioxide. *Int. J. Greenhouse Gas Control* 5 (1), 88–98.
- Zhou, Z., et al., 2011. Predicting CO₂ EOR and geological sequestration processes with artificial noble gas tracers. *Mineral. Mag.* 75 (3), 1149.
- Zhou, Z., Ballentine, C.J., Schoell, M., Stevens, S.H., 2012. Identifying and quantifying natural CO₂ sequestration processes over geological timescales: the Jackson Dome CO₂ Deposit, USA. *Geochim. Cosmochim. Acta* 86, 257–275.
- Zhu, C., Lu, P., 2013. The coupling of dissolution and precipitation reactions as the main contributor to the apparent field–lab rate discrepancy. *Procedia Earth Planet. Sci.* 7, 948–952.
- Zhu, C., Veblen, D., Blum, A., Chipera, S., 2006. Naturally weathered feldspar surfaces in the Navajo Sandstone aquifer, Black Mesa, Arizona: electron microscopic characterization. *Geochim. Cosmochim. Acta* 70 (18), 4600–4616.
- Zimmer, M., Erzinger, J., Kujawa, C., 2011. The gas membrane sensor (GMS): a new method for gas measurements in deep boreholes applied at the CO₂SINK site. *Int. J. Greenhouse Gas Control* 5 (4), 995–1001.
- Zweigel, P., Hamborg, M., Arts, R., Lothe, A., Sylta, Ø., Tømmerås, A., 2000. Prediction of migration of CO₂ injected into an underground depository: reservoir geology and migration modelling in the Sleipner case (North Sea). 5th International Conference on Greenhouse Gas Control Technologies, Cairns (Australia).